PHYSICAL REVIEW D **93,** 052002 (2016)

Search for the electroweak production of supersymmetric particles in $\sqrt{s} = 8$ TeV pp collisions with the ATLAS detector

G. Aad *et al.*[*]
(ATLAS Collaboration)
(Received 23 September 2015; published 4 March 2016)

The ATLAS experiment has performed extensive searches for the electroweak production of charginos, neutralinos, and staus. This article summarizes and extends the search for electroweak supersymmetry with new analyses targeting scenarios not covered by previously published searches. New searches use vector-boson fusion production, initial-state radiation jets, and low-momentum lepton final states, as well as multivariate analysis techniques to improve the sensitivity to scenarios with small mass splittings and low-production cross sections. Results are based on 20 fb^{-1} of proton-proton collision data at $\sqrt{s} = 8$ TeV recorded with the ATLAS experiment at the Large Hadron Collider. No significant excess beyond Standard Model expectations is observed. The new and existing searches are combined and interpreted in terms of 95% confidence-level exclusion limits in simplified models, where a single production process and decay mode is assumed, as well as within phenomenological supersymmetric models.

DOI: 10.1103/PhysRevD.93.052002

I. INTRODUCTION

Supersymmetry (SUSY) [1–9] is a space-time symmetry that postulates for each Standard Model (SM) particle the existence of a partner state whose spin differs by one-half unit. The introduction of these new SUSY particles (sparticles) provides a potential solution to the hierarchy problem [10–13]. If R-parity is conserved [14–18], as assumed in this article, sparticles are always produced in pairs and the lightest supersymmetric particle (LSP) emerges as a stable dark-matter candidate.

The charginos and neutralinos are mixtures of the bino, winos, and higgsinos, collectively referred to as the electroweakinos, that are superpartners of the U(1), SU(2) gauge bosons and the Higgs bosons, respectively. Their mass eigenstates are referred to as $\tilde{\chi}_i^{\pm}$ ($i = 1, 2$) and $\tilde{\chi}_j^0$ ($j = 1, 2, 3, 4$) in order of increasing mass. The direct production of charginos, neutralinos, and sleptons ($\tilde{\ell}$) through electroweak (EW) interactions may dominate the SUSY production at the Large Hadron Collider (LHC) if the masses of the gluinos and squarks are large. Previous searches for electroweak SUSY production at ATLAS targeted the production of $\tilde{\ell}^+\tilde{\ell}^-$, $\tilde{\tau}^+\tilde{\tau}^-$, $\tilde{\chi}_1^+\tilde{\chi}_1^-$ (decaying through $\tilde{\ell}$ or W bosons), $\tilde{\chi}_1^{\pm}\tilde{\chi}_2^0$ (decaying through $\tilde{\ell}$ or W and Z/h bosons), and $\tilde{\chi}_2^0\tilde{\chi}_3^0$ (decaying through $\tilde{\ell}$ or Z bosons) [19–23], and found no significant excess beyond SM expectations. These searches are typically sensitive to scenarios where there is a relatively large $O(m_{W,Z})$ splitting between the produced sparticles and the LSP, leaving uncovered territory for smaller mass splittings.

This article addresses EW SUSY production based on the 20.3 fb^{-1} of $\sqrt{s} = 8$ TeV proton-proton collisions collected by the ATLAS experiment in 2012. A series of new analyses targeting regions in parameter space not covered by previous ATLAS analyses [19–23] are presented. The results from new and published searches are combined and reinterpreted to provide the final 8 TeV ATLAS limits on the production of EW SUSY particles in a variety of models. The dependence of the limits on the mass of the intermediate slepton in models of electroweakino production with $\tilde{\ell}$-mediated decays is also studied, thus generalizing the results of Refs. [19–21].

In cases where the LSP is wino or higgsino dominated, the lighter electroweakino states $\tilde{\chi}_1^{\pm}$, $\tilde{\chi}_2^0$ can have mass differences with the $\tilde{\chi}_1^0$ ranging from a few GeV to a few tens of GeV, depending on the values of the other parameters in the mixing matrix [24]. In particular, in naturalness-inspired models [25,26] the higgsino must be light, so the $\tilde{\chi}_1^0$, $\tilde{\chi}_2^0$, and $\tilde{\chi}_1^{\pm}$ are usually higgsino-dominated and have a small mass splitting. Therefore, a situation with a light $\tilde{\chi}_1^0$ approximately mass degenerate with the $\tilde{\chi}_1^{\pm}$ and $\tilde{\chi}_2^0$ has a strong theoretical motivation. A relatively low mass splitting between the produced sparticles and the LSP (referred to as compressed scenarios) results in low-momentum decay products that are difficult to reconstruct efficiently, and probing these signatures is experimentally challenging. The new analyses introduced in this article improve the sensitivity to the compressed spectra. The two- and three-lepton searches for $\tilde{\chi}_1^+\tilde{\chi}_1^-$ and $\tilde{\chi}_1^{\pm}\tilde{\chi}_2^0$ production in Refs. [19,20] are extended by lowering the transverse momentum threshold on reconstructed leptons, and by boosting the electroweak SUSY system through the

[*]Full author list given at the end of the article.

Published by the American Physical Society under the terms of the Creative Commons Attribution 3.0 License. Further distribution of this work must maintain attribution to the author(s) and the published article's title, journal citation, and DOI.

source: https://doi.org/10.7892/boris.100023 | downloaded: 12.10.2024

 © 2016 CERN, for the ATLAS Collaboration

requirement of QCD initial state radiation (ISR). The search for the vector-boson fusion (VBF) production of $\tilde{\chi}_1^{\pm}\tilde{\chi}_1^{\pm}$ uses the signature of a same-sign light lepton (e, μ) pair with two jets to probe compressed spectra.

In many SUSY scenarios with large $\tan\beta$, the stau ($\tilde{\tau}$) is lighter than the selectron and smuon [27], resulting in tau-rich final states. Coannihilation processes [28] favor a light $\tilde{\tau}$ that has a small mass splitting with a bino LSP, as it can set the relic density to the observed value [29]. An additional new search is presented here, which uses a final state with two hadronically decaying τ leptons and multivariate techniques to improve the sensitivity to direct $\tilde{\tau}$ production compared to the search presented in Ref. [22].

Searches for the electroweak production of SUSY particles have been conducted at the Tevatron [30,31] and by the CMS Collaboration [32–34]. At LEP [35–39], searches set lower limits of 103.5 GeV, 99.9 GeV, 94.6 GeV, and 86.6 GeV at 95% confidence level (CL) on the mass of promptly decaying charginos, selectrons, smuons, and staus, respectively. For the interval $0.1 \lesssim \Delta m(\tilde{\chi}_1^{\pm}, \tilde{\chi}_1^0) \lesssim 3$ GeV, the chargino mass limit set by LEP degrades to 91.9 GeV. The slepton mass limits from LEP assume gaugino mass unification, which is not assumed in the results presented here.

The article is organized as follows: Sec. II describes the signal models studied in this article; Sec. III provides a brief description of the ATLAS detector; Secs. IV and V outline the Monte Carlo (MC) simulation and event selection, respectively; Sec. VI discusses the analysis strategy common to all analyses studied in this article; Sec. VII presents the direct stau production search; Sec. VIII presents the compressed spectra searches in direct production; Sec. IX presents the search for same-sign chargino-pair production via VBF; Sec. X provides a global overview of the results of the ATLAS searches for electroweakino production at 8 TeV, integrating the results of the new analyses with published analyses in the framework of several relevant signal models; and finally conclusions are drawn in Sec. XI.

II. SUSY SCENARIOS

The SUSY scenarios considered in this article can be divided into two categories: simplified models and phenomenological models. The simplified models [40] target the production of charginos, neutralinos, and sleptons, where the masses and the decay modes of the relevant particles are the only free parameters. In each of the simplified models, a single production process with a fixed decay chain is considered for optimization of the event selection and interpretation of the results. To illustrate the range of applicability of the searches, several classes of phenomenological models that consider all relevant SUSY production and decay processes are also used to interpret the results. These models include the five-dimensional EW phenomenological minimal supersymmetric standard model (pMSSM) [41], the nonuniversal Higgs masses (NUHM) model [42,43], and a gauge-mediated SUSY breaking (GMSB) model [44–49].

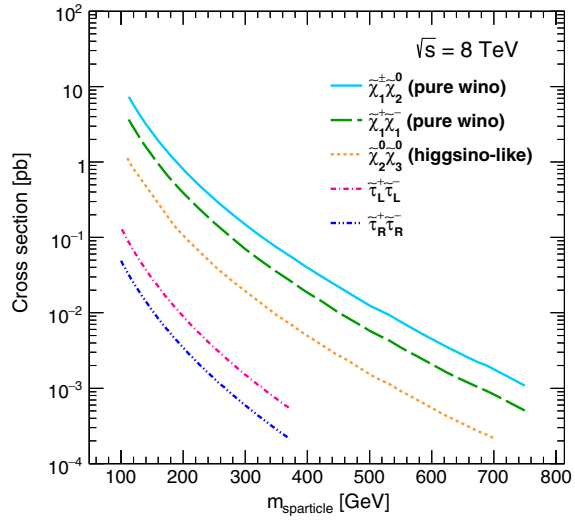

FIG. 1. The production cross sections for the simplified models of the direct production of $\tilde{\chi}_1^{+}\tilde{\chi}_1^{-}$, $\tilde{\chi}_1^{\pm}\tilde{\chi}_2^0$ [where $m(\tilde{\chi}_1^{\pm}) = m(\tilde{\chi}_2^0)$], $\tilde{\chi}_2^0\tilde{\chi}_3^0$ [where $m(\tilde{\chi}_2^0) = m(\tilde{\chi}_3^0)$], and $\tilde{\tau}^{+}\tilde{\tau}^{-}$ studied in this article. The left-handed and right-handed stau-pair production cross sections are shown separately.

R-parity is assumed to be conserved in all SUSY scenarios considered in this article. The LSP is assumed to be the lightest neutralino $\tilde{\chi}_1^0$ except in the GMSB scenarios, where it is the gravitino $\tilde{G}$. The next-to-LSP (NLSP) is usually one or more of the charginos, neutralinos, or sleptons. All SUSY particles are assumed to decay promptly, with the exception of the LSP, which is stable. Finally, SUSY particles that are not considered in a given model are decoupled by setting their masses to values inaccessible at the LHC.

Unless stated otherwise, signal cross sections are calculated to next-to-leading order (NLO) in the strong coupling constant using PROSPINO2 [50] and are shown in Fig. 1 for a number of selected simplified-model production modes. The cross sections for the production of charginos and neutralinos are in agreement with the NLO calculations matched to resummation at next-to-leading logarithmic (NLL) accuracy (NLO + NLL) within about 2% [51–53]. The nominal cross section and the uncertainty are taken from the center and spread, respectively, of the envelope of cross-section predictions using different parton distribution function (PDF) sets and factorization and renormalization scales, as described in Ref. [54].

A. Direct stau-pair production simplified model

Two simplified models describing the direct production of $\tilde{\tau}^{+}\tilde{\tau}^{-}$ are used in this article: one considers stau partners of the left-handed τ lepton ($\tilde{\tau}_L$), and a second considers stau partners of the right-handed τ lepton ($\tilde{\tau}_R$). In both models,

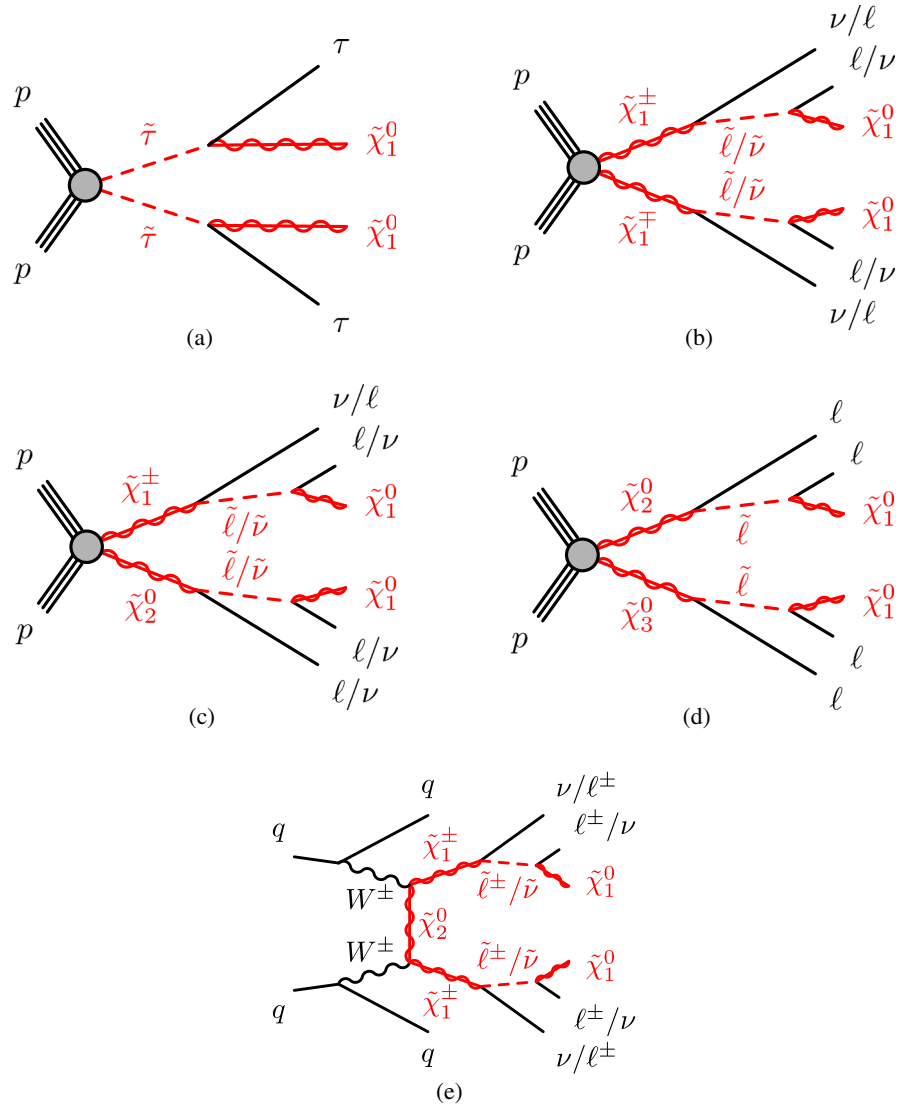

FIG. 2. The diagrams for the simplified models of the direct pair production of staus and the direct production of $\tilde{\chi}_1^+\tilde{\chi}_1^-$, $\tilde{\chi}_1^\pm\tilde{\chi}_2^0$, and $\tilde{\chi}_2^0\tilde{\chi}_3^0$, and the VBF production of $\tilde{\chi}_1^\pm\tilde{\chi}_1^\pm$ studied in this article. All three generations are included in the definition of $\tilde{\ell}/\tilde{\nu}$, except for the direct production of $\tilde{\chi}_2^0\tilde{\chi}_3^0$ where only the first two generations are assumed. The different decay modes are discussed in the text.

the stau decays with a branching fraction of 100% to the SM tau lepton and the LSP. The diagram for this model can be seen in Fig. 2(a).

B. Direct chargino-pair, chargino-neutralino, and neutralino-pair production simplified models

In the simplified models describing the direct production of $\tilde{\chi}_1^+\tilde{\chi}_1^-$ and $\tilde{\chi}_1^\pm\tilde{\chi}_2^0$, both the $\tilde{\chi}_1^\pm$ and $\tilde{\chi}_2^0$ are assumed to be pure wino and mass degenerate, while the $\tilde{\chi}_1^0$ is assumed to be pure bino. However, it is possible to reinterpret the results from these simplified models by assuming different compositions of the $\tilde{\chi}_1^0$, $\tilde{\chi}_2^0$, and $\tilde{\chi}_1^\pm$ for the same masses of the states. Two different scenarios for the decays of the $\tilde{\chi}_1^\pm$ and $\tilde{\chi}_2^0$ are considered, as shown in Figs. 2(b) and 2(c):

(i) $\tilde{\chi}_1^+\tilde{\chi}_1^-/\tilde{\chi}_1^\pm\tilde{\chi}_2^0$ *production with* $\tilde{\ell}_L$*-mediated decays:* The $\tilde{\chi}_1^\pm$ and $\tilde{\chi}_2^0$ decay with a branching fraction of 1/6 via $\tilde{e}_L$, $\tilde{\mu}_L$, $\tilde{\tau}_L$, $\tilde{\nu}_e$, $\tilde{\nu}_\mu$, or $\tilde{\nu}_\tau$ with masses $m_{\tilde{\nu}_\ell} = m_{\tilde{\ell}_L} = x(m_{\tilde{\chi}_1^\pm} - m_{\tilde{\chi}_1^0}) + m_{\tilde{\chi}_1^0}$ with $x = 0.05$, 0.25, 0.5, 0.75, or 0.95,

(ii) $\tilde{\chi}_1^\pm\tilde{\chi}_2^0$ *production with* $\tilde{\tau}_L$*-mediated decay:* The first- and second-generation sleptons and sneutrinos are assumed to be very heavy, so that the $\tilde{\chi}_1^\pm$ and $\tilde{\chi}_2^0$ decay with a branching fraction of 1/2 via $\tilde{\tau}_L$ or $\tilde{\nu}_\tau$ with masses $m_{\tilde{\nu}_\tau} = m_{\tilde{\tau}_L} = 0.5(m_{\tilde{\chi}_1^\pm} + m_{\tilde{\chi}_1^0})$.

In the simplified models considered here, the slepton mass is assumed to lie between the $\tilde{\chi}_1^0$ and $\tilde{\chi}_1^\pm/\tilde{\chi}_2^0$ masses, which increases the branching fraction to leptonic final states compared to scenarios without sleptons.

The compressed spectra searches in this article are less sensitive to scenarios where the $\tilde{\chi}_1^\pm/\tilde{\chi}_2^0$ decay through SM W, Z, or Higgs bosons, as the branching fraction to leptonic final states is significantly suppressed. The results of the ATLAS searches for $\tilde{\chi}_1^+\tilde{\chi}_1^-$ production with WW-mediated decays [19], $\tilde{\chi}_1^\pm\tilde{\chi}_2^0$ production with WZ-mediated decays [20], and $\tilde{\chi}_1^\pm\tilde{\chi}_2^0$ production with Wh-mediated decays [23] are summarized in Sec. X E. In these scenarios with decays mediated by SM bosons, the W, Z, and h bosons are assumed to decay with SM branching fractions.

In the simplified models of the direct production of $\tilde{\chi}_2^0\tilde{\chi}_3^0$, the $\tilde{\chi}_2^0$ and $\tilde{\chi}_3^0$ are assumed to be pure higgsino and mass degenerate, while the $\tilde{\chi}_1^0$ is assumed to be pure bino. The $\tilde{\chi}_2^0$ and $\tilde{\chi}_3^0$ are assumed to decay with a branching fraction of one-half via $\tilde{e}_R$, $\tilde{\mu}_R$ with mass $m_{\tilde{\ell}_R} = x(m_{\tilde{\chi}_2^0} - m_{\tilde{\chi}_1^0}) + m_{\tilde{\chi}_1^0}$ with $x = 0.05$, 0.25, 0.5, 0.75, or 0.95 ($\tilde{\chi}_2^0\tilde{\chi}_3^0$ production with $\tilde{\ell}_R$-mediated decay). The associated diagram is shown in Fig. 2(d). In this $\tilde{\chi}_2^0\tilde{\chi}_3^0$ simplified model, the choice of right-handed sleptons in the decay chain ensures high lepton multiplicities in the final state while suppressing the leptonic branching fraction of any associated chargino, thus enhancing the rate of four-lepton events with respect to events with lower lepton multiplicities.

C. Simplified model of same-sign chargino-pair production via vector-boson fusion

A simplified model for $\tilde{\chi}_1^\pm\tilde{\chi}_1^\pm$ production via VBF [55,56] is also considered. As in the case of direct production, the $\tilde{\chi}_1^\pm$ is assumed to be pure wino, and mass degenerate with the $\tilde{\chi}_2^0$, and the $\tilde{\chi}_1^0$ is assumed to be pure bino. The $\tilde{\chi}_1^\pm$ decays with a branching fraction of 1/6 via $\tilde{e}_L$, $\tilde{\mu}_L$, $\tilde{\tau}_L$, $\tilde{\nu}_e$, $\tilde{\nu}_\mu$, or $\tilde{\nu}_\tau$ with masses $m_{\tilde{\nu}_\ell} = m_{\tilde{\ell}_L} = 0.5(m_{\tilde{\chi}_1^\pm} + m_{\tilde{\chi}_1^0})$. The diagram for $\tilde{\chi}_1^\pm\tilde{\chi}_1^\pm$ production via VBF, where the sparticles are produced along with two jets, is shown in Fig. 2(e). The jets are widely separated in pseudorapidity[1] η and have a relatively high dijet invariant mass m_{jj}. Because of the VBF topology, the charginos are often boosted in the transverse plane, forcing the decay products to be more collinear and energetic, even in highly compressed spectra. This feature of VBF production makes it a good candidate to probe compressed SUSY scenarios that are experimentally difficult to explore via the direct production modes. The signal cross sections are calculated to leading order (LO) in the strong coupling constant using MadGraph 5-1.3.33 [57] (more details on the cross-section calculation are given in the Appendix). The uncertainties on the signal cross sections are calculated by using different PDF sets (2%) and by varying the renormalization and factorization scales between 0.5 and 2 times the nominal values (6%) [58]. For a $\tilde{\chi}_1^\pm$ with mass of 120 GeV, the cross section for $\tilde{\chi}_1^\pm\tilde{\chi}_1^\pm$ production in association with two jets satisfying the criteria $m_{jj} > 350$ GeV and $|\Delta\eta_{jj}| > 1.6$ is 1.1 fb. For the assumed mixings in the chargino-neutralino sector, and the mass values considered in the analysis, the cross section for $\tilde{\chi}_1^\pm\tilde{\chi}_1^\pm$ VBF production is found to be independent of the $\tilde{\chi}_1^0$ mass.

[1]ATLAS uses a right-handed coordinate system with its origin at the nominal interaction point (IP) in the center of the detector and the z axis along the beam pipe. The x axis points from the IP to the center of the LHC ring, and the y axis points upward. Cylindrical coordinates (r, ϕ) are used in the transverse plane, ϕ being the azimuthal angle around the z axis. The pseudorapidity is defined in terms of the polar angle θ as $\eta = -\ln\tan(\theta/2)$.

D. Phenomenological minimal supersymmetric standard model

The analysis results are interpreted in a pMSSM scenario. The masses of the sfermions, the gluino, and the CP-odd Higgs boson are set to high values (2 TeV, 2 TeV, and 500 GeV, respectively), thus decoupling the production of these particles and allowing only the direct production of charginos and neutralinos decaying via SM gauge bosons and the lightest Higgs boson. The remaining four parameters, the ratio of the expectation values of the two Higgs doublets ($\tan\beta$), the gaugino mass parameters M_1 and M_2, and the higgsino mass parameter μ, determine the phenomenology of direct electroweak SUSY production. For the analysis presented here, μ and M_2 are treated as free parameters. The remaining parameters are fixed to $\tan\beta = 10$ and $M_1 = 50$ GeV, so that the relic dark-matter density is below the cosmological bound [29] across most of the μ-M_2 grid. The lightest Higgs boson has a mass close to 125 GeV, which is set by tuning the mixing in the top squark sector, and decays to SUSY as well as SM particles where kinematically allowed.

E. Two-parameter nonuniversal Higgs masses model

Radiatively driven natural SUSY [59] allows the Z and Higgs boson masses to be close to 100 GeV, with gluino and squark masses beyond the TeV scale. In the two-parameter NUHM model (NUHM2) that is considered in this article, the direct production of charginos and neutralinos is dominant in a large area of the parameter space considered. The mass hierarchy, composition, and production cross section of the SUSY particles are governed by the universal soft SUSY-breaking scalar mass m_0, the soft SUSY-breaking gaugino mass $m_{1/2}$, the trilinear SUSY-breaking parameter A_0, the pseudoscalar Higgs boson mass m_A, $\tan\beta$, and μ. Both μ and $m_{1/2}$ are treated as free parameters, and the other parameters are fixed to $m_0 = 5$ TeV, $A_0 = -1.6m_0$, $\tan\beta = 15$, $m_A = 1$ TeV, and $\mathrm{sign}(\mu) > 0$. These conditions ensure a low level of electroweak fine-tuning, while keeping the lightest Higgs boson mass close to 125 GeV and the squark masses to a few TeV. The gluino mass typically satisfies $m_{\tilde{g}} \simeq 2.5m_{1/2}$. For low gluino masses, the production of strongly interacting

SUSY particles dominates; as the gluino mass increases, the production of electroweakinos becomes more important. The charginos and neutralinos decay via W, Z, and Higgs bosons.

F. Gauge-mediated SUSY breaking model

Minimal GMSB models are described by six parameters: the SUSY-breaking mass scale in the low-energy sector (Λ), the messenger mass (M_{mess}), the number of SU(5) messenger fields (N_5), the scale factor for the gravitino mass (C_{grav}), $\tan\beta$, and μ. In the model presented here, Λ and $\tan\beta$ are treated as free parameters, and the remaining parameters are fixed to $M_{\mathrm{mess}} = 250$ TeV, $N_5 = 3$, $C_{\mathrm{grav}} = 1$, and $\mathrm{sign}(\mu) > 0$. For high Λ values, the EW production of SUSY particles dominates over other SUSY processes. In most of the relevant parameter space, the NLSP is the $\tilde{\tau}$ for large values of $\tan\beta$ ($\tan\beta > 20$), and the final states contain two, three, or four tau leptons. In the region where the mass difference between the stau and selectron/smuon is smaller than the sum of the tau and the electron/muon masses, the stau, selectron, and smuon decay directly into the LSP and a lepton, defining the phenomenology. The charginos and neutralinos decay as $\tilde{\chi}_1^{\pm} \to W^{\pm}\tilde{\chi}_1^0$ and $\tilde{\chi}_2^0 \to Z\tilde{\chi}_1^0$, where the $\tilde{\chi}_1^0$ decays as $\tilde{\chi}_1^0 \to \ell^{\pm}\tilde{\ell}^{\mp} \to \ell^+\ell^-\tilde{G}$ and the LSP is the gravitino $\tilde{G}$.

III. THE ATLAS DETECTOR

The ATLAS detector [60] is a multipurpose particle physics detector with forward-backward symmetric cylindrical geometry. The inner tracking detector (ID) covers $|\eta| < 2.5$ and consists of a silicon pixel detector, a semiconductor microstrip detector, and a transition radiation tracker. The ID is surrounded by a thin superconducting solenoid providing a 2 T axial magnetic field. A high-granularity lead/liquid-argon sampling calorimeter measures the energy and the position of electromagnetic showers within $|\eta| < 3.2$. Sampling calorimeters with liquid argon as the active medium are also used to measure hadronic showers in the end cap ($1.5 < |\eta| < 3.2$) and forward ($3.1 < |\eta| < 4.9$) regions, while a steel/scintillator tile calorimeter measures hadronic showers in the central region ($|\eta| < 1.7$). The muon spectrometer (MS) surrounds the calorimeters and consists of three large superconducting air-core toroid magnets, each with eight coils, a system of precision tracking chambers ($|\eta| < 2.7$), and fast trigger chambers ($|\eta| < 2.4$). A three-level trigger system [61] selects events to be recorded for off-line analysis.

IV. MONTE CARLO SIMULATION

Monte Carlo generators are used to simulate SM processes and new physics signals. The SM processes considered are those that can lead to leptonic signatures. Details of the signal and background MC simulation samples used in this article, as well as the order of cross-section calculations in perturbative QCD used for yield normalization, are shown in Table I.

For all MC simulation samples, the propagation of particles through the ATLAS detector is modeled with Geant 4 [96] using the full ATLAS detector simulation [97], or a fast simulation using a parametric response of the electromagnetic and hadronic calorimeters [98] and Geant 4 elsewhere. The effect of multiple proton-proton collisions in the same or nearby beam bunch crossings (in-time and out-of-time pileup) is incorporated into the simulation by overlaying additional minimum-bias events generated with Pythia -8 onto hard-scatter events. Simulated events are weighted to match the distribution of the mean number of interactions per bunch crossing in data and are reconstructed in the same manner as data. The simulated MC samples are corrected to account for differences with respect to the data in the heavy-flavor quark jet selection efficiencies and misidentification probabilities, lepton efficiencies, tau misidentification probabilities, as well as the energy and momentum measurements of leptons and jets. The $\tilde{\chi}_1^+\tilde{\chi}_1^-$ ($\tilde{\chi}_1^{\pm}\tilde{\chi}_2^0$) signal samples simulated with Herwig++ are reweighted to match the $\tilde{\chi}_1^+\tilde{\chi}_1^-$ ($\tilde{\chi}_1^{\pm}\tilde{\chi}_2^0$) system transverse momentum distribution obtained from the MadGraph samples that are generated with an additional parton in the matrix element to give a better description of the ISR.

V. EVENT RECONSTRUCTION

Events recorded during stable data-taking conditions are analyzed if the reconstructed primary vertex has five or more tracks with transverse momentum $p_{\mathrm{T}} > 400$ GeV associated with it. The primary vertex of an event is identified as the vertex with the highest $\Sigma {p_{\mathrm{T}}}^2$ of associated tracks. After the application of beam, detector, and data-quality requirements, the total luminosity considered in these analyses corresponds to 20.3 fb^{-1} (20.1 fb^{-1} for the direct stau production analysis due to a different trigger requirement).

Electron candidates are required to have $|\eta| < 2.47$ and $p_{\mathrm{T}} > 7$ GeV, where the p_{T} and η are determined from the calibrated clustered energy deposits in the electromagnetic calorimeter and the matched ID track, respectively. Electrons must satisfy "medium" identification criteria, following Ref. [99]. Muon candidates are reconstructed by combining tracks in the ID and tracks in the MS [100], and are required to have $|\eta| < 2.5$ and $p_{\mathrm{T}} > 5$ GeV. Events containing one or more muons that have transverse impact parameter with respect to the primary vertex $|d_0| > 0.2$ mm or longitudinal impact parameter with respect to the primary vertex $|z_0| > 1$ mm are rejected to suppress cosmic-ray muon background. In the direct stau production analysis, and the two-lepton compressed spectra analyses, electrons and muons are required to have $p_{\mathrm{T}} > 10$ GeV.

Jets are reconstructed with the anti-k_t algorithm [101] with a radius parameter of $R = 0.4$. Three-dimensional

TABLE I. The MC simulation samples used in this article for background and signal estimates. Shown are the generator type, the order of cross-section calculations used for yield normalization, the names of the sets of tunable parameters (tunes) used for the underlying-event generation, and the PDF sets.

Process	Generator + fragmentation/hadronization	Cross section	Tune	PDF set
Diboson (VV)				
W^+W^-, WZ, ZZ	Powheg Box-r2129 [62,63] + Pythia-8.165 [64] (or + Pythia-6.426)	NLO QCD with MCFM-6.2 [65,66]	AU2 [67]	CT10 [68]
$W^\pm W^\pm$	Sherpa-1.4.0 [69]	NLO	(Sherpa internal)	CT10
$W^\pm W^\pm$ via vector-boson fusion	Sherpa-1.4.0	NLO	(Sherpa internal)	CT10
ZZ, W^+W^- via gluon fusion (*not incl. in)* powheg box)	gg2VV [70] + Herwig-6.520	NLO	AUET2B [71]	CT10
$W\gamma$, $Z\gamma$	Sherpa-1.4.1	NLO	(Sherpa internal)	CT10
Triboson (VVV)				
WWW, ZWW	MadGraph5-1.3.33 + Pythia-6.426	NLO [72]	AUET2B	CTEQ6L1 [73]
Higgs				
Via gluon fusion	PowhegBox-r2092 + Pythia-8.165	NNLO + NNLL QCD, NLO EW [74]	AU2	CT10
Via vector-boson fusion	Powheg Box-r2092 + Pythia-8.165	NNLO QCD, NLO EW [74]	AU2	CT10
Associated W/Z production	Pythia-8.165	NNLO QCD, NLO EW [74]	AU2	CTEQ6L1
Associated $t\bar{t}$-production	Pythia-8.165	NNLO QCD [74]	AU2	CTEQ6L1
Top + Boson $t\bar{t}V$				
$t\bar{t}W$, $t\bar{t}Z$	Alpgen-2.14 [75] Herwig-6.520	NLO [76,77]	AUET2B	CTEQ6L1
$t\bar{t}WW$	MadGraph 5-1.3.33 + Pythia-6.426	NLO [77]	AUET2B	CTEQ6L1
$\mathbf{t\bar{t}}$	Powheg Box-r2129 + Pythia-6.426	NNLO + NNLL [78–83]	Perugia2011C [84]	CT10
Single top				
t-channel	AcerMC-38 [85] + Pythia-6.426	NNLO + NNLL [86]	AUET2B	CTEQ6L1
s-channel, Wt	MC@NLO-4.06 [87,88] + Herwig-6.520	NNLO + NNLL [89,90]	AUET2B	CT10
tZ	MadGraph 5-1.5.11 + Pythia-6.426	NLO [91]	AUET2B	CTEQ6L1
W + jets, Z + jets	Alpgen-2.14 + Pythia-6.426 (or + Herwig-6.520) or Sherpa-1.4.0	NNLO QCD using DYNNLO-1.1 [92] with MSTW2008 NNLO [93] NNLO QCD using DYNNLO-1.1 with MSTW2008 NNLO	Perugia 2011C	CTEQ6L1 CT10
Low-mass resonances				
J/Ψ, Υ	Pythia -8.165	NLO	AU2	CTEQ6L1
SUSY signal				
$\tilde{\tau}\tilde{\tau}$, $\tilde{\chi}_1^+\tilde{\chi}_1^-$, $\tilde{\chi}_1^\pm\tilde{\chi}_2^0$ simplified models	Herwig + + -2.5.2 [94]	NLO using Prospino2 [50]	UE-EE-3 [95]	CTEQ6L1
$\tilde{\chi}_2^0\tilde{\chi}_3^0$ simplified models	MadGraph 5-1.5.12 + Pythia-6.426	NLO using Prospino2	AUET2B	CTEQ6L1
VBF $\tilde{\chi}_1^+\tilde{\chi}_1^-$ simplified models	MadGraph 5_aMC@NLO-2.1.1 + Pythia -6.426	LO using MadGraph 5-1.3.33 [57]	AUET2B	CTEQ6L1
NUHM2, GMSB	Herwig + + -2.5.2	NLO using Prospino2	UE-EE-3	CTEQ6L1

calorimeter energy clusters are used as input to the jet reconstruction. The clusters are calibrated using the local hadronic calibration [102], which gives different weights to the energy deposits from the electromagnetic and hadronic components of the showers. The final jet energy calibration corrects the calorimeter response to the particle-level jet energy [102,103], where correction factors are obtained from simulation and then refined and validated using data. Corrections for in-time and out-of-time pileup are also applied based on the jet area method [102]. Central jets must have $|\eta| < 2.4$ and $p_{\mathrm{T}} > 20$ GeV, and a "jet vertex fraction" (JVF) [102] larger than 0.5 if $p_{\mathrm{T}} < 50$ GeV. The JVF is the p_{T}-weighted fraction of the tracks in the jet that are associated with the primary vertex. Requiring large JVF values suppresses jets from pileup. Forward jets are those with $2.4 < |\eta| < 4.5$ and $p_{\mathrm{T}} > 30$ GeV. Events containing jets failing to satisfy the quality criteria described in Ref. [102] are rejected to suppress events with large calorimeter noise and noncollision backgrounds.

Central jets are identified as containing b-hadrons (referred to as b-tagged) using a multivariate technique based on quantities related to reconstructed secondary vertices. The chosen working point of the b-tagging algorithm [104] correctly identifies b-hadrons in simulated $t\bar{t}$ samples with an efficiency of 80%, with a light-flavor jet misidentification probability of about 4% and a c-jet misidentification probability of about 30%.

Hadronically decaying τ leptons (τ_{had}) are reconstructed using jets described above with $|\eta| < 2.47$ and a lower p_{T} threshold of 10 GeV. The τ_{had} reconstruction algorithm uses information about the tracks within $\Delta R \equiv \sqrt{(\Delta\phi)^2 + (\Delta\eta)^2} = 0.2$ of the seed jet, in addition to the electromagnetic and hadronic shower shapes in the calorimeters. The τ_{had} candidates are required to have one or three associated tracks (prongs), as τ leptons predominantly decay to either one or three charged pions together with a neutrino and often additional neutral pions. The τ_{had} candidates are required to have $p_{\mathrm{T}} > 20$ GeV and unit total charge of their constituent tracks. A boosted decision tree algorithm (BDT) uses discriminating track and cluster variables to optimize τ_{had} identification, where "loose," "medium," and "tight" working points are defined [105]. Electrons misidentified as τ_{had} candidates are vetoed using transition radiation and calorimeter information. The τ_{had} candidates are corrected to the τ energy scale [105] using an η- and p_{T}-dependent calibration. Kinematic variables built using taus in this article use only the visible decay products from the hadronically decaying tau.

The missing transverse momentum is the negative vector sum of the transverse momenta of all muons with $p_{\mathrm{T}} > 10$ GeV, electrons with $p_{\mathrm{T}} > 10$ GeV, photons with $p_{\mathrm{T}} > 10$ GeV [99], jets with $p_{\mathrm{T}} > 20$ GeV, and calibrated calorimeter energy clusters with $|\eta| < 4.9$ not associated with these objects. Hadronically decaying τ leptons are included in the $E_{\mathrm{T}}^{\mathrm{miss}}$ calculation as jets. Clusters associated with electrons, photons, and jets are calibrated to the scale of the corresponding objects. Calorimeter energy clusters not associated with these objects are calibrated using both calorimeter and tracker information [106]. For jets, the calibration includes the pileup correction described above, while the JVF requirement is not considered when selecting jet candidates.

To avoid potential ambiguities among objects, "tagged" leptons are candidate leptons separated from each other and from jets in the following order:

(1) If two electron candidates are reconstructed with $\Delta R < 0.1$, the lower energy candidate is discarded.
(2) Jets within $\Delta R = 0.2$ of an electron candidate, and τ_{had} candidates within $\Delta R = 0.2$ of an electron or muon, are discarded.
(3) Electron and muon candidates are discarded if found within $\Delta R = 0.4$ of a remaining jet to suppress leptons from semileptonic decays of c- and b-hadrons.
(4) To reject bremsstrahlung from muons, $e\mu$ ($\mu\mu$) pairs are discarded if the two leptons are within $\Delta R = 0.01$ (0.05) of one another.
(5) Jets found within $\Delta R = 0.2$ of a "signal" τ lepton (see below) are discarded.

Finally, to suppress low-mass decays, if tagged electrons and muons form a same-flavor opposite-sign (SFOS) pair with $m_{\mathrm{SFOS}} < 2$ GeV, both leptons in the pair are discarded.

Tagged leptons satisfying additional identification criteria are called signal leptons. To maximize the search sensitivity, some analyses presented in this article require different additional criteria for signal leptons, and these are highlighted where necessary. Signal τ leptons must satisfy medium identification criteria [105], while for the final signal-region selections, both the medium and tight criteria are used. Unless stated otherwise, signal electrons (muons) are tagged electrons (muons) for which the scalar sum of the transverse momenta of tracks within a cone of $\Delta R = 0.3$ around the lepton candidate is less than 16% (12%) of the lepton p_{T}. Tracks used for the electron (muon) isolation requirement defined above are those that have $p_{\mathrm{T}} > 0.4$ (1.0) GeV and $|z_0| < 2$ mm with respect to the primary vertex of the event. Tracks of the leptons themselves as well as tracks closer in z_0 to another vertex (that is not the primary vertex) are not included. The isolation requirements are imposed to reduce the contributions from semileptonic decays of hadrons and jets misidentified as leptons. Signal electrons must also satisfy tight identification criteria [99], and the sum of the extra transverse energy deposits in the calorimeter (corrected for pileup effects) within a cone of $\Delta R = 0.3$ around the electron candidate must be less than 18% of the electron p_{T}. To further suppress electrons and muons originating from secondary vertices, the d_0 normalized to its uncertainty is required to be small, with $|d_0|/\sigma(d_0) < 5(3)$, and $|z_0 \sin\theta| < 0.4$ mm (1 mm) for electrons (muons).

TABLE II. The triggers used in the analyses and the off-line p_T threshold used, ensuring that the lepton(s) or E_T^{miss} triggering the event are in the plateau region of the trigger efficiency. Where multiple triggers are listed for an analysis, events are used if any of the triggers is passed. Muons are triggered within a restricted range of $|\eta| < 2.4$.

Trigger	p_T threshold [GeV]	Analysis
Single τ	150	Direct stau production
Double τ	40,25	
Single isolated e	25	Compressed spectra $\ell^+\ell^-$, 3ℓ
Single isolated μ	25	
Double e	14,14 25,10	Compressed spectra $\ell^+\ell^-$, $\ell^\pm\ell^\pm$, 3ℓ
Double μ	14,14 18,10	Compressed spectra $\ell^+\ell^-$, $\ell^\pm\ell^\pm$, 3ℓ
Triple e	20,9,9	Compressed spectra 3ℓ
Triple μ	7,7,7 19,5,5	Compressed spectra 3ℓ
Combined $e\mu$	$14(e)$,$10(\mu)$ $18(\mu)$,$10(e)$ $9(e)$, $9(e)$, $7(\mu)$ $9(e)$, $7(\mu)$, $7(\mu)$	Compressed spectra 3ℓ
E_T^{miss}	120	Chargino production via VBF

Events must satisfy the relevant trigger for the analysis and satisfy the corresponding p_T-threshold requirements shown in Table II.

VI. GENERAL ANALYSIS STRATEGY

The broad range of EW SUSY scenarios considered by the ATLAS experiment is accompanied by a large number of experimental signatures: from the two-tau signature from direct stau production to three-lepton signatures from $\tilde{\chi}_1^\pm\tilde{\chi}_2^0$ production. As much as possible the individual analyses follow a common approach. Signal regions (SR) are defined to target one or more EW SUSY scenarios, using kinematic variables with good signal-background separation, as described in Sec. VI A. The optimization of key selection variables is performed by maximizing the expected sensitivity to the signal model. A common background estimation strategy is used for the analyses in this article: the main SM backgrounds are estimated by normalizing MC simulation samples to data in dedicated control regions (CRs); backgrounds due to nonprompt and fake leptons are derived from data as outlined in Sec. VI B, while small backgrounds are estimated purely using MC simulation samples. The HistFitter [107] software framework is used in all analyses for constraining the background normalizations and the statistical interpretation of the results.

The CRs are defined with kinematic properties similar to the SRs, yet are disjoint from the SR, and have high purity for the background process under consideration. The CRs are designed in a way that minimizes the contamination from the signal model, and cross contamination between multiple CRs is taken into account in the normalization to data. To validate the modeling of the SM backgrounds, the yields and shapes of key kinematic variables are compared to data in validation regions (VR). The VRs are defined to be close to, yet disjoint from the SR and CR, and be dominated by the background process under consideration. The VRs are designed such that the contamination from the signal model is low. Three different fit configurations are used. The "background-only fit" is used for estimating the expected background in the SRs and VRs using observations in the CRs, with no assumptions made on any signal model. In the absence of an observed excess of events in one or more signal regions, the "model-dependent signal fit" is used to set exclusion limits in a particular model, where the signal contribution from the particular model that is being tested is taken into account in all CR and SR. Finally, in the "model-independent signal fit," both the CRs and SRs are used in the same manner as for the model-dependent signal fit, but signal contamination is not accounted for in the CRs. A likelihood function is built as the product of Poisson probability functions, describing the observed and expected number of events in the CRs and SRs. The observed number of events in various CRs and SRs are used in a combined profile likelihood fit to determine the expected SM background yields in each of the SRs. The systematic uncertainties on the expected background yields described in Sec. VI C are included as nuisance parameters, constrained to be Gaussian with a width determined by the size of the uncertainty. Correlations between control and signal regions, and background processes, are taken into account with common nuisance parameters. The free parameters and the nuisance parameters are determined by maximizing the product of the Poisson probability functions and the Gaussian constraints on the nuisance parameters.

After the background modeling is understood and validated, the predicted background in the SR is compared to the observed data. In order to quantify the probability for the background-only hypothesis to fluctuate to the observed number of events or higher, the one-sided p_0-value is calculated. For this calculation, the profile likelihood ratio is used as a test statistic to exclude the signal-plus-background hypothesis if no significant excess is observed. A signal model can be excluded at 95% CL if the CL_s [108] of the signal plus background hypothesis is < 0.05. For each signal region, the expected and observed upper limits at 95% CL on the number of beyond-the-SM

events ($S^{95}_{\rm exp}$ and $S^{95}_{\rm obs}$) are calculated using the model-independent signal fit. The 95% CL upper limits on the signal cross section times efficiency ($\langle\epsilon\sigma\rangle^{95}_{\rm obs}$) and the CL_b value for the background-only hypothesis are also calculated for each analysis in this article.

A. Event variables

A large set of discriminating variables is used in the analysis strategies presented here. The following kinematic variables are defined and their use in the various analyses is detailed in Secs. VII–IX:

$p_{\rm T}^X$ The transverse momentum of a reconstructed object X.

$\Delta\phi(X,Y)$, $\Delta\eta(X,Y)$ The separation in ϕ or η between two reconstructed objects X and Y, e.g. $\Delta\phi(E_{\rm T}^{\rm miss},\ell)$.

$|\Delta\eta_{jj}|$ The separation in η between the leading two jets.

$E_{\rm T}^{\rm miss}$ The magnitude of the missing transverse momentum in the event.

$E_{\rm T}^{\rm miss,rel}$ The quantity $E_{\rm T}^{\rm miss,rel}$ is defined as

$$E_{\rm T}^{\rm miss,rel} = \begin{cases} E_{\rm T}^{\rm miss} & \text{if } \Delta\phi(E_{\rm T}^{\rm miss},\ell/j) \geq \pi/2 \\ E_{\rm T}^{\rm miss} \times \sin\Delta\phi(E_{\rm T}^{\rm miss},\ell/j) & \text{if } \Delta\phi(E_{\rm T}^{\rm miss},\ell/j) < \pi/2 \end{cases}, \tag{1}$$

where $\Delta\phi(E_{\rm T}^{\rm miss},\ell/j)$ is the azimuthal angle between the direction of $E_{\rm T}^{\rm miss}$ and that of the nearest electron, muon, or central jet.

$p_{\rm T}^{\ell\ell}$ The transverse momentum of the two-lepton system.

$H_{\rm T}$ The scalar sum of the transverse momenta of the leptons and jets in the event.

$m_{\rm T}$ The transverse mass formed using the $E_{\rm T}^{\rm miss}$ and the leading lepton or tau in the event

$$m_{\rm T}(\vec{p}_{\rm T}^{\,\ell/\tau}, E_{\rm T}^{\rm miss}) = \sqrt{2{p_{\rm T}}^{\ell/\tau}E_{\rm T}^{\rm miss} - 2\vec{p}_{\rm T}^{\,\ell/\tau}\cdot E_{\rm T}^{\rm miss}}. \tag{2}$$

In the three-lepton analysis, the lepton not forming the SFOS lepton pair with mass closest to the Z boson mass is used. In cases where the second lepton or tau is used, the variable is labeled as $m_{\rm T}^X$, where X is the object used with the $E_{\rm T}^{\rm miss}$ to form the transverse mass.

$m_{\rm SFOS}$ The invariant mass of the SFOS lepton pair in the event. In the three-lepton analysis, the SFOS pair with mass closest to the Z boson mass is used.

$m_{\rm SFOS}^{\rm min}$ The lowest $m_{\rm SFOS}$ value among the possible SFOS combinations.

$m_{\ell\ell\ell}$ The three-lepton invariant mass.

$m_{\tau\tau}$ The two-tau invariant mass.

$m_{\rm T2}$ The "stransverse mass" is calculated as

$$m_{\rm T2} = \min_{\vec{q}_{\rm T}}[\max(m_{\rm T}({\vec{p}_{\rm T}}^{\ell 1/\tau 1}, \vec{q}_{\rm T}), m_{\rm T}({\vec{p}_{\rm T}}^{\ell 2/\tau 2}, E_{\rm T}^{\rm miss} - \vec{q}_{\rm T}))], \tag{3}$$

where $\ell 1/\tau 1$ and $\ell 2/\tau 2$ denote the highest- and second-highest-$p_{\rm T}$ leptons or taus in the event, respectively, and $\vec{q}_{\rm T}$ is a test transverse vector that minimizes the larger of the two transverse masses

m_{T}. The m_{T2} distribution has a kinematic end point for events where two massive pair-produced particles each decay to two particles, one of which is detected and the other escapes undetected [109,110].

m_{eff} The scalar sum of the transverse momenta of the signal leptons, taus, jets, and $E_{\mathrm{T}}^{\mathrm{miss}}$ in the event

$$m_{\mathrm{eff}} = E_{\mathrm{T}}^{\mathrm{miss}} + \Sigma p_{\mathrm{T}}{}^{\mathrm{leptons}} + \Sigma p_{\mathrm{T}}{}^{\mathrm{taus}} + \Sigma p_{\mathrm{T}}{}^{\mathrm{jets}}. \tag{4}$$

In the case of the two-tau analysis, only the sum of the $E_{\mathrm{T}}^{\mathrm{miss}}$ and two taus is used.

R_2 The quantity R_2 is defined as

$$R_2 = \frac{E_{\mathrm{T}}^{\mathrm{miss}}}{E_{\mathrm{T}}^{\mathrm{miss}} + p_{\mathrm{T}}{}^{\ell 1} + p_{\mathrm{T}}{}^{\ell 2}}. \tag{5}$$

The R_2 distribution is shifted toward unity for signal events compared to the background, due to the existence of the LSPs that results in a larger $E_{\mathrm{T}}^{\mathrm{miss}}$.

M_{Δ}^{R}, $\Delta\phi_{R}^{\beta}$ The super-razor quantities M_{Δ}^{R} and $\Delta\phi_{R}^{\beta}$ are defined in Ref. [111]. These variables are motivated by the generic process of the pair production of two massive particles, each decaying into a set of visible and invisible particles (i.e. $\tilde{\chi}_1^{\pm} \to \ell\nu_{\ell}\tilde{\chi}_1^0$). Similar to m_{T2}, M_{Δ}^{R} is sensitive to the squared mass difference of the pair-produced massive particle and the invisible particle, via a kinematic end point. These two variables are expected to provide a similar performance for discriminating the signal from the background. For systems where the invisible particle has a mass that is comparable to the pair-produced massive particle (i.e. compressed spectra), the variable $\Delta\phi_{R}^{\beta}$ has a pronounced peak near π. The effect is magnified as the spectrum becomes more and more compressed, making this variable a good discriminator for compressed spectra searches.

B. Common reducible background estimation

Electron and muon candidates can be classified into three main types, depending on their origin: "real" leptons are prompt and isolated leptons from a W or Z boson, a prompt tau, or a SUSY particle decay; "fake" leptons can originate from a misidentified light-flavor quark or gluon jet (referred to as "light flavor"); "nonprompt" leptons can originate from a semileptonic decay of a heavy-flavor quark, from the decay of a meson, or from an electron from a photon conversion. The background due to nonprompt and fake electrons and muons, collectively referred to as "reducible," is commonly estimated using the matrix method described in Ref. [112]. The matrix method extracts the number of events with one or two fake or nonprompt leptons from a system of linear equations relating the number of events with two signal or tagged leptons (before signal lepton identification requirements are applied) to the number of events with two candidates that are either real, fake, or nonprompt. The coefficients of the linear equations are functions of the real-lepton identification efficiencies and of the fake and nonprompt lepton misidentification probabilities, both defined as a fraction of the corresponding tagged leptons satisfying the signal lepton requirements.

The real-lepton identification efficiencies are obtained from MC simulation samples in the region under consideration to account for detailed kinematic dependencies and are multiplied by correction factors to account for residual differences with respect to the data. The correction factors are obtained from a control region rich in $Z \to e^+e^-$ and $Z \to \mu^+\mu^-$ decays. The fake and nonprompt lepton misidentification probabilities are calculated as the weighted averages of the corrected type- and process-dependent misidentification probabilities defined below according to their relative contributions in a given signal or validation region. The type- and process-dependent misidentification probabilities for each relevant fake and nonprompt lepton type (heavy-flavor, light-flavor, or conversion) and for each reducible background process are corrected using the ratio ("correction factor") of the misidentification probability in data to that in simulation obtained from dedicated control samples. The correction factors are assumed to be independent of the selected regions and of any potential composition or kinematic differences. For nonprompt electrons and muons from heavy-flavor quark decays, the correction factor is measured in a $b\bar{b}$-dominated control sample. The correction factor for the conversion candidates is determined in events with a converted photon radiated from a muon in $Z \to \mu\mu$ decays.

C. Common systematic uncertainties

Several sources of systematic uncertainty are considered for the SM background estimates and signal yield predictions. When the MC simulation samples are normalized to data yields in the CR, there is a partial cancellation of both the experimental and theoretical modeling systematic uncertainties.

The experimental systematic uncertainties affecting the simulation-based estimates include the following: the uncertainties due to the jet energy scale and resolution [100,102]; the uncertainties due to the lepton energy scale, energy resolution, and identification efficiency [99,100,105]; the uncertainty due to the hadronic tau misidentification probability [105]; the uncertainty on the $E_{\mathrm{T}}^{\mathrm{miss}}$ from energy deposits not associated with reconstructed objects ($E_{\mathrm{T}}^{\mathrm{miss}}$ soft-term resolution) [106]; and the uncertainties due to b-tagging efficiency and mistag probability [104]. The uncertainty on the integrated luminosity is $\pm 2.8\%$ and is derived following the same methodology as that detailed in Ref. [113]. The uncertainty due to the modeling of the pileup in the MC simulation samples is estimated by varying the distribution of the number of interactions per bunch crossing overlaid in the MC samples by $\pm 10\%$. An uncertainty is applied to MC samples to cover differences in efficiency observed between the trigger in data and the MC trigger simulation.

The systematic uncertainties due to the limitations in theoretical models or calculations affecting the simulation-based background estimates include the cross-section uncertainties that are estimated by varying the renormalization and factorization scales and the PDFs, and the acceptance uncertainties due to PDFs and the choice of MC generator and parton shower. The cross-section uncertainties for the irreducible backgrounds used here are 30% for $t\bar{t}V$ [76,77], 50% for tZ, 5% for ZZ, 7% for WZ, and 100% for the triboson samples. For the Higgs boson samples, a 20% uncertainty is used for VH and VBF production, while a 100% uncertainty is assigned to $t\bar{t}H$ and Higgs boson production via gluon fusion [74]. For the $\tilde{\chi}_1^+\tilde{\chi}_1^-$ and $\tilde{\chi}_1^\pm\tilde{\chi}_2^0$ signal simulations that are sensitive to ISR, the impact of the choice of renormalization scales, factorization scales, the scale for the first emission in the so-called MLM matching scheme [114], and MLM matching scale are evaluated by varying these individually between 0.5 and 2 times the nominal values in MadGraph.

VII. DIRECT STAU PRODUCTION

This section presents a search for direct stau-pair production with subsequent decay into final states with two taus and $E_{\mathrm{T}}^{\mathrm{miss}}$. The search for direct stau production is very challenging, as the final state is difficult to trigger on and to separate from the SM background. In Ref. [22], the best observed upper limit on the direct stau production cross section was found for a stau mass of 80 GeV and a massless $\tilde{\chi}_1^0$, where the theoretical cross section at NLO is 0.07 (0.17) pb for right-handed (left-handed) stau-pair production and the excluded cross section is 0.22 (0.28) pb. This analysis is an update of Ref. [22], using a multivariate analysis technique instead of a simple cut-based method to improve the sensitivity to direct stau-pair production.

A. Event selection

Events are selected using the basic reconstruction, object, and event selection criteria described in Sec. V. In addition, if taus form an SFOS pair with $m_{\mathrm{SFOS}} < 12$ GeV, the event is rejected. Events with exactly two hadronically decaying tau candidates are selected, where the two tau candidates are required to have opposite-sign (OS) charge. At least one tau must satisfy the tight tau identification BDT requirement, and events with additional tagged light leptons are vetoed. Events must satisfy either the single-tau or ditau trigger criteria, as described in Sec. V.

To suppress events from Z boson decays, events are rejected if the invariant mass of the tau pair lies within ± 10 GeV of the peak value of 81 GeV for Z boson candidates.[2] To suppress background from events containing a top quark, events with b-tagged jets are vetoed. To further select SUSY events from direct stau production and suppress WW and $t\bar{t}$ production, m_{T2} is calculated using the two taus and the $E_{\mathrm{T}}^{\mathrm{miss}}$ in the event. The additional requirement of $m_{\mathrm{T2}} > 30$ GeV is applied to select events for the training and optimization of the multivariate analysis (MVA).

After applying the preselection listed above, both the signal and background MC samples are split in two. Half is used for the BDT training and the other half for testing. Twelve variables with good discriminatory power are considered as input for the BDT training procedure: $E_{\mathrm{T}}^{\mathrm{miss}}$, m_{eff}, m_{T2}, $m_{\tau\tau}$, $\Delta\phi(\tau,\tau)$, $\Delta\eta(\tau,\tau)$, $p_{\mathrm{T}}^{\tau 1}$, $p_{\mathrm{T}}^{\tau 2}$, $m_{\mathrm{T}\tau 1}$, $m_{\mathrm{T}\tau 2}$, $\Delta\phi(E_{\mathrm{T}}^{\mathrm{miss}},\tau 1)$, and $\Delta\phi(E_{\mathrm{T}}^{\mathrm{miss}},\tau 2)$. The MC simulation samples are compared to data for these variables and their correlations to ensure that they are modeled well.

A direct stau production scenario with $m(\tilde{\tau}_R,\tilde{\chi}_1^0) = (109, 0)$ GeV is used for the training and optimization of the BDT, and the BDT response requirement (t_{cut}) is chosen based on the best expected sensitivity for discovery. The two-tau MVA SR definition is shown in Table III.

B. Background determination

The main SM backgrounds in the two-tau MVA SR are $W+$jets and diboson production. Contributions from diboson, $t\bar{t}$, and $Z+$jets processes are estimated using MC simulation samples and validated using data in WW-rich, $t\bar{t}$-rich, or Z-rich validation regions, as defined in Ref. [22].

[2]The Z boson mass in ditau decays is reconstructed lower than the Z boson mass value due to the neutrinos from the tau decay.

TABLE III. Two-tau MVA signal region and validation region definitions for the direct stau-pair production analysis, where t_{cut} is the BDT response requirement.

	Common				
	Exactly 2 medium OS taus ≥1 tight tau tagged ℓ veto b-jet veto Z-veto				
	Signal region SR	Multijet VR1	Multijet VR2	W-VR1	W-VR2
m_{T2}	>30 GeV	30–50 GeV	50–80 GeV	>30 GeV	>30 GeV
$E_{\mathrm{T}}^{\mathrm{miss}}$	...	...	...	>100 GeV	>90 GeV
t_{cut}	>0.07	<0.07	<0.07	$-0.2-0.07$	$-0.2-0.07$

The $W+$jets contribution in the signal region is dominated by events where the W decays to a tau lepton and a jet is misidentified as another tau. The contribution is estimated by normalizing the yields from MC simulation samples to data in a dedicated control region. The $W+$jets control region selects events with the W boson decaying to a muon and neutrino to suppress the multijet background, which is larger for the electron channel. Events containing exactly one isolated muon and one tau satisfying the tight identification requirement are selected, where the muon and tau must have opposite electrical charge. To reduce the contribution from $Z+$jets production, $m_{\mathrm{T}}^{\tau}+m_{\mathrm{T}}^{\mu}>80$ GeV is required, and the reconstructed invariant mass of the muon and tau must be outside the Z mass window (12 GeV $< m_{\tau\mu} <$ 40 GeV or $m_{\tau\mu} >$ 100 GeV). To further suppress multijet and $Z+$jets processes, $E_{\mathrm{T}}^{\mathrm{miss}}>40$ GeV is required, and the muon and tau must not be back-to-back [$\Delta\phi(\tau,\mu)<2.7$ and $\Delta\eta(\tau,\mu)<2.0$]. The contribution from events with top quarks is suppressed by rejecting events containing b-tagged jets. The multijet background in the $W+$jets control region is estimated using a region with the same requirements, but with a same-sign muon and tau. The contribution from other SM processes is subtracted using MC simulation samples, and the ratio of opposite-sign muon and tau events to same-sign events is assumed to be unity for the multijet background.

The contribution from multijet events in the signal region, where both selected taus are misidentified jets, is small and is estimated using the so-called ABCD method. Four exclusive regions (A, B, C, D) are defined in a two-dimensional plane as a function of the two uncorrelated

TABLE IV. Numbers of events observed in data and expected from SM processes and the SUSY reference point $m(\tilde{\tau}_R,\tilde{\chi}_1^0)=(109,0)$ GeV in the two-tau MVA validation and signal regions. The uncertainties shown include both statistical and systematic components. The "top" contribution includes the single top, $t\bar{t}$, and $t\bar{t}V$ processes. The multijet background estimation is taken from data, as described in the text. In the VR, the multijet scale factor from fitting the background is not applied, while the $W+$jets scale factor is applied. In the SR, both the multijet and the $W+$jets scale factors are applied. Also shown are the model-independent limits calculated from the signal region observations: the one-sided p_0-value; the expected and observed upper limits at 95% CL on the number of beyond-the-SM events (S_{exp}^{95} and S_{obs}^{95}) for each signal region, calculated using pseudoexperiments and the CL_s prescription; the observed 95% CL upper limit on the signal cross section times efficiency ($\langle\epsilon\sigma\rangle_{\mathrm{obs}}^{95}$); and the CL_b value for the background-only hypothesis.

SM process	Multijet VR1	Multijet VR2	W-VR1	W-VR2	SR
Top	30 ± 9	19 ± 6	5.4 ± 2.6	8.1 ± 3.4	1.2 ± 0.9
$Z+$jets	590 ± 100	86 ± 21	2.3 ± 1.7	4.4 ± 2.5	0.9 ± 1.2
$W+$jets	570 ± 190	210 ± 70	20 ± 8	33 ± 13	7.3 ± 3.4
Diboson	29 ± 8	16 ± 5	4.7 ± 2.4	7.1 ± 3.1	4.4 ± 1.6
Multijet	19400 ± 1200	3840 ± 230	5.9 ± 2.7	17 ± 12	0.9 ± 2.6
SM total	20700 ± 1200	4170 ± 250	38 ± 9	70 ± 19	15 ± 5
Observed	21107	4002	33	65	15
$m(\tilde{\tau}_R,\tilde{\chi}_1^0)=(109,0)$ GeV	17 ± 7	13 ± 5	3.4 ± 2.2	5.6 ± 2.9	21 ± 5
p_0	...	...	...	...	0.48
S_{obs}^{95}	...	...	...	...	15.3
S_{exp}^{95}	...	...	...	...	$15.1^{+5.1}_{-3.5}$
$\langle\epsilon\sigma\rangle_{\mathrm{obs}}^{95}$ [fb]	...	...	...	...	0.76
CL_b	...	...	...	...	0.52

discriminating variables m_{T2} and the tau identification criterion. Regions A and B are required to have two medium taus where at least one meets the tight tau identification criteria, while regions C and D are required to have two loose taus that fail to satisfy the tight tau identification criteria. In regions A and C (B and D) $m_{T2} > 30$ GeV ($m_{T2} < 20$ GeV) is also required. The multijet background in signal region A can be estimated from $N_A = N_C \times N_B/N_D$, where N_A, N_B, N_C, and N_D are the numbers of events in regions A, B, C, and D, respectively. The assumption that the ratios N_A/N_C and N_B/N_D are the same is confirmed using MC simulation samples and in validation regions using data.

A simultaneous likelihood fit to the multijet estimation and $W+$jets CR is performed to normalize the corresponding background estimates and obtain the expected yields in the SR (as described in Sec. VI). After the simultaneous fit, the multijet and $W+$jets normalization factors are found to be $1.4^{+2.5}_{-1.4}$ and 0.98 ± 0.30, respectively. Because of the small number of events in some of the ABCD regions, the uncertainty on the multijet normalization factor is large; however, the multijet contribution to the total background is very small and the effect on the total signal region background uncertainty is small.

Two multijet validation regions are defined with the same selection as for the signal region, but with $t_{cut} < 0.07$ and intermediate m_{T2}. These multijet validation regions are enriched in events with jets misidentified as hadronic tau decays, and good agreement is seen between the data and expectation across the BDT input kinematic variables. A further two validation regions are defined to check the modeling of the $W+$jets background. The intermediate BDT region $-0.2 < t_{cut} < 0.07$ is used, with a high E_T^{miss} selection, where the $W+$jets background is seen to be

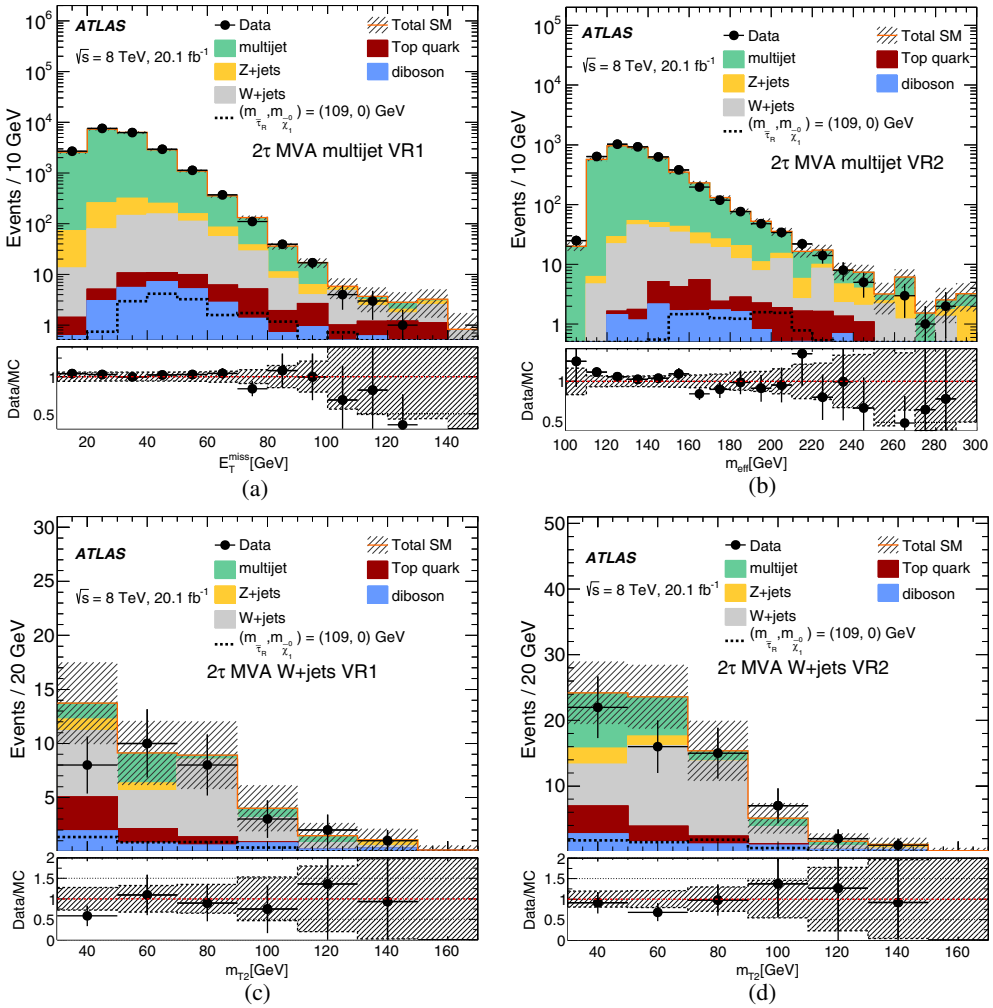

FIG. 3. Distributions in the two-tau MVA validation regions: (a) missing transverse momentum E_T^{miss} in multijet VR1, (b) effective mass m_{eff} in multijet VR2, (c) stransverse mass m_{T2} in W-VR1, and (d) m_{T2} in W-VR2. The lower panel of each plot shows the ratio of data to the SM background prediction. The last bin in each distribution includes the overflow. The uncertainty band includes both the statistical and systematic uncertainties on the SM prediction.

TABLE V. The relative systematic uncertainty (%) on the background estimate in the two-tau MVA SR from the leading sources. Uncertainties from different sources may be correlated and do not necessarily add in quadrature to the total uncertainty.

Systematic source	Uncertainty
Statistical uncertainty on MC samples	20%
$E_{\mathrm{T}}^{\mathrm{miss}}$ soft-term resolution	20%
Statistical uncertainty on the $W+$jets scale factor	15%
Tau misidentification probability	14%
$W+$jets theory and modeling	13%
Jet energy scale	11%
$E_{\mathrm{T}}^{\mathrm{miss}}$ soft-term scale	10%
Total	35%

modeled well. The validation region definitions are shown in Table III. Table IV and Figs. 3(a), 3(b), 3(c), and 3(d) show the agreement between data and expectation in the validation regions. The purity of the multijet and $W+$jets validation regions is ~90% and ~50%, respectively, while the signal contamination from the $m(\tilde{\tau}_R,\tilde{\chi}_1^0)=(109,0)$ GeV scenario is $<1\%$ and $<10\%$, respectively.

C. Results

The observed number of events in the signal region is shown in Table IV along with the background expectations, uncertainties, p_0-value, S_{exp}^{95}, S_{obs}^{95}, $\langle\epsilon\sigma\rangle_{\mathrm{obs}}^{95}$, and the CL_b value. The individual sources of uncertainty on the background estimation in the SR are shown in Table V, where the dominant sources are the statistical uncertainty on the MC simulation samples, the uncertainty on the $E_{\mathrm{T}}^{\mathrm{miss}}$ from energy deposits not associated with reconstructed objects, and the statistical uncertainty on the normalization factor applied to the $W+$jets background. Generator modeling uncertainties for the $W+$jets background are estimated by varying the renormalization and factorization scales individually between 0.5 and 2 times the nominal values in Alpgen. Additionally, the impact of the jet p_{T} threshold used for parton-jet matching in Alpgen $W+$jets simulation is assessed by changing the jet p_{T} threshold from 15 GeV to 25 GeV. Figures 4(a), 4(b), 4(c), and 4(d) show the distributions of the BDT response prior to the t_{cut} selection, and the $E_{\mathrm{T}}^{\mathrm{miss}}$, m_{eff}, and m_{T2} quantities in the SR, where good agreement between the expected background and the observed data is seen.

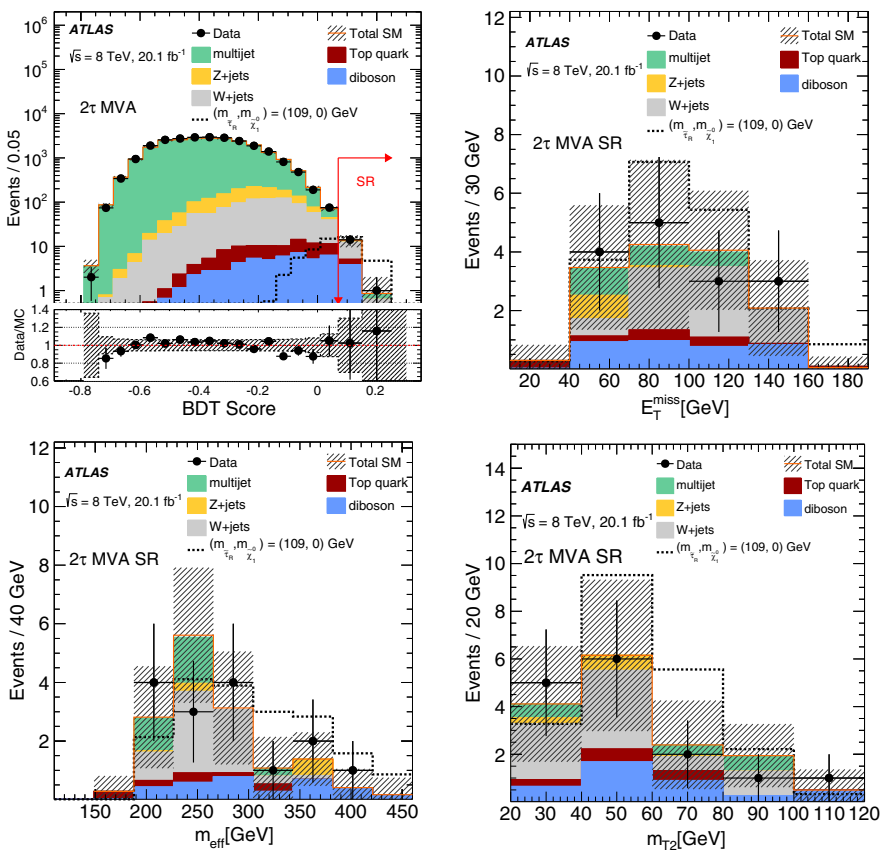

FIG. 4. The BDT response is shown in (a) prior to applying the SR t_{cut} requirement. Also shown are distributions in the two-tau MVA SR: (b) $E_{\mathrm{T}}^{\mathrm{miss}}$, (c) m_{eff}, and (d) m_{T2}. The lower panel in (a) shows the ratio of data to the SM background prediction. The uncertainty band includes both the statistical and systematic uncertainties on the SM prediction. The multijet and $W+$jets normalization factors from the background fits are applied in (b)–(d); only the $W+$jets normalization factor is applied in (a).

VIII. COMPRESSED SPECTRA IN DIRECT PRODUCTION OF $\tilde{\chi}_1^+\tilde{\chi}_1^-$ OR $\tilde{\chi}_1^+\tilde{\chi}_2^0$

In many SUSY scenarios, one or more of the mass differences between the charginos and neutralinos is small, resulting in final states with low-momentum leptons that require dedicated searches. The two-lepton analysis in Ref. [19] excluded $\tilde{\chi}_1^+\tilde{\chi}_1^-$ scenarios with $\tilde{\ell}_L$-mediated decays with $\tilde{\chi}_1^\pm$-$\tilde{\chi}_1^0$ mass splittings down to approximately 100 GeV, while the three-lepton analysis in Ref. [20] excluded $\tilde{\chi}_1^\pm\tilde{\chi}_2^0$ scenarios with $\tilde{\ell}_L$-mediated decays down to $\tilde{\chi}_2^0$-$\tilde{\chi}_1^0$ mass splittings of 20 GeV. The analyses presented in this section focus on event selections based on low-momentum leptons, and also on the production in association with ISR jets to provide improved sensitivity to the compressed spectra scenarios not covered by previous searches. As discussed in Sec. II, simplified models describing $\tilde{\chi}_1^+\tilde{\chi}_1^-$ and $\tilde{\chi}_1^\pm\tilde{\chi}_2^0$ production are considered for these compressed spectra searches, where the $\tilde{\chi}_1^\pm/\tilde{\chi}_2^0$ decay only through sleptons or sneutrinos. The compressed spectra searches are less sensitive to scenarios where the $\tilde{\chi}_1^\pm/\tilde{\chi}_2^0$ decay through SM W, Z, or Higgs bosons, as the branching fraction to leptonic final states is significantly suppressed. The experimental sensitivity to these scenarios is expected to be recovered with a larger data set.

A. Searches with two opposite-sign light leptons

Previous searches for direct $\tilde{\chi}_1^+\tilde{\chi}_1^-$ production using two opposite-sign light-lepton final states are extended here to increase the sensitivity to compressed SUSY scenarios. The opposite-sign, two-lepton analysis presented here probes $\tilde{\chi}_1^\pm$-$\tilde{\chi}_1^0$ mass splittings below 100 GeV using an ISR-jet selection.

1. Event selection

Events are reconstructed as described in Sec. V, with the signal light-lepton p_T threshold raised to $p_T = 10$ GeV. In addition, in events where tagged light leptons form an SFOS pair with $m_{SFOS} < 12$ GeV, both leptons in the pair are rejected. Events must have exactly two signal light leptons with opposite charge and satisfy the symmetric or asymmetric dilepton trigger criteria, as described in Sec. V.

To suppress the top-quark ($t\bar{t}$ and Wt) production contribution to the background, events containing central b-tagged jets or forward jets are rejected. To suppress events from Z boson decays, events with invariant mass of the reconstructed SFOS pair within 10 GeV of the Z boson mass (91.2 GeV) are rejected in the same-flavor channel.

Two SRs, collectively referred to as SR2ℓ-1, are defined. Both are designed to provide sensitivity to $\tilde{\chi}_1^+\tilde{\chi}_1^-$ production with $\tilde{\ell}_L$-mediated decays and low $\tilde{\chi}_1^\pm$-$\tilde{\chi}_1^0$ mass splittings and rely on a high-p_T ISR jet to boost the leptons, which would otherwise have too low momentum to be reconstructed. The super-razor variables that are discussed in Sec. VI A are used to discriminate between signal and backgrounds. Both the same-flavor (SF) and different-flavor (DF) channels are used. The first SR, SR2ℓ-1a, requires $R_2 > 0.5(0.7)$ in the SF (DF) channel, whereas the second SR, SR2ℓ-1b, requires $R_2 > 0.65(0.75)$. Both SRs require $M_\Delta^R > 20$ GeV to reduce SM $Z+$jets background, and $\Delta\phi_R^\beta > 2(2.5)$ in the SF (DF) to further increase the signal sensitivity. Table VI summarizes the complete definitions of the SRs. SR2ℓ-1a provides sensitivity for moderate $\tilde{\chi}_1^\pm$-$\tilde{\chi}_1^0$ mass splittings from 50 GeV to 100 GeV, while SR2ℓ-1b provides sensitivity for $\tilde{\chi}_1^\pm$-$\tilde{\chi}_1^0$ mass splittings less than 50 GeV.

2. Background determination

The SM background is dominated by WW diboson and top-quark production. The MC predictions for these SM sources, in addition to contributions from ZV production, where $V = W$ or Z, are normalized in dedicated control regions for each background. The reducible background is estimated using the matrix method as described in Sec. VI B. Finally, contributions from remaining sources of SM background, which include Higgs boson production and $Z+$jets, are small and are estimated from simulation. These are collectively referred to as "Others."

TABLE VI. The selection requirements for the opposite-sign, two-lepton signal and control regions, targeting $\tilde{\chi}_1^+\tilde{\chi}_1^-$ production with small mass splittings between the $\tilde{\chi}_1^\pm$ and LSP.

	Common						
Central light-flavor jets	=1 Veto >20						
Forward jets M_Δ^R [GeV]	SR2ℓ-1a		SR2ℓ-1b		CR2ℓ-Top	CR2ℓ-WW	CR2ℓ-ZV
ℓ flavor/sign	$\ell^\pm\ell^\mp$	$\ell^\pm\ell'^\mp$	$\ell^\pm\ell^\mp$	$\ell^\pm\ell'^\mp$	$\ell^\pm\ell'^\mp$	$\ell^\pm\ell'^\mp$	$\ell^\pm\ell^\mp$
Central b-tagged jets	Veto				≥1	Veto	Veto
m_{SFOS} [GeV]	Veto 81.2–101.2				···	···	Select 81.2–101.2
$p_T^{\ell\ell}$ [GeV]	···	···	<40	<50	···	>70	>70
p_T^{jet} [GeV]	>80	>80	>60	>80	···	···	···
R_2	>0.5	>0.7	>0.65	>0.75	···	···	···
$\Delta\phi_R^\beta$ [rad]	>2	>2.5	>2	>2.5	···	<2	>2
$p_T^{\text{central light jet}}$ [GeV]	···	···	···	···	>80	···	···

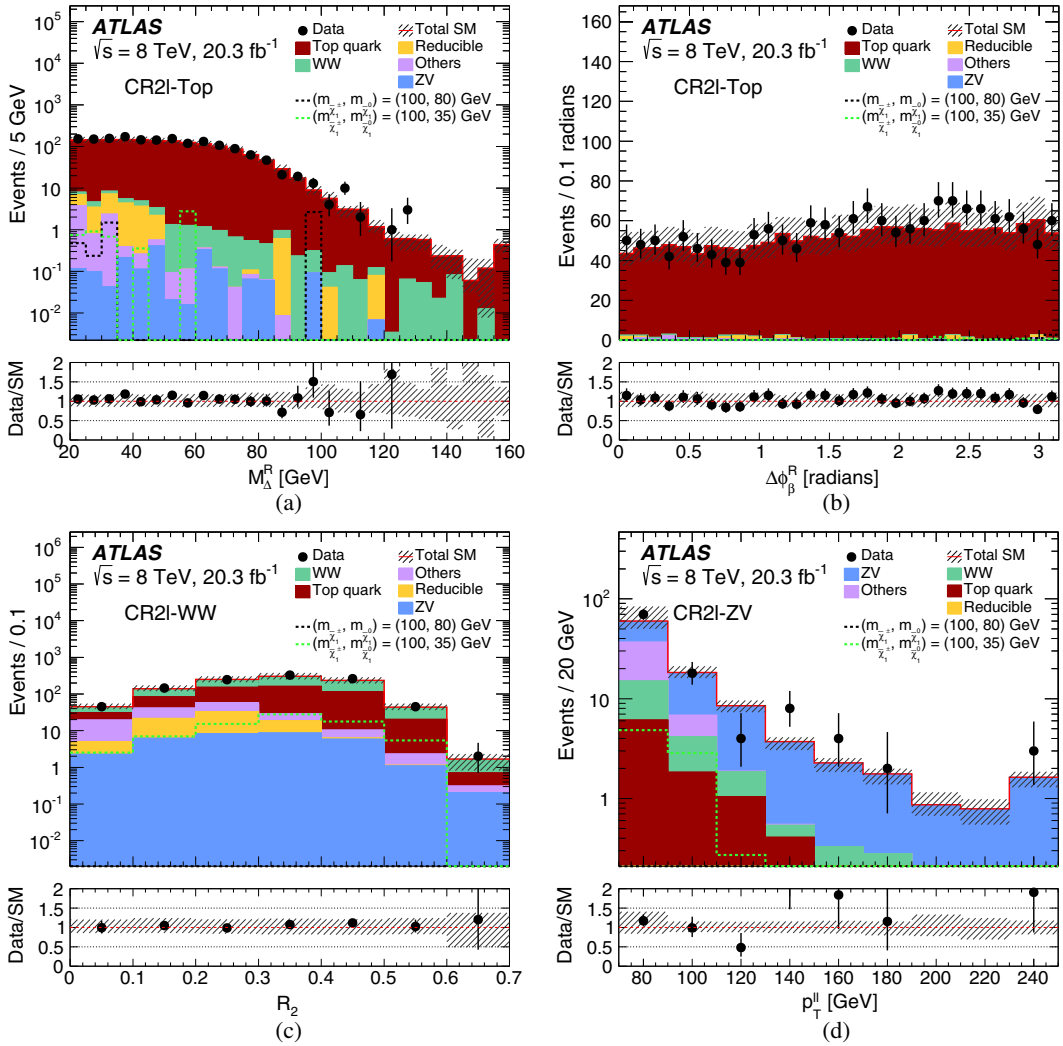

FIG. 5. Distributions in the opposite-sign, two-lepton control regions: (a) super-razor quantity M_Δ^R and (b) super-razor quantity $\Delta\phi_R^\beta$ in the top CR, (c) ratio R_2 in the WW CR, and (d) transverse momentum of the two-lepton system $p_T^{\ell\ell}$ in the ZV CR. No data-driven normalization factors are applied to the distributions. The "Others" background category includes $Z+$jets and SM Higgs boson production. The hashed regions represent the total uncertainties on the background estimates. The rightmost bin of each plot includes overflow. The lower panel of each plot shows the ratio of data to the SM background prediction. SM background prediction. Predicted signal distributions in simplified models are also shown.

The top CR is defined using the DF sample in order to suppress events from SM Z boson production. Events are required to have exactly one central light-flavor jet with $p_T > 80$ GeV, no forward jet, and $M_\Delta^R > 20$ GeV. At least one b-tagged jet is required to enrich the purity in top-quark production and ensure orthogonality to the SRs. Figures 5(a) and 5(b) show the M_Δ^R and $\Delta\phi_R^\beta$ distributions in this CR, respectively. The estimated signal contamination in this CR is less than 1% for the signal models considered.

The WW CR is also defined using the DF sample. Events are required to have exactly one central light jet, no forward jet or b-tagged jet, $p_T^{\ell\ell} > 70$ GeV, and $M_\Delta^R > 20$ GeV. In order to ensure orthogonality to the SRs, $\Delta\phi_R^\beta < 2$ is required. Figure 5(c) shows the R_2 distribution in this CR. The estimated signal contamination in this CR is less than 20% for the signal models considered.

The ZV CR is defined by using the SF samples and by requiring exactly one central light jet, no forward jet, or b-tagged jet, $p_T^{\ell\ell} > 70$ GeV, $\Delta\phi_R^\beta > 2$, and $M_\Delta^R > 20$ GeV. In order to increase the purity in ZV production, events with invariant mass of the reconstructed SFOS pair within 10 GeV of the Z boson mass are used. This requirement also ensures orthogonality to the SRs. Figure 5(d) shows the $p_T^{\ell\ell}$ distribution in this CR. The estimated signal contamination in this CR is less than 10% for the signal models considered.

A simultaneous likelihood fit to the top, WW, and ZV CRs is performed to normalize the corresponding background estimates to obtain yields in the SR (as described

TABLE VII. Numbers of observed and predicted events in the opposite-sign, two-lepton control regions, data/MC normalization factors, and composition of the CRs obtained from the background-only fit. The "Others" background category includes $Z+$jets and SM Higgs boson production. The $Z+$jets production is the dominant contribution to this category in the CR2ℓ-ZV.

CR	CR2ℓ-top	CR2ℓ-WW	CR2ℓ-ZV
Observed events	1702	1073	109
MC prediction	1600 ± 80	1020 ± 140	98 ± 14
Normalization	1.06	1.04	1.19
Total uncertainty	0.07	0.35	0.42
Composition			
WW	1%	43%	12%
Top	98%	41%	9%
ZV	<1%	4%	56%
Reducible	1%	5%	<1%
Others	<1%	7%	22%

TABLE VIII. The dominant systematic uncertainties (in %) on the total background estimated in the opposite-sign two-lepton signal regions. Because of correlations between the systematic uncertainties and the fitted backgrounds, the total uncertainty is different from the sum in quadrature of the individual uncertainties.

SR	SR2ℓ-1a		SR2ℓ-1b	
ℓ flavor/sign	$\ell^\pm\ell^\mp$	$\ell^\pm\ell'^\mp$	$\ell^\pm\ell^\mp$	$\ell^\pm\ell'^\mp$
Statistical uncertainty on MC samples	2%	6%	4%	10%
Jet energy scale/resolution	10%	9%	13%	11%
Theory and modeling	22%	22%	24%	25%
Total	23%	23%	26%	28%

in Sec. VI). Table VI summarizes the definitions of the CRs, and Table VII summarizes the numbers of observed and predicted events in these CRs, data/MC normalizations, and CR compositions obtained from the simultaneous fit.

Systematic uncertainties affect the estimates of the backgrounds and signal event yields in the control and signal regions. A breakdown of the different sources of systematic uncertainty on the background estimate as described in Sec. VI C is shown in Table VIII. Generator modeling uncertainties are estimated by comparing the results from the Powheg Box and MC@NLO event generators for top-quark events, and Powheg Box and aMC@NLO for WW events, using Herwig for parton showering in all cases. Parton showering uncertainties are estimated in top-quark and WW events by comparing Powheg Box+Herwig with Powheg Box+Pythia. Both generator modeling and parton showering uncertainties are estimated for ZV events by comparing Powheg Box +Pythia to sherpa. Top-quark samples are generated using AcerMC+Pythia to evaluate the uncertainties related to the amount of initial- and final-state radiation [115]. The impact of the choice of renormalization and factorization scales is evaluated by varying these individually between 0.5 and 2 times the nominal values in Powheg Box for top-quark events and in aMC@NLO for diboson events. The dominant contributions among the "Theory and modeling" uncertainties come from the generator modeling and parton showering uncertainties.

TABLE IX. Observed and expected number of events in the opposite-sign two-lepton signal regions. The "Others" background category includes $Z+$jets and SM Higgs boson production. The numbers of signal events are shown for the $\tilde{\chi}_1^+\tilde{\chi}_1^-$ simplified models with $\tilde{\ell}_L$-mediated decays and different $\tilde{\chi}_1^\pm$ and $\tilde{\chi}_1^0$ masses in GeV. The uncertainties shown include both statistical and systematic components. Also shown are the model-independent limits calculated from the opposite-sign two-lepton signal region observations: the one-sided p_0 values; the expected and observed upper limits at 95% CL on the number of beyond-the-SM events ($S^{95}_{\rm exp}$ and $S^{95}_{\rm obs}$) for each signal region, calculated using pseudoexperiments and the CL$_s$ prescription; the observed 95% CL upper limit on the signal cross section times efficiency ($\langle\epsilon\sigma\rangle^{95}_{\rm obs}$); and the CL$_b$ value for the background-only hypothesis.

SR	SR2ℓ-1a		SR2ℓ-1b	
ℓ flavor/sign	$\ell^\pm\ell^\mp$	$\ell^\pm\ell'^\mp$	$\ell^\pm\ell^\mp$	$\ell^\pm\ell'^\mp$
Expected background				
WW	67 ± 27	12 ± 5	22 ± 9	5.7 ± 2.4
Top	69 ± 19	12 ± 4	21 ± 7	5.0 ± 2.0
ZV	7.3 ± 3.4	1.7 ± 0.8	2.4 ± 1.5	0.6 ± 0.4
Reducible	12 ± 6	5.8 ± 2.0	10 ± 4	2.8 ± 1.1
Others	18 ± 5	2.1 ± 1.3	9.4 ± 3.4	1.0 ± 0.7
Total	173 ± 23	34 ± 5	65 ± 9	15.0 ± 2.5
Observed events	153	24	73	8
Predicted signal				
$(m_{\tilde{\chi}_1^\pm}, m_{\tilde{\chi}_1^0})=(100,35)$	81 ± 16	25 ± 7	44 ± 8	14 ± 4
$(m_{\tilde{\chi}_1^\pm}, m_{\tilde{\chi}_1^0})=(100,80)$	41 ± 10	23 ± 6	31 ± 7	18 ± 5
p_0	0.50	0.50	0.26	0.50
$S^{95}_{\rm obs}$	35.7	9.3	30.8	5.6
$S^{95}_{\rm exp}$	46^{+18}_{-12}	15^{+6}_{-4}	25^{+10}_{-7}	$9.4^{+4.2}_{-2.8}$
$\langle\epsilon\sigma\rangle^{95}_{\rm obs}$ [fb]	1.76	0.46	1.52	0.27
CL$_b$	0.22	0.09	0.73	0.07

3. Results

The observed number of events in each signal region is shown in Table IX along with the background expectations and uncertainties, p_0-values, $S^{95}_{\rm exp}$, $S^{95}_{\rm obs}$, $\langle\epsilon\sigma\rangle^{95}_{\rm obs}$, and the CL$_b$ values. Figures 6(a)–6(d) show the distributions of the quantities R_2 and M^R_Δ in the SR2ℓ-1a and SR2ℓ-1b regions, respectively, prior to the requirements on these variables. For illustration, the distributions are also shown for two $\tilde{\chi}_1^+\tilde{\chi}_1^-$ simplified models with $\tilde{\ell}_L$-mediated decays and different mass splittings.

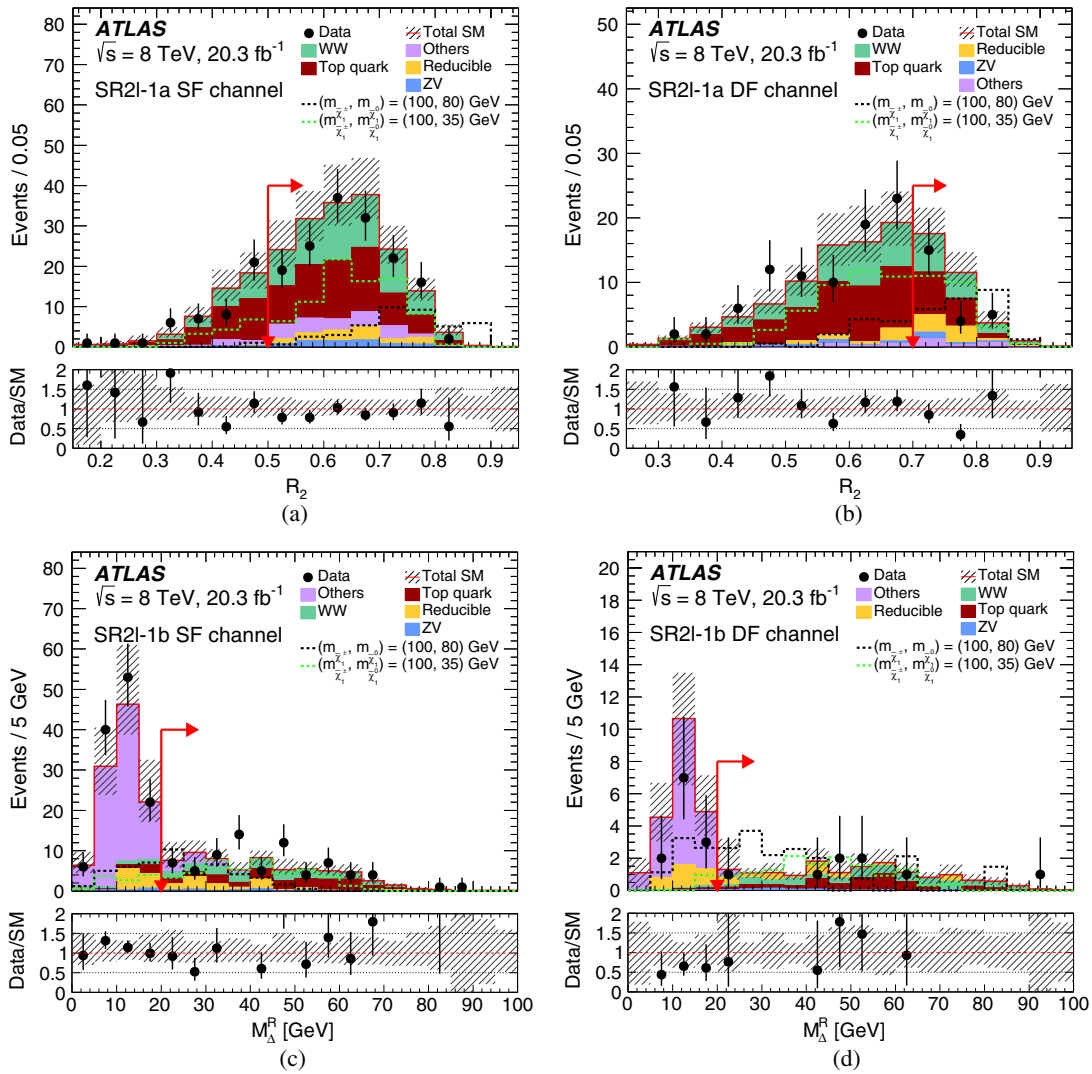

FIG. 6. Distributions of R_2 in the (a) same flavor and (b) different flavor channels in SR2ℓ-1a, and of M_Δ^R in the (c) same flavor and (d) different flavor channels in SR2ℓ-1b, prior to the requirements on these variables. The "Others" background category includes $Z+$jets and SM Higgs boson production. Arrows indicate the limits on the values of the variables used to define the signal regions. The lower panel of each plot shows the ratio of data to the SM background prediction. The uncertainty band includes both the statistical and systematic uncertainties on the SM prediction. The last bin in each distribution includes the overflow. Predicted signal distributions in simplified models are also shown.

B. Searches with two same-sign light leptons

In compressed mass scenarios, one or more of the three leptons from $\tilde{\chi}_1^\pm\tilde{\chi}_2^0$ production may have momentum too low to be reconstructed. Therefore, the search for $\tilde{\chi}_1^\pm\tilde{\chi}_2^0$ production using two same-sign leptons can complement the three-lepton search documented in Ref. [20] and extend the reach for small mass splittings. The search for same-sign lepton pairs is preferable to opposite-sign pairs, due to the comparatively small SM background. A multivariate analysis technique is used here to discriminate between signal and backgrounds.

1. Event selection

Events are selected using the basic reconstruction, object, and event selection criteria described in Sec. V. In addition, if tagged light leptons form an SFOS pair with $m_{\mathrm{SFOS}} < 12$ GeV, both leptons in the pair are rejected. Signal electrons with $p_{\mathrm{T}} < 60$ GeV have a tightened track (calorimeter) isolation of 7% (13%) of the electron p_{T} applied, whereas for electrons with $p_{\mathrm{T}} > 60$ GeV, a track isolation requirement of 4.2 GeV (7.8 GeV) is used. For signal muons, the track (calorimeter) isolation requirement is tightened to 6% (14%) of the muon p_{T} for $p_{\mathrm{T}} < 60$ GeV, and 4.2 GeV (8.4 GeV) otherwise. The stricter lepton isolation requirements are optimized to suppress the

TABLE X. Same-sign, two-lepton MVA signal region BDT requirements, targeting $\tilde{\chi}_1^\pm\tilde{\chi}_2^0$ production with small mass splittings between the $\tilde{\chi}_1^\pm/\tilde{\chi}_2^0$ and LSP. The selection on the BDT output, $t_{\rm cut}$, is independent for each SR.

		$\ell^\pm\ell^\pm$ pair, b-jet veto				
Common		SR ΔM20	SR ΔM35	SR ΔM65	SR ΔM100	VR
ISR	$t_{\rm cut}$	>0.071	>0.087	>0.103	>0.119	−0.049 − 0.051
No-ISR	$t_{\rm cut}$	>0.071	>0.087	>0.135	>0.135	−0.049 − 0.051

TABLE XI. The expected and observed yields in the same-sign, two-lepton MVA validation regions, separated into ee events, $e\mu$ events, and $\mu\mu$ events. The uncertainties shown include both statistical and systematic components.

	VR ISR			VR no-ISR		
	ee	$e\mu$	$\mu\mu$	ee	$e\mu$	$\mu\mu$
Reducible background	260 ± 140	670 ± 330	160 ± 110	410 ± 190	1100 ± 400	310 ± 170
Charge-flip	289 ± 15	15.0 ± 1.2	⋯	711 ± 34	28.1 ± 2.0	⋯
Diboson	58 ± 23	155 ± 37	110 ± 26	678 ± 25	199 ± 34	154 ± 34
Higgs	0.42 ± 0.30	0.7 ± 0.5	0.7 ± 0.5	0.23 ± 0.18	0.6 ± 0.4	0.50 ± 0.33
$t\bar{t}V$	0.23 ± 0.18	0.7 ± 0.4	0.44 ± 0.29	0.01 ± 0.022	0.01 ± 0.022	0.01 ± 0.022
$W\gamma$	61 ± 25	94 ± 23	1.0 ± 0.9	120 ± 50	200 ± 40	2.3 ± 2.0
Total	670 ± 140	940 ± 330	270 ± 120	1300 ± 200	1500 ± 400	470 ± 180
Data	585	799	363	1134	1349	612

reducible SM backgrounds with semileptonically decaying b/c-hadrons, which are an important background in this search.

Events must have exactly two light leptons with the same charge, $e^\pm e^\pm$, $\mu^\pm\mu^\pm$, or $e^\pm\mu^\pm$, and satisfy the symmetric or asymmetric dilepton trigger criteria, as described in Sec. V. Eight BDTs are independently trained to define eight signal regions optimized for four mass splitting scenarios, $m(\tilde{\chi}_2^0) - m(\tilde{\chi}_1^0) = 20$, 35, 65, 100 GeV, referred to as ΔM20, ΔM35, ΔM65, and ΔM100, respectively, each with and without the presence of a central light jet with $p_{\rm T} > 20$ GeV, referred to as ISR and no-ISR. For the BDT training, signal scenarios of $\tilde{\chi}_1^\pm\tilde{\chi}_2^0$ production with $\tilde{\ell}_L$-mediated decays are used, where the slepton mass is set at 95% between the $\tilde{\chi}_1^\pm$ and the $\tilde{\chi}_1^0$ masses. Seven variables are considered as input for the BDT training procedure: $m_{\rm T2}$, $p_{\rm T}{}^{\ell\ell}$, $E_{\rm T}^{\rm miss,rel}$, $H_{\rm T}$, $m_{\rm T}^{\rm lep1}$, $m_{\rm T}^{\rm lep2}$, and $\Delta\phi(\ell,\ell)$. Three further variables are also considered for the ISR signal regions: $\Delta\phi(,{\rm jet1})$ and the ratios $E_{\rm T}^{\rm miss,rel}/p_{\rm T}{}^{\rm jet1}$ and $p_{\rm T}{}^{\rm lep1}/p_{\rm T}{}^{\rm jet1}$. These variables exploit the kinematic properties of a compressed mass SUSY system, with and without a high-$p_{\rm T}$ ISR jet. The MC simulation samples are compared to data for these variables and their correlations to ensure that they are modeled well.

For the training and testing of the BDT, the signal and background samples are split into two halves, including those backgrounds estimated from data as described in Sec. VIII B 2. The eight signal region definitions are shown in Table X. Since the selection on the BDT output, $t_{\rm cut}$, is independent for each SR, the overlap between SRs with looser and tighter selections is small.

2. Background determination

Several SM processes produce events with two same-sign signal leptons. The SM background processes are classified as irreducible background if they lead to events with two real, prompt, same-sign leptons, reducible background if the event has at least one fake or nonprompt lepton, or "charge flip" if the event has one lepton with mismeasured charge.

Irreducible processes include diboson ($W^\pm W^\pm$, WZ, ZZ), triboson (VVV), $t\bar{t}V$, tZ, and Higgs boson production and are determined using the corresponding MC samples. The reducible $W\gamma$ process is estimated with MC simulation samples; other reducible processes are estimated with the matrix method, similar to that described in Sec. VI B.

In this implementation of the matrix method, the fake and nonprompt lepton misidentification probabilities are measured in control regions that are kinematically close and similar in composition to the signal regions. The regions where the misidentification probabilities are measured are required to have large $H_{\rm T}$ ($H_{\rm T} > 50$ GeV) and large transverse mass using the leading lepton ($m_{\rm T} > 50$ GeV). The contamination from signal events in these measurement regions is $< 1\%$. The charge-flip, irreducible, and $W\gamma$ backgrounds are subtracted from the control regions before calculating lepton misidentification probabilities.

Charge-flip processes include sources of opposite-sign prompt leptons for which the charge of one lepton is mismeasured (Z, $t\bar{t}$, W^+W^-). In the relevant momentum range the muon charge-flip background is found to be negligible. Control samples of e^+e^- and $e^\pm e^\pm$ with invariant mass near the Z boson mass

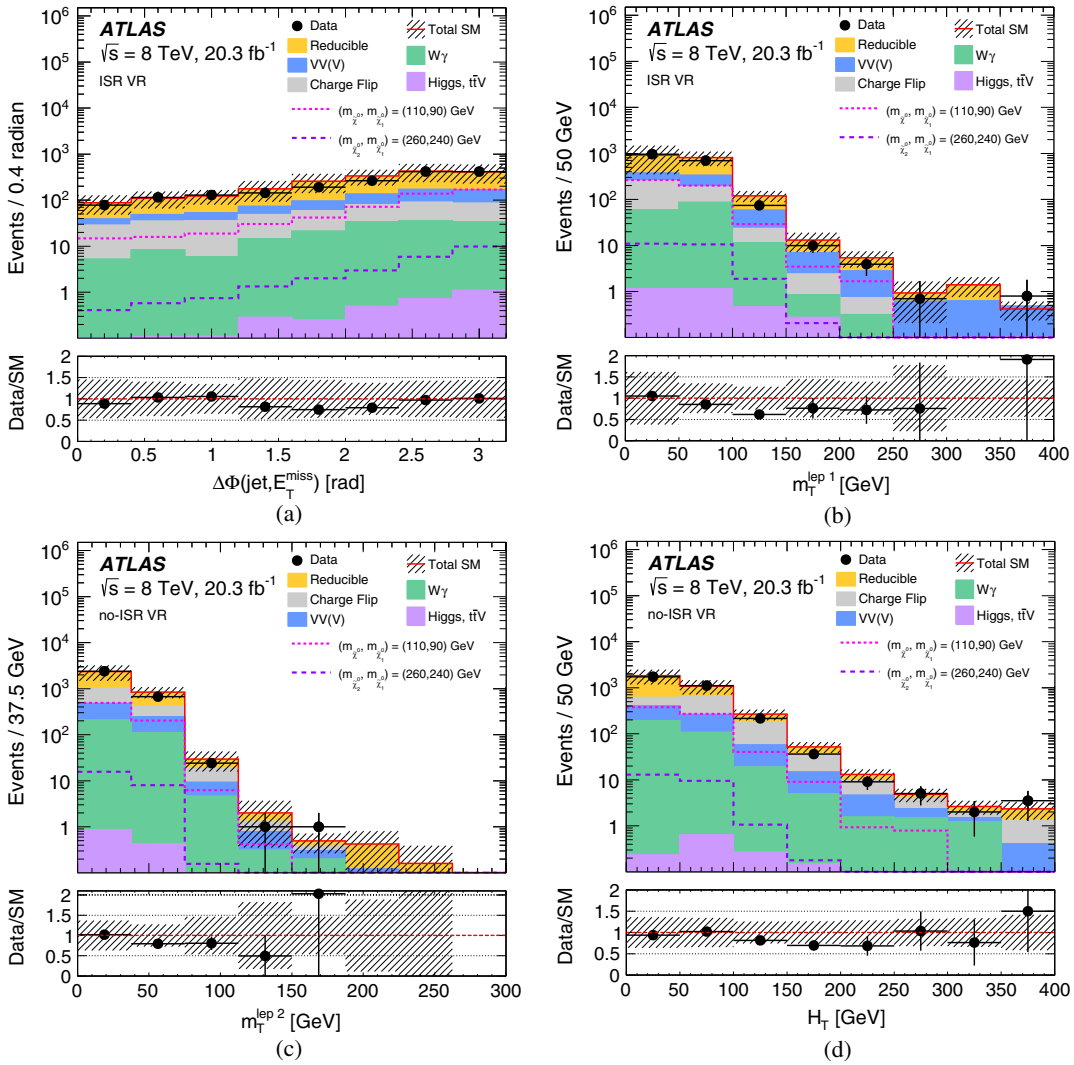

FIG. 7. For events in a selection of the same-sign, two-lepton MVA validation regions: (a) separation in ϕ between the leading jet and the $E_{\mathrm{T}}^{\mathrm{miss}}$, $\Delta\phi(\mathrm{jet}, E_{\mathrm{T}}^{\mathrm{miss}})$ and (b) transverse mass using the leading lepton $m_{\mathrm{T}}^{\mathrm{lep1}}$ in the ISR VR, (c) transverse mass using the second leading lepton $m_{\mathrm{T}}^{\mathrm{lep2}}$ and (d) scalar sum H_{T} of the p_{T} of the leptons and jets in the non-ISR VR. The lower panel of each plot shows the ratio of data to the SM background prediction. The uncertainty band includes both the statistical and systematic uncertainties on the SM prediction.

($75 < m_{\ell\ell} < 100$ GeV) are used to extract the electron charge-flip rate. A small background due to misidentified jets is subtracted by interpolating the mass sidebands and subtracting them from the observed data events. A likelihood fit is used that takes the numbers of e^+e^- and $e^\pm e^\pm$ pairs observed in the charge-flip control regions as input. The charge-flip probability is a free parameter of the fit and is extracted as a function of the electron p_{T} and η. The charge-flip background event yield is found by applying the charge-flip probability to control regions in data with the same kinematic requirements as the signal and validation regions, but with opposite-sign light lepton pairs. The contamination from fake and nonprompt leptons, and from signal events, is negligible in the e^+e^- and $e^\pm e^\pm$ control regions.

Generator modeling uncertainties for the diboson processes are estimated by comparing the results from the Powheg Box and MC@NLO event generators, while parton showering uncertainties are estimated by comparing MC@NLO+Herwig with MC@NLO+Pythia. The impact of the choice of renormalization and factorization scales is evaluated by varying these individually between 0.5 and 2 times the nominal values in aMC@NLO for diboson events.

To test the background prediction methods, two validation regions with looser selection on the BDT output than the SRs are defined; the definitions are shown in Table X. The light-lepton flavor content (ee, $\mu\mu$, or $e\mu$) is checked separately in each validation region. Table XI and Figures 7(a)–7(d) show the agreement between data and expectation in the validation regions.

TABLE XII. The model-independent limits calculated from the same-sign two-lepton MVA signal region observations: the observed 95% CL upper limit on the signal cross section times efficiency ($\langle\epsilon\sigma\rangle^{95}_{\rm obs}$); the expected and observed upper limits at 95% CL on the number of beyond-the-SM events ($S^{95}_{\rm exp}$ and $S^{95}_{\rm obs}$) for each signal region, calculated using pseudoexperiments and the CL_s prescription; the CL_b value for the background-only hypothesis; and the one-sided p_0 values.

SR		$N_{\rm exp}$	$N_{\rm obs}$	$\langle\epsilon\sigma\rangle^{95}_{\rm obs}$ [fb]	$S^{95}_{\rm obs}$	$S^{95}_{\rm exp}$	CL_b	p_0
ΔM20	ISR ee	3.2 ± 0.9	5	0.36	7.3	$5.4^{+2.2}_{-1.2}$	0.81	0.19
	$e\mu$	9.7 ± 2.8	9	0.44	8.9	$9.0^{+3.5}_{-2.5}$	0.47	0.50
	$\mu\mu$	4.3 ± 2.6	5	0.47	9.5	$8.8^{+2.8}_{-1.8}$	0.63	0.44
	No-ISR ee	28 ± 5	23	0.57	11.6	14^{+6}_{-4}	0.27	0.50
	$e\mu$	25 ± 8	29	1.08	21.9	19^{+7}_{-5}	0.68	0.33
	$\mu\mu$	7.6 ± 1.7	12	0.59	12.1	$8.0^{+2.7}_{-2.0}$	0.90	0.10
ΔM35	ISR ee	3.9 ± 1.2	1	0.17	3.5	$4.9^{+2.3}_{-1.1}$	0.09	0.50
	$e\mu$	6.5 ± 1.8	10	0.53	10.8	$7.4^{+3.2}_{-1.9}$	0.85	0.14
	$\mu\mu$	5.4 ± 2.1	5	0.37	7.6	$7.6^{+2.7}_{-1.7}$	0.51	0.50
	No-ISR ee	23 ± 5	19	0.56	11.4	$13.4^{+4.8}_{-3.4}$	0.30	0.50
	$e\mu$	46 ± 11	39	0.94	19.0	22^{+8}_{-6}	0.32	0.50
	$\mu\mu$	27 ± 10	21	0.79	15.9	$17.6^{+2.4}_{-4.0}$	0.34	0.50
ΔM65	ISR ee	1.7 ± 0.8	4	0.36	7.3	$4.7^{+1.8}_{-0.8}$	0.90	0.09
	$e\mu$	2.4 ± 0.8	4	0.33	6.7	$5.0^{+1.9}_{-1.3}$	0.54	0.34
	$\mu\mu$	1.4 ± 0.6	2	0.24	4.9	$4.1^{+1.6}_{-0.6}$	0.70	0.30
	No-ISR ee	1.2 ± 0.6	0	0.11	2.1	$3.4^{+1.3}_{-0.4}$	0.20	0.50
	$e\mu$	1.3 ± 0.5	2	0.24	4.9	$4.1^{+1.4}_{-0.7}$	0.73	0.26
	$\mu\mu$	1.5 ± 0.5	2	0.23	4.7	$4.1^{+1.6}_{-0.8}$	0.68	0.32
ΔM100	ISR ee	0.9 ± 0.6	0	0.13	2.6	$3.06^{+1.25}_{-0.09}$	0.29	0.50
	$e\mu$	0.57 ± 0.29	0	0.14	2.9	$3.00^{+1.20}_{-0.10}$	0.29	0.50
	$\mu\mu$	0.38 ± 0.35	0	0.15	3.0	$3.15^{+0.96}_{-0.11}$	0.38	0.50
	No-ISR ee	0.31 ± 0.22	0	0.16	3.2	$2.99^{+0.78}_{-0.05}$	0.38	0.50
	$e\mu$	0.55 ± 0.30	1	0.19	3.9	$3.33^{+0.93}_{-0.22}$	0.75	0.27
	$\mu\mu$	0.25 ± 0.21	0	0.16	3.2	$2.94^{+0.73}_{-0.09}$	0.37	0.50

TABLE XIII. Overview of the dominant systematic uncertainties on the background estimates in the same-sign, two-lepton MVA signal regions. The percentages show the sizes of the uncertainty relative to the total expected background; the range shows the variation among the flavor channels.

	SRΔM20		SRΔM35		SRΔM65		SRΔM100	
	ISR	No-ISR	ISR	No-ISR	ISR	No-ISR	ISR	No-ISR
Reducible background								
-Fake lepton composition	7%–14%	15%–20%	4%–14%	5%–17%	5%–17%	21%	9%–24%	20%–22%
-Real lepton subtraction	13%–32%	12%–25%	10%–20%	18%–26%	8%–18%	26%	15%–32%	22%–33%
-Statistical uncertainty on data	5%–8%	9%–12%	3%–7%	4%–8%	3%–9%	9%	5%–11%	9%–11%
Statistical uncertainty on MC samples	15%–37%	7%–12%	15%–28%	8%–16%	15%–43%	16%–32%	30%–45%	35%–74%
Choice of generator for WZ	9%–17%	4%–20%	15%–17%	5%–11%	13%–20%	6%–21%	3%–27%	4%–20%
Choice of generator for $W\gamma$	2%–3%	3%–7%	2%	4%–8%	3%–9%	...	...	...
Jet energy resolution	1%–18%	1%–7%	1%–7%	6%–12%	1%–10%	1%–6%	5%–70%	4%–35%
Total	28%–60%	18%–32%	28%–39%	22%–37%	33%–47%	33%–50%	51%–92%	55%–84%

3. Results

The observed number of events in each signal region is shown in Table XII along with the background expectation and uncertainties, p_0-values, $S^{95}_{\rm exp}$, $S^{95}_{\rm obs}$, $\langle\epsilon\sigma\rangle^{95}_{\rm obs}$, and the CL_b values. No significant excess with respect to the SM expectation is observed. The sizes and sources of uncertainty on the background estimation in the signal regions are shown in Table XIII, where the dominant sources of uncertainty are the statistical uncertainty on the reducible background estimation,

TABLE XIV. The selection requirements for the three-lepton signal regions, targeting $\tilde{\chi}_1^{\pm}\tilde{\chi}_2^0$ production with small mass splittings between the $\tilde{\chi}_1^{\pm}/\tilde{\chi}_2^0$ and LSP.

	Common			
ℓ flavor/sign	$\ell^{\pm}\ell^{\mp}\ell$, $\ell^{\pm}\ell^{\mp}\ell'$			
$p_{\mathrm{T}}^{\mathrm{lep1}}$	<30 GeV			
b-jet	Veto			
$E_{\mathrm{T}}^{\mathrm{miss}}$	>50 GeV			
m_{SFOS}	Veto 8.4–10.4 GeV			
SR	SR3ℓ-0a	SR3ℓ-0b	SR3ℓ-1a	SR3ℓ-1b
Central jets	No jets $p_{\mathrm{T}}>50$ GeV		$\geq$1jet $p_{\mathrm{T}}>50$ GeV	
$m_{\mathrm{SFOS}}^{\mathrm{min}}$	4–15 GeV	15–25 GeV	5–15 GeV	15–25 GeV
Other	$30<m_{\ell\ell\ell}<60$ GeV $m_{\mathrm{T}}<20$ GeV	$30<m_{\ell\ell\ell}<60$ GeV	$\Delta\phi(E_{\mathrm{T}}^{\mathrm{miss}},\mathrm{jet1})>2.7$ rad $p_{\mathrm{T}}^{\mathrm{lep1}}/p_{\mathrm{T}}^{\mathrm{jet1}}<0.2$	$\Delta\phi(E_{\mathrm{T}}^{\mathrm{miss}},3\ell)>0.7\pi$ rad

the statistical uncertainty on the MC simulation samples, and the uncertainty related to the choice of generator for the WZ MC simulation sample.

C. Searches with three light leptons

Previous searches for $\tilde{\chi}_1^{\pm}\tilde{\chi}_2^0$ production using the three-lepton final state are extended here to increase the sensitivity to compressed SUSY scenarios. The three-lepton analysis presented here probes $\tilde{\chi}_2^0$-$\tilde{\chi}_1^0$ mass splittings below 25 GeV using low-p_{T} leptons and ISR jets.

1. Event selection

Events are selected as described in Sec. V. In addition, signal muons with $p_{\mathrm{T}} < 15$ GeV have tightened track and calorimeter isolation requirements of 7% of the muon p_{T}. The stricter muon isolation requirements suppress SM backgrounds with semileptonically decaying b/c-hadrons, which are larger for muons rather than electrons due to the lower muon-p_{T} threshold. Events must satisfy a single-lepton, dilepton, or trilepton trigger.

Four signal regions are defined with exactly three light leptons, all with $p_{\mathrm{T}} < 30$ GeV, and at least one SFOS pair present among the leptons. All signal regions veto events with b-tagged jets to reduce the $t\bar{t}$ SM background and events with $8.4 < m_{\mathrm{SFOS}} < 10.4$ GeV to suppress backgrounds with leptonic Υ decays. The three-lepton signal region selections are summarized in Table XIV.

The first two signal regions, SR3ℓ-0a and SR3ℓ-0b, closely follow the selection in Ref. [20], using $E_{\mathrm{T}}^{\mathrm{miss}}$, m_{T}, and m_{SFOS} selections. SR3ℓ-0a and SR3ℓ-0b are defined with $E_{\mathrm{T}}^{\mathrm{miss}} > 50$ GeV and $30 < m_{\ell\ell\ell} < 60$ GeV to reject diboson processes. Events with a jet with $p_{\mathrm{T}} > 50$ GeV are vetoed to be disjoint from the ISR signal region. The first signal region, SR3ℓ-0a, targets the smallest $\tilde{\chi}_2^0$-$\tilde{\chi}_1^0$ mass splittings by selecting events with $m_{\mathrm{SFOS}}^{\mathrm{min}}$ between 4 and 15 GeV. In addition, SR3ℓ-0a requires small m_{T} to reduce the WZ SM background. The second signal region, SR3ℓ-0b, targets the slightly larger $\tilde{\chi}_2^0$-$\tilde{\chi}_1^0$ mass splittings by selecting events with $m_{\mathrm{SFOS}}^{\mathrm{min}}$ between 15 and 25 GeV.

The third and fourth signal regions, SR3ℓ-1a and SR3ℓ-1b, both require the presence of a $p_{\mathrm{T}} > 50$ GeV jet to target signal production with ISR. The leptons from a

TABLE XV. The selection requirements for the three-lepton validation regions. The "Z boson" requirement is defined as m_{SFOS} in the range 81.2–101.2 GeV.

	Common			
ℓ flavor/sign	$\ell^{\pm}\ell^{\mp}\ell$, $\ell^{\pm}\ell^{\mp}\ell'$			
$m_{\mathrm{SFOS}}^{\mathrm{min}}$	>4 GeV			
m_{SFOS}	Veto 8.4–10.4 GeV			
SR	VR3ℓ-0a	VR3ℓ-0b	VR3ℓ-1a	VR3ℓ-1b
Central jets	No jets $p_{\mathrm{T}}>50$ GeV		$\geq$1 jet $p_{\mathrm{T}}>50$ GeV	
$N_{b-\mathrm{jets}}$	0	1	0	1
$E_{\mathrm{T}}^{\mathrm{miss}}$	<30 GeV	>30 GeV	<50 GeV	>50 GeV
Z boson	Veto	⋯	Veto	Veto
$p_{\mathrm{T}}^{\mathrm{lep1}}$	<30 GeV	⋯	⋯	⋯
Target process				
Irreducible	WZ	WZ	WZ	WZ
Reducible	$Z+$jets, Υ	$t\bar{t}$	$Z+$jets	$t\bar{t}$

TABLE XVI. Estimated and observed yields in the three-lepton validation regions. The uncertainties shown include both statistical and systematic components. The "Others" background category includes $t\bar{t}V$, VVV, and SM Higgs boson production.

	VR3ℓ-0a	VR3ℓ-0b	VR3ℓ-1a	VR3ℓ-1b
WZ	108 ± 20	35 ± 7	36 ± 7	$9.7^{+2.0}_{-2.2}$
ZZ	63 ± 11	5.9 ± 1.3	5.2 ± 1.1	$0.33^{+0.08}_{-0.07}$
Reducible	990^{+300}_{-270}	159^{+40}_{-35}	56 ± 16	102^{+23}_{-19}
Others	1.0 ± 0.8	4.8 ± 1.7	1.5 ± 0.6	$9.9^{+3.4}_{-3.5}$
Total SM	1160^{+300}_{-280}	200 ± 40	99 ± 17	122^{+24}_{-20}
Data	1247	212	95	93

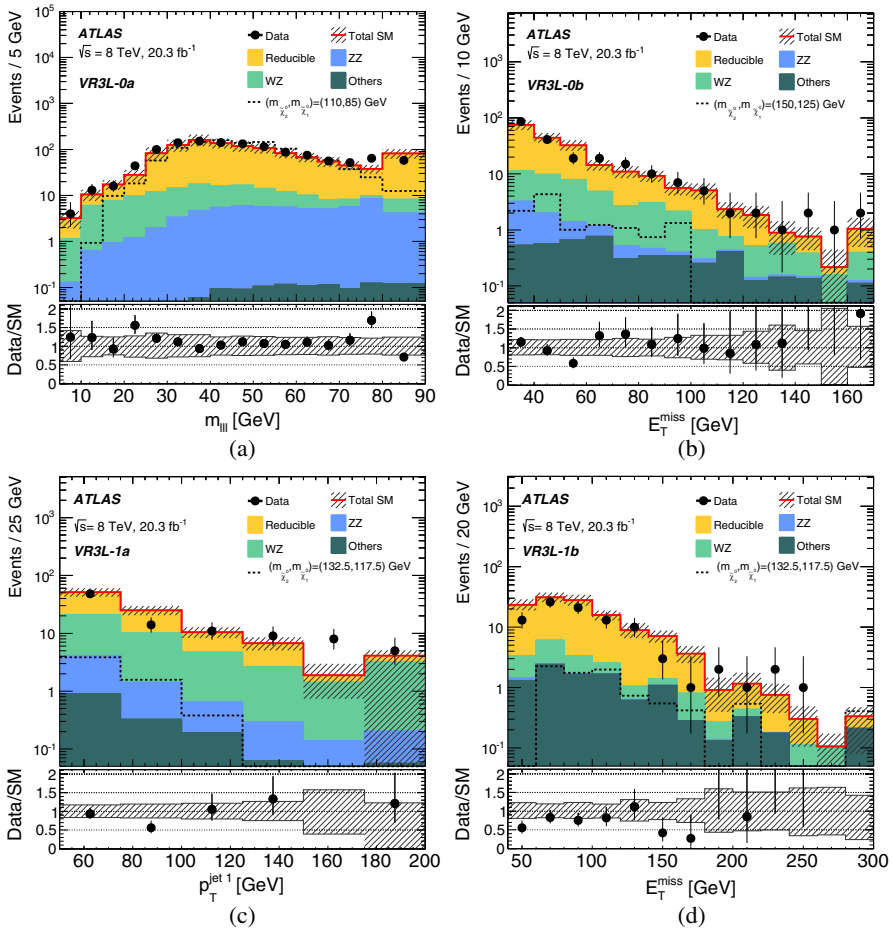

FIG. 8. Distributions in the three-lepton validation regions: (a) three-lepton invariant mass $m_{\ell\ell\ell}$ in VR3ℓ-0a, (b) $E_{\mathrm{T}}^{\mathrm{miss}}$ in VR3ℓ-0a, (c) transverse momentum of the leading jet $p_{\mathrm{T}}^{\mathrm{jet1}}$ in VR3ℓ-1a, and (d) $E_{\mathrm{T}}^{\mathrm{miss}}$ in VR3ℓ-1a. The "Others" background category includes $t\bar{t}V + tZ$, VVV, and SM Higgs boson production. The lower panel of each plot shows the ratio of data to the SM background prediction. The uncertainty band includes both the statistical and systematic uncertainties on the SM prediction. The last bin in each distribution includes the overflow.

compressed SUSY decay chain would have too low p_{T} to be reconstructed; however, because of the recoil against the high-p_{T} ISR jet, all three leptons can be boosted enough to meet the selection requirements. The third signal region, SR3ℓ-1a, targets the smallest $\tilde{\chi}_2^0$-$\tilde{\chi}_1^0$ mass splittings and selects events with $5 < m_{\mathrm{SFOS}}^{\mathrm{min}} < 15$ GeV. Here the leading jet is required to be back-to-back in the transverse plane with the $E_{\mathrm{T}}^{\mathrm{miss}}$, $\Delta\phi(E_{\mathrm{T}}^{\mathrm{miss}}, \mathrm{jet1}) > 2.7$ rad, and the ratio of leading lepton p_{T} to the jet p_{T} is required to be small, $p_{\mathrm{T}}^{\mathrm{lep1}}/p_{\mathrm{T}}^{\mathrm{jet1}} < 0.2$, to suppress the diboson and $t\bar{t}$ backgrounds. The fourth signal region, SR3ℓ-1b, targets the slightly larger $\tilde{\chi}_2^0$-$\tilde{\chi}_1^0$ mass splittings by selecting events with $15 < m_{\mathrm{SFOS}}^{\mathrm{min}} < 25$ GeV. To suppress the WZ and $t\bar{t}$ backgrounds in SR3ℓ-1b, the angle between the $E_{\mathrm{T}}^{\mathrm{miss}}$ and the three-lepton system is required to be large, $\Delta\phi(E_{\mathrm{T}}^{\mathrm{miss}}, 3\ell) > 0.7\pi$ rad.

2. Background determination

Several SM processes produce events with three signal leptons. The SM background processes are classified as irreducible background if they lead to events with three or more real leptons, or as reducible background if the event has at least one fake or nonprompt lepton. The predictions for irreducible and reducible backgrounds are tested in validation regions. For this search, irreducible processes include diboson (WZ and ZZ), VVV, $t\bar{t}V$, tZ, and Higgs boson production and are determined from MC simulation samples.

Reducible processes include single and pair production of top quarks, WW production, and a single W or Z boson produced in association with jets or photons. The dominant reducible background component is $t\bar{t}$, followed by $Z +$ jets. The reducible background is estimated using the matrix method, similar to that described in Sec. VI B. In this implementation of the matrix method, the highest-p_{T} signal electron or muon is taken to be real, and only the second and third leptons are used in the matrix method. Simulation studies show that neglecting the case that the leading lepton is nonprompt or fake is valid in more than 95% of the events.

TABLE XVII. Expected and observed yields in the three-lepton signal regions. The uncertainties shown include both statistical and systematic components. The "Others" background category includes $t\bar{t}V$, VVV, and SM Higgs boson production. Also shown are the model-independent limits calculated from the three-lepton signal region observations: the one-sided p_0-values; the expected and observed upper limits at 95% CL on the number of beyond-the-SM events (S^{95}_{exp} and S^{95}_{obs}) for each signal region, calculated using pseudoexperiments and the CL_s prescription; the observed 95% CL upper limit on the signal cross section times efficiency ($\langle\epsilon\sigma\rangle^{95}_{\mathrm{obs}}$); and the CL_b value for the background-only hypothesis.

	SR3ℓ-0a	SR3ℓ-0b	SR3ℓ-1a	SR3ℓ-1b
WZ	$0.59^{+0.47}_{-0.32}$	$5.0^{+1.5}_{-1.2}$	$0.54^{+0.20}_{-0.19}$	1.6 ± 0.4
ZZ	$0.23^{+0.09}_{-0.07}$	0.66 ± 0.16	0.024 ± 0.013	$0.10^{+0.05}_{-0.04}$
Reducible	$2.8^{+1.5}_{-2.2}$	$9.7^{+3.1}_{-3.6}$	0.09 ± 0.08	$1.4^{+1.0}_{-1.1}$
Others	$0.0033^{+0.0036}_{-0.0033}$	0.07 ± 0.05	0.013 ± 0.010	0.038 ± 0.021
Total SM	$3.7^{+1.6}_{-2.2}$	$15.4^{+3.5}_{-3.9}$	$0.67^{+0.22}_{-0.21}$	$3.1^{+1.1}_{-1.2}$
Data	4	15	1	3
p_0	0.47	0.50	0.36	0.50
S^{95}_{obs}	8.3	12.6	4.0	6.1
S^{95}_{exp}	$8.2^{+1.7}_{-2.2}$	$12.6^{+5.2}_{-3.0}$	$3.8^{+0.6}_{-0.3}$	$6.0^{+2.1}_{-1.3}$
$\langle\epsilon\sigma\rangle^{95}_{\mathrm{obs}}$ [fb]	0.41	0.62	0.20	0.30
CL_b	0.59	0.50	0.69	0.54

The uncertainty on the reducible background includes the MC statistical uncertainty on the weights for the process-dependent misidentification probabilities, the uncertainty on the correction factors for the misidentification probability, the statistical uncertainty on the data events to which the matrix equation is applied, and the statistical uncertainty from the misidentification probability measured in simulation.

The systematic uncertainty related to the theoretical modeling of the WZ and ZZ backgrounds is assessed by comparing MC estimates with data in dedicated regions. The WZ region requires three light leptons with $p_{\mathrm{T}} > 30$ GeV, an SFOS pair among the three leptons, $30 < E_{\mathrm{T}}^{\mathrm{miss}} < 50$ GeV, and one jet with $p_{\mathrm{T}} > 50$ GeV. Events with an SFOS pair or three-lepton invariant mass within 10 GeV of the Z boson mass are vetoed. The ZZ region is defined with four light leptons with $p_{\mathrm{T}} > 10$ GeV, two SFOS pairs with invariant mass within 10 GeV of the Z boson mass, and $E_{\mathrm{T}}^{\mathrm{miss}} < 50$ GeV. This approach for estimating the systematic uncertainties is used here instead of the MC-based approach discussed in Sec. VI C. The WZ and ZZ MC simulation samples are both found to agree with observations in the dedicated regions within 15%, which is applied as a systematic uncertainty in the three-lepton validation and signal regions.

The background predictions are tested in validation regions that are defined to be adjacent to, yet disjoint from, the signal regions. Low-$E_{\mathrm{T}}^{\mathrm{miss}}$ validation regions ("a" regions) and high-$E_{\mathrm{T}}^{\mathrm{miss}} + b$-jet validation regions ("b" regions) are defined to target different background processes. The definition of the regions and the targeted processes are shown in Table XV. In the three-lepton validation regions, the observed data counts and SM expectations are in good agreement within statistical and systematic uncertainties, as shown in Table XVI and Figs. 8(a)–8(d).

TABLE XVIII. Breakdown of the dominant systematic uncertainties on background estimates in the three-lepton signal regions. The percentages show the size of the uncertainty relative to the total expected background.

Source of uncertainty	SR3ℓ-0a	SR3ℓ-0b	SR3ℓ-1a	SR3ℓ-1b
Reducible background				
- Statistical uncertainty	34%	14%	11%	30%
- Muon misidentification probability	30%	11%	<1%	11%
- Electron misidentification probability	21%	10%	2%	9%
- Heavy-flavor relative contribution	22%	5%	<1%	2%
- Light-flavor relative contribution	23%	4%	N/a	<1%
- Conversion relative contribution	2%	6%	<1%	10%
$E_{\mathrm{T}}^{\mathrm{miss}}$ soft-term scale	12%	7%	<1%	1%
Statistical uncertainty on MC samples	4%	3%	25%	10%
Theoretical modeling of WZ	2%	5%	12%	8%
Cross section	2%	2%	6%	4%
Total	59%	25%	33%	39%

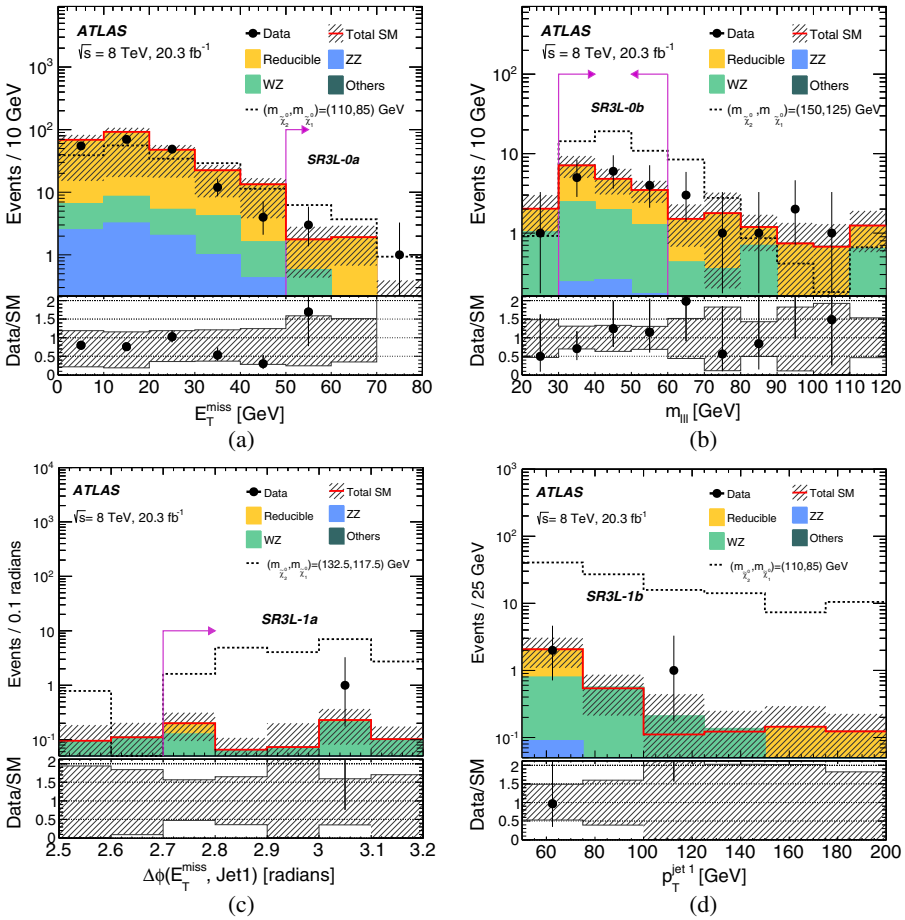

FIG. 9. Distributions in the three-lepton signal regions: (a) $E_{\mathrm{T}}^{\mathrm{miss}}$ in SR3ℓ-0a, (b) $m_{\ell\ell\ell}$ in SR3ℓ-0b, (c) $\Delta\phi(E_{\mathrm{T}}^{\mathrm{miss}}, \mathrm{jet1})$ in SR3ℓ-1a, and (d) $p_{\mathrm{T}}^{\mathrm{jet1}}$ in SR3ℓ-1b. All are shown prior to the requirements on these variables. The "Others" background category includes $t\bar{t}V + tZ$, VVV, and SM Higgs boson production. The lower panel of each plot shows the ratio of data to the SM background prediction. Arrows indicate the limits on the values of the variables used to define the signal regions. The uncertainty band includes both the statistical and the systematic uncertainties on the SM prediction. The last bin in each distribution includes the overflow.

TABLE XIX. The selection requirements for the same-sign, two-lepton VBF signal region, targeting $\tilde{\chi}_1^{\pm}\tilde{\chi}_1^{\pm}$ production via VBF with small mass splittings between the $\tilde{\chi}_1^{\pm}$ and LSP.

	SR2ℓ-2
ℓ flavor/sign	$\ell^{\pm}\ell^{\pm}$, $\ell^{\pm}\ell'^{\pm}$
Jets	≥ 2
Central b-jets	Veto
$E_{\mathrm{T}}^{\mathrm{miss}}$ [GeV]	>120
m_{T2} [GeV]	<40
$m_{\ell\ell}$ [GeV]	<100
$p_{\mathrm{T}}^{\mathrm{jet1}}$ [GeV]	>95
m_{jj} [GeV]	>350
$\eta^{\mathrm{jet1}} \cdot \eta^{\mathrm{jet2}}$	<0
$\lvert\Delta\eta_{jj}\rvert$	>1.6
$p_{\mathrm{T}}^{\ell\ell}/E_{\mathrm{T}}^{\mathrm{miss}}$	<0.4
$p_{\mathrm{T}}^{\mathrm{jet1}}/E_{\mathrm{T}}^{\mathrm{miss}}$	<1.9
$p_{\mathrm{T}}^{\ell\ell}/p_{\mathrm{T}}^{jj}$	<0.35

3. Results

The observed number of events in each signal region is shown in Table XVII along with the background expectations and uncertainties, p_0-values, S_{exp}^{95}, S_{obs}^{95}, $\langle\epsilon\sigma\rangle_{\mathrm{obs}}^{95}$, and the CL_b values. The sizes and sources of uncertainty on the background estimation in the three-lepton signal regions are shown in Table XVIII, where the dominant sources of uncertainty are the statistical uncertainty on the data for the reducible background estimate, and the uncertainty on the electron and muon misidentification probabilities. Figures 9(a), 9(b), 9(c), and 9(d) show the distributions of the quantities $E_{\mathrm{T}}^{\mathrm{miss}}$, $m_{\ell\ell\ell}$, $\Delta\phi(E_{\mathrm{T}}^{\mathrm{miss}}, \mathrm{jet1})$, and $p_{\mathrm{T}}^{\mathrm{jet1}}$ in SR3ℓ-0a, SR3ℓ-0b, SR3ℓ-1a, and SR3ℓ-1b regions, respectively, prior to the requirements on these variables. For illustration, the distributions are also shown for a $\tilde{\chi}_1^{\pm}\tilde{\chi}_2^{0}$ scenario with $\tilde{\ell}_L$-mediated decays, where the slepton mass is set halfway between the $\tilde{\chi}_1^{\pm}$ and the $\tilde{\chi}_1^{0}$ masses.

IX. SAME-SIGN CHARGINO-PAIR PRODUCTION VIA VECTOR-BOSON FUSION

This section presents a search for the same-sign chargino-pair production via VBF with subsequent $\tilde{\ell}_L$-mediated chargino decays into final states with two same-sign light leptons, at least two jets, and $E_{\mathrm{T}}^{\mathrm{miss}}$. Although the cross section for VBF production is significantly lower than that for direct production, the two additional jets in the event provide a means to separate the signal from the background for compressed spectra scenarios and complement the direct production searches that use low-momentum leptons and ISR jets.

A. Event selection

Events are selected using the basic reconstruction, object, and event selection criteria described in Sec. V. In addition, signal muons with $p_{\mathrm{T}} < 15$ GeV have tightened isolation requirements as in the three-lepton analysis described in Sec. VIII C. A tighter isolation is needed for muons rather than electrons due to the lower p_{T} threshold for muons. The stringent lepton isolation suppresses the dominant reducible background processes. Events are required to satisfy an $E_{\mathrm{T}}^{\mathrm{miss}}$ trigger.

One signal region, SR2ℓ-2, is defined with exactly two same-sign light leptons, at least two jets (central light or forward) and large missing transverse momentum $E_{\mathrm{T}}^{\mathrm{miss}} > 120$ GeV. In order to select events that originate from VBF production, the highest-p_{T} jet (jet 1) and the second highest-p_{T} jet (jet 2) are required to have large invariant mass, $m_{jj} > 350$ GeV, to be well separated in pseudorapidity, $|\Delta\eta_{jj}| > 1.6$, and to be in opposite sides of the detector, $\eta^{\mathrm{jet1}} \cdot \eta^{\mathrm{jet2}} < 0$. The last requirement greatly reduces the SM background originating from non-VBF diboson and Higgs boson production. The residual SM background originating from diboson and top-quark production is minimized by requiring the events to have no b-tagged jets, moderate invariant mass of the two leptons ($m_{\ell\ell} < 100$ GeV), small stransverse mass ($m_{\mathrm{T2}} < 40$ GeV), and a high-p_{T} jet ($p_{\mathrm{T}}^{\mathrm{jet1}} > 95$ GeV). In addition, requirements are made on the ratios of the jet p_{T}, $E_{\mathrm{T}}^{\mathrm{miss}}$, p_{T}^{jj}, and $p_{\mathrm{T}}^{\ell\ell}$. The SR definition is summarized in Table XIX.

B. Background determination

Several SM processes lead to events with two same-sign signal leptons. The irreducible background is dominated by diboson production, which is estimated using MC simulation samples. The dominant reducible background component is from $W+$jets production, followed by $t\bar{t}$ production, and these are estimated using a data-driven technique called the "fake factor method," similar to that described in Ref. [116]. The production of $W\gamma$ is also an important background component and is modeled using MC simulation samples. The charge-flip background is estimated by applying data-driven corrections to the MC simulation samples, following the procedure outlined in Sec. VIII B 2.

The fake factor method estimates the contributions from processes that produce one or two fake or nonprompt

TABLE XX. The selection requirements for the same-sign, two-lepton VBF validation regions.

	Common	
ℓ flavor/sign	$\ell^\pm\ell^\pm$, $\ell^\pm\ell'^\pm$	
$E_{\mathrm{T}}^{\mathrm{miss}}$ [GeV]	>120	
Jets	≥2	
	VR-VV	VR-Fakes
$p_{\mathrm{T}}^{\mathrm{lep1}}$ [GeV]	>40 GeV	⋯
$p_{\mathrm{T}}^{\mathrm{lep2}}$ [GeV]	>40 GeV	⋯
Central b-jets	Veto	⋯
Target process	Dibosons	Nonprompt and fake leptons

TABLE XXI. Observed and expected number of events in the same-sign, two-lepton VBF validation and signal regions. The numbers of signal events are shown for the $\tilde{\chi}_1^\pm\tilde{\chi}_1^\pm$ VBF simplified model with $\tilde{\ell}_L$-mediated decays, with the $\tilde{\chi}_1^\pm$ and $\tilde{\chi}_1^0$ masses in GeV. The uncertainties shown include both statistical and systematic components. The model-independent limits are also shown: the one-sided p_0 value; the expected and observed upper limits at 95% CL on the number of beyond-the-SM events (S_{exp}^{95} and S_{obs}^{95}) for the signal region, calculated using pseudoexperiments and the CL_s prescription; the observed 95% CL upper limit on the signal cross section times efficiency ($\langle\epsilon\sigma\rangle_{\mathrm{obs}}^{95}$); and the CL_b value for the background-only hypothesis.

	VR-VV	VR-Fakes	SR2ℓ-2
ℓ flavor/sign	$\ell^\pm\ell^\pm$, $\ell^\pm\ell'^\pm$	$\ell^\pm\ell^\pm$, $\ell^\pm\ell'^\pm$	$\ell^\pm\ell^\pm$, $\ell^\pm\ell'^\pm$
Expected background			
$W^\pm W^\pm$	$8.9^{+1.0}_{-1.1}$	41 ± 13	$1.95^{+0.21}_{-0.23}$
$W\gamma$	3.5 ± 0.8	$22.8^{+4.2}_{-2.5}$	$0.67^{+0.52}_{-0.31}$
WZ	11.0 ± 3.0	65 ± 16	$2.3^{+0.8}_{-0.9}$
ZZ	$0.65^{+0.20}_{-0.19}$	1.7 ± 0.4	$0.05^{+0.11}_{-0.17}$
Reducible	4.0 ± 2.2	280 ± 100	5.2 ± 2.0
Charge-flip	0.7 ± 0.7	8 ± 4	$0.03^{+0.04}_{-0.02}$
Others	$0.32^{+0.07}_{-0.06}$	13.6 ± 1.5	0.013 ± 0.007
Total	29 ± 5	430 ± 100	10.3 ± 2.3
Observed events	20	400	10
Predicted signal $(m_{\tilde{\chi}_1^\pm}, m_{\tilde{\chi}_1^0}) = (120, 95)$	0.25 ± 0.03	8.32 ± 0.19	3.47 ± 0.12
p_0	⋯	⋯	0.50
S_{obs}^{95}	⋯	⋯	8.4
S_{exp}^{95}	⋯	⋯	$8.7^{+3.9}_{-2.5}$
$\langle\epsilon\sigma\rangle_{\mathrm{obs}}^{95}$ [fb]	⋯	⋯	0.41
CL_b	⋯	⋯	0.47

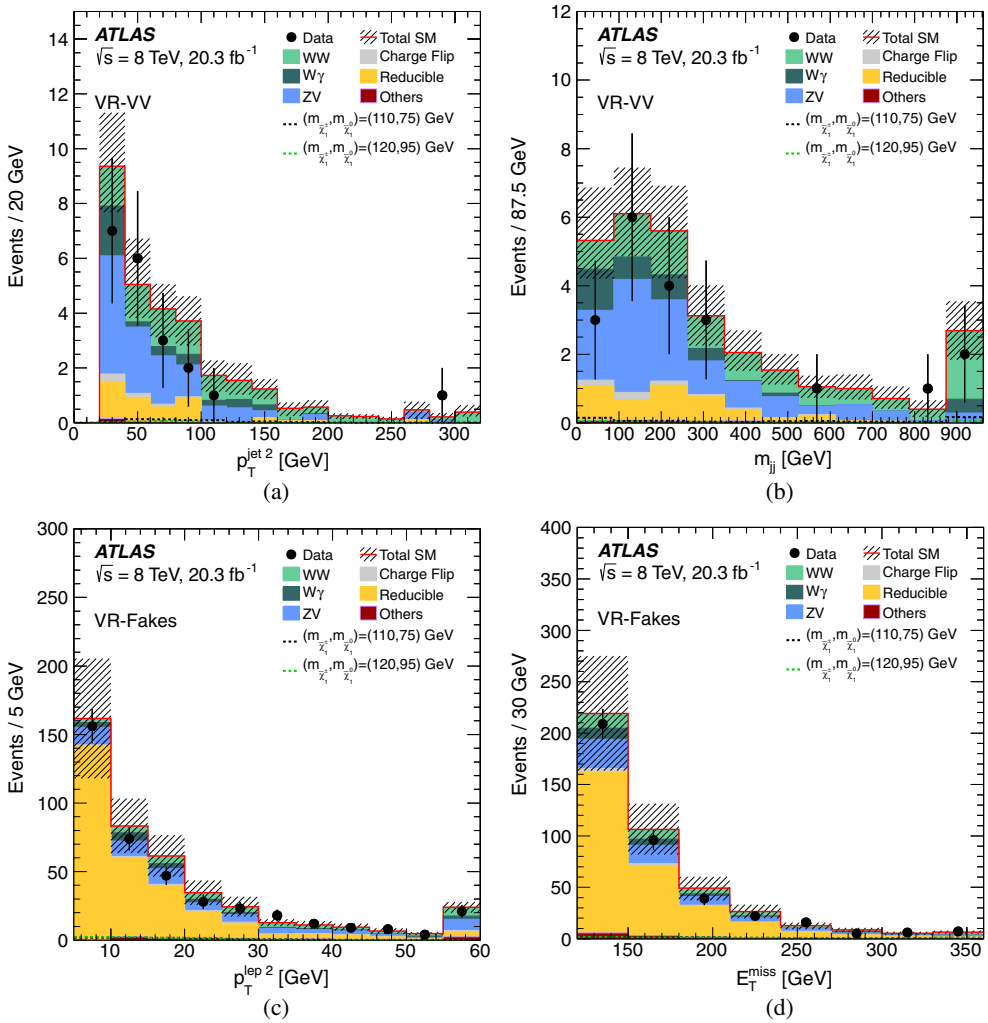

FIG. 10. For events in the same-sign VBF validation region VR-Fakes, the (a) transverse momentum of the second leading jet $p_{\mathrm{T}}^{\mathrm{jet2}}$ and (b) invariant mass of the two leading jets m_{jj} in VR-VV, and (c) transverse momentum of the second leading lepton $p_{\mathrm{T}}^{\mathrm{lep2}}$ and (d) $E_{\mathrm{T}}^{\mathrm{miss}}$. The "Others" background category includes $t\bar{t}V + tV$, VVV, and SM Higgs boson production. The uncertainty band includes both the statistical and the systematic uncertainties on the SM prediction. The last bin in each distribution includes the overflow.

leptons using data events that contain one signal lepton and one lepton failing to satisfy the signal lepton requirements. These events are scaled by a "fake factor" to predict the reducible background in the signal region. The fake factor is defined as the ratio of events with two signal leptons to events with one signal lepton and one lepton failing the signal lepton requirements. It is measured in data using a control sample of jets faking leptons in $Z \to \ell\ell$ events. The SM background process dependence of the fake factor is studied using simulation, and no strong dependence is observed. Residual differences are covered by assigning a 30% uncertainty, independent of the lepton p_{T}, to the fake factor. The uncertainty on the reducible background estimate ranges from 37% to 42%, depending on the channel (ee, $\mu\mu$, or $e\mu$), and is dominated by the prompt lepton contamination in the control sample and the uncertainty on the extrapolation of fake factors into the signal region.

The contributions from diboson processes are estimated using MC simulation samples. SHERPA is used to produce all diboson samples, taking into account both the strong and the electroweak production of associated jets. The $W^{\pm}W^{\pm} + 2$jets and $WZ + 2$jets processes are normalized to NLO cross sections using corrections evaluated in dedicated VBF fiducial regions at the parton level. The corrections are calculated separately for strong and electroweak jet production. For the $W^{\pm}W^{\pm} + 2$jets production, the fiducial cross section is calculated using POWHEG BOX +PYTHIA [62,63,117], and the fiducial region is defined to be identical to the signal region at the parton level, except for the lepton isolation requirement. For the $WZ + 2$jets production, the fiducial cross sections are calculated using VBFNLO-2.7.0 [118]. Since it is not possible to define a fiducial region that is identical to the signal region using VBFNLO-2.7.0, a looser set of requirements is imposed.

TABLE XXII. The dominant systematic uncertainties on the background estimates for the same-sign, two-lepton VBF signal region. The percentages show the size of the uncertainty relative to the total expected background. Because of correlations between the systematic uncertainties, the total uncertainty is different from the sum in quadrature of the individual uncertainties.

Source of uncertainty	SR2ℓ-2
Fake factor closure test	13%
Statistical uncertainty on the reducible background	11%
$WZ + 2$jets scale and PDF	5%
Statistical uncertainty on $WZ + 2$jets	4%
Statistical uncertainty on the electron fake factor	3%
Jet energy resolution	3%
Statistical uncertainty on $W^{\pm}W^{\pm} + 2$jets	3%
$W^{\pm}W^{\pm} + 2$jets scale and PDF	1%
Total	21%

The generator modeling uncertainty is estimated by comparing POWHEG BOX+PYTHIA with VBFNLO-2.7.0 for $W^{\pm}W^{\pm}$+2jets production, and parton showering uncertainties are estimated by comparing POWHEG BOX+HERWIG with POWHEG BOX+PYTHIA. The impact of the choice of renormalization and factorization scales is evaluated by varying each between 0.5 and 2 times the nominal values. The uncertainties due to the PDFs are evaluated using 90% CL CT10 PDF eigenvectors. Finally, the interference between the strong and electroweak jet production is studied at LO accuracy using SHERPA and is found to have a negligible effect on the combined fiducial cross section in the signal region.

The background predictions are tested in VRs that are defined to be as kinematically close to the SR as possible. The first VR, VR-Fakes, is defined with two signal light

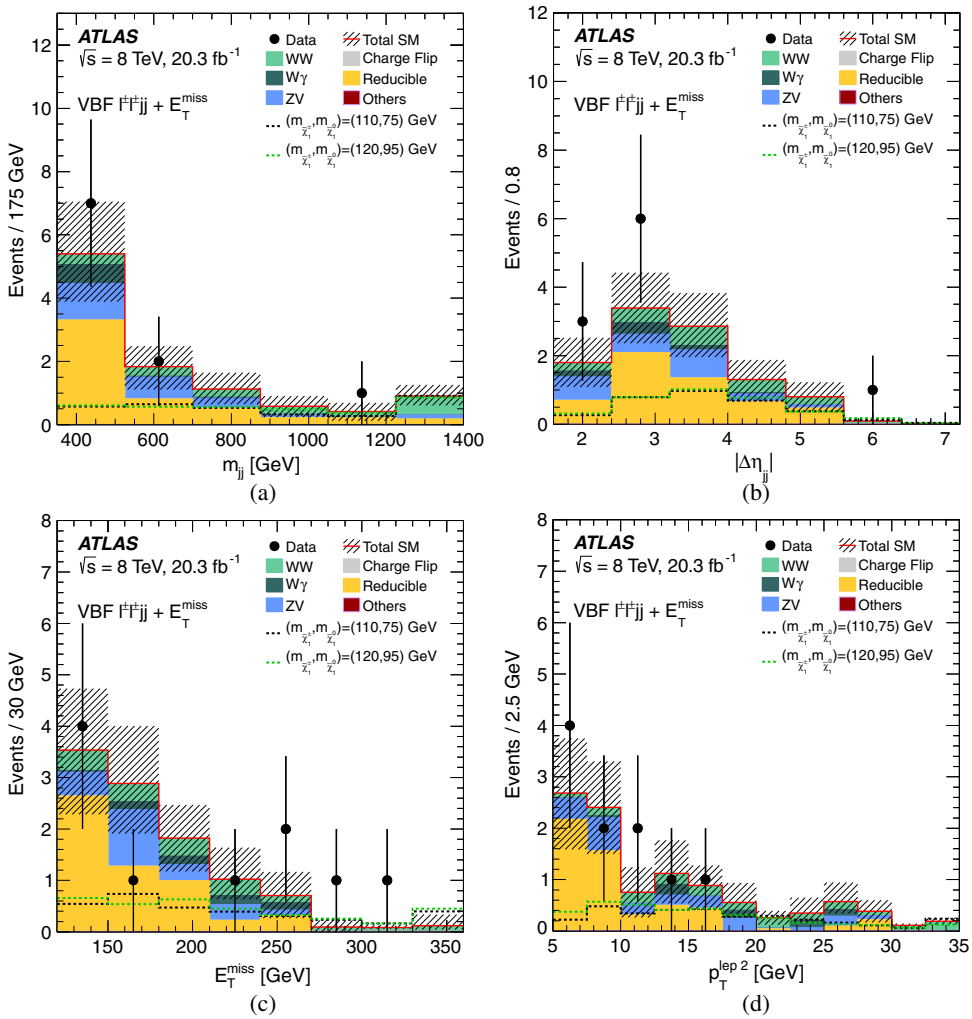

FIG. 11. For events in the same-sign VBF signal region, the (a) m_{jj}, (b) separation in η between the two leading jets $|\Delta\eta_{jj}|$, (c) $E_{\mathrm{T}}^{\mathrm{miss}}$, and (d) $p_{\mathrm{T}}^{\ell 2}$ in SR2ℓ-2. The "Others" background category includes $t\bar{t}V + tZ$, VVV, and SM Higgs boson production. The uncertainty band includes both the statistical and systematic uncertainties on the SM prediction. The last bin in each distribution includes the overflow.

leptons, large $E_{\mathrm{T}}^{\mathrm{miss}}$, and at least two jets to test backgrounds with fake and nonprompt leptons modeled by the fake factor method. The second VR, VR-VV, adopts the same requirements as the VR-Fakes, in addition to higher lepton-p_{T} thresholds and a b-jet veto that allow it to test the MC modeling of the diboson background. By definition, the VRs are not disjoint from the SR, but have negligible overlaps. The overlap between the VR-Fakes (VR-VV) and the SR is 2.4% (0.2%), and the largest signal contamination is 1.9% (0.9%) of the total expected background in the VR-Fakes (VR-VV). The definitions of the validation regions are shown in Table XX, along with the targeted processes. The yields in the VRs are shown in Table XXI, where the background expectation is in good agreement with the observed data, within the total uncertainties. Figures 10(a), 10(b), 10(c), and 10(d) show the distributions of $p_{\mathrm{T}}^{\mathrm{lep2}}$ and m_{jj} in VR-VV, along with $p_{\mathrm{T}}^{\mathrm{lep2}}$ and $E_{\mathrm{T}}^{\mathrm{miss}}$ in VR-Fakes, with good agreement observed.

C. Results

The observed number of events in the signal region is shown in Table XXI along with the background expectation and uncertainties, p_0-value, S_{exp}^{95}, S_{obs}^{95}, $\langle\epsilon\sigma\rangle_{\mathrm{obs}}^{95}$, and the CL_b value. No significant excess with respect to the SM expectation is observed. A breakdown of the different sources of systematic uncertainty in the signal region, including those described in Sec. VI C, is shown in Table XXII. Figures 11(a)–11(d) show the distributions of the quantities m_{jj}, $|\Delta\eta_{jj}|$, $E_{\mathrm{T}}^{\mathrm{miss}}$, and $p_{\mathrm{T}}^{\mathrm{lep2}}$ in the signal region.

X. INTERPRETATION OF RESULTS

Previous ATLAS searches for EW SUSY production [19–23] are combined with the new analyses presented in Secs. VII–IX. The combined results are interpreted in the SUSY models discussed in Sec. II. The analyses combined for each SUSY model are shown in Table XXIII. Limits in the simplified models targeted by the analysis presented in the previous sections are presented in Secs. X A–X D. A summary is provided in Sec. X E, including the limits previously obtained from the ATLAS searches for $\tilde{\chi}_1^+\tilde{\chi}_1^-$ production with WW-mediated decays [19], $\tilde{\chi}_1^\pm\tilde{\chi}_2^0$ production with WZ-mediated decays [20], and $\tilde{\chi}_1^\pm\tilde{\chi}_2^0$ production with Wh-mediated decays [23]. Finally, limits on phenomenological models are presented in Secs. X F–X H. For these models, the new searches presented in this article are not included, since they target very specific areas of parameter space and their sensitivity is small.

Exclusion limits are calculated by statistically combining results from a number of disjoint signal regions. In general, the analyses in Table XXIII are mutually exclusive by design (the exceptions are indicated in the table), using the lepton multiplicity and charge, and are statistically combined. Where overlapping signal regions exist within an analysis, the signal region with the best-expected exclusion is used. During the combinations, all experimental uncertainties are treated as correlated between regions and processes, with the exception of the experimental uncertainties on data-driven backgrounds, which are correlated between regions only. Theoretical uncertainties on the irreducible background and signal are treated as correlated between regions, while statistical uncertainties are treated as

TABLE XXIII. Searches used to probe each of the models described in Sec. II.

Model	Wh [23]	2ℓ [†][19]	2τ[*] [22]	3ℓ[◇] [20]	4ℓ [21]	2τ MVA[*]	SR2ℓ-1[†]	SS MVA [§]	SR3ℓ-0/1[◇]	SR2ℓ-2[§]
$\tilde{\tau}\tilde{\tau}$			√			√				
$\tilde{\chi}_1^+\tilde{\chi}_1^-$ via $\tilde{\ell}_L$ with $x = 0.5$		√					√			
$\tilde{\chi}_1^+\tilde{\chi}_1^-$ via $\tilde{\ell}_L$ with variable x		√								
$\tilde{\chi}_1^+\tilde{\chi}_1^-$ via WW		√								
$\tilde{\chi}_1^\pm\tilde{\chi}_1^\pm$ via VBF										√
$\tilde{\chi}_1^\pm\tilde{\chi}_2^0$ via $\tilde{\tau}_L$			√	√						
$\tilde{\chi}_1^\pm\tilde{\chi}_2^0$ via $\tilde{\ell}_L$ with $x = 0.5$				√				√	√	
$\tilde{\chi}_1^\pm\tilde{\chi}_2^0$ via $\tilde{\ell}_L$ with variable x				√						
$\tilde{\chi}_1^\pm\tilde{\chi}_2^0$ via WZ		√		√						
$\tilde{\chi}_1^\pm\tilde{\chi}_2^0$ via Wh	√	√		√						
$\tilde{\chi}_2^0\tilde{\chi}_3^0$ via $\tilde{\ell}_L$ with $x = 0.5$				√	√					
$\tilde{\chi}_2^0\tilde{\chi}_3^0$ via $\tilde{\ell}_L$ with variable x				√	√					
pMSSM	√	√		√						
NUHM2		√		√	√					
GMSB					√					

[†]The opposite-sign, two-lepton signal regions in Ref. [19] and Sec. VIII A overlap.
[*]The two-tau signal regions in Ref. [22] and Sec. VII overlap.
[◇]The three-lepton signal regions in Ref. [20] and Sec. VIII C overlap.
[§]The same-sign, two-lepton signal regions in Sec. VIII B and Sec. IX overlap.

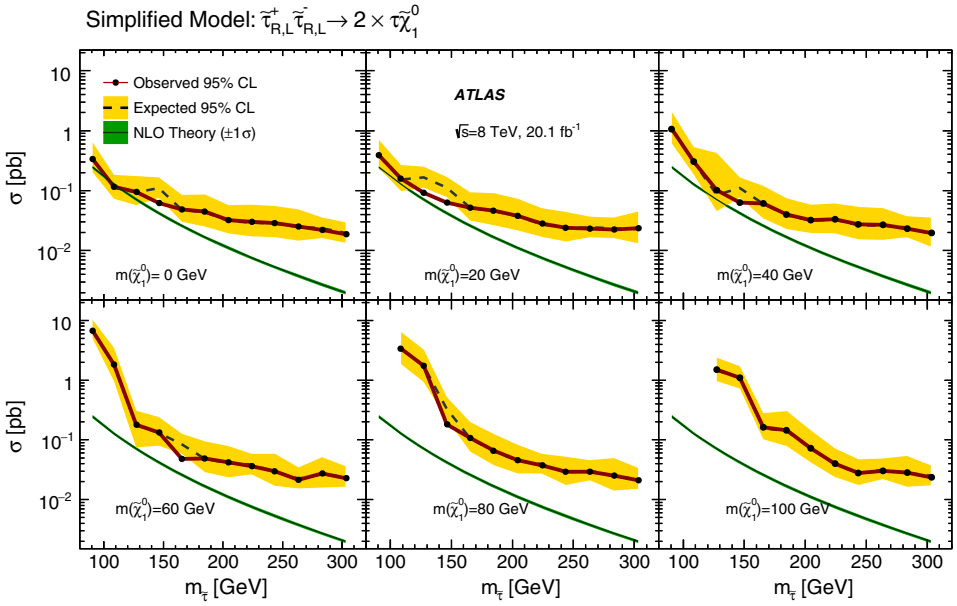

FIG. 12. The 95% CL exclusion limits on the cross section for production of left- and right-handed stau pairs for various $\tilde{\chi}^0_1$ masses. The NLO theoretical cross section for left- and right-handed stau pair production is also shown.

uncorrelated between regions and processes. For the exclusion limits, the observed and expected 95% CL limits are calculated using asymptotic formulas for each SUSY model point, taking into account the theoretical and experimental uncertainties on the SM background and the experimental uncertainties on the signal. Where the three-lepton [20] analysis is used in the combination, 95% CL limits are calculated using pseudoexperiments as the asymptotic approximation becomes inappropriate where the expected and observed yields are close to zero. The impact of the theoretical uncertainties on the signal cross section is shown for the observed mass limit; where quoted in the text, mass limits refer to the -1σ variation on the observed limit.

A. Direct stau production

The combination of the two-tau MVA results in Sec. VII with the simple cut-based analysis from Ref. [22] is used to set limits on the direct production of stau pairs. For each

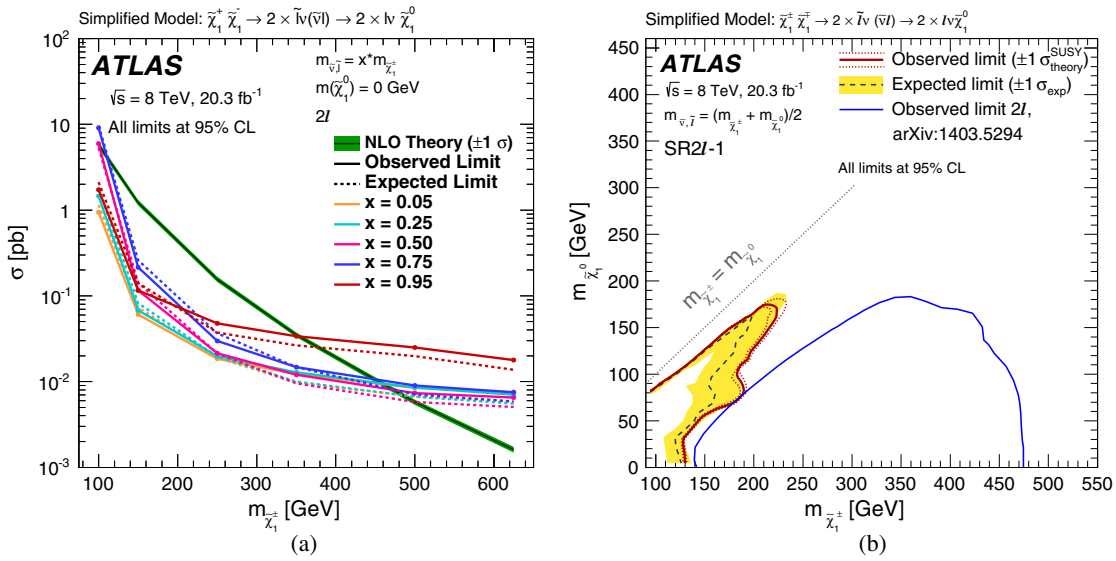

FIG. 13. The 95% CL exclusion limits on $\tilde{\chi}^+_1\tilde{\chi}^-_1$ production with $\tilde{\ell}_L$-mediated decays, (a) where the $\tilde{\chi}^0_1$ is massless and the intermediate slepton mass is set to 5%, 25%, 50%, 75%, and 95% of the $\tilde{\chi}^\pm_1$ mass, and (b) as a function of the $\tilde{\chi}^\pm_1$ and $\tilde{\chi}^0_1$ masses, where the slepton mass is halfway between the $\tilde{\chi}^0_2$ and $\tilde{\chi}^0_1$ masses. The limits in (a) are set using the 2ℓ analysis from Ref. [19], while the limits in (b) use the opposite-sign, two-lepton analysis from this article. The limit from Ref. [19] is also shown in (b).

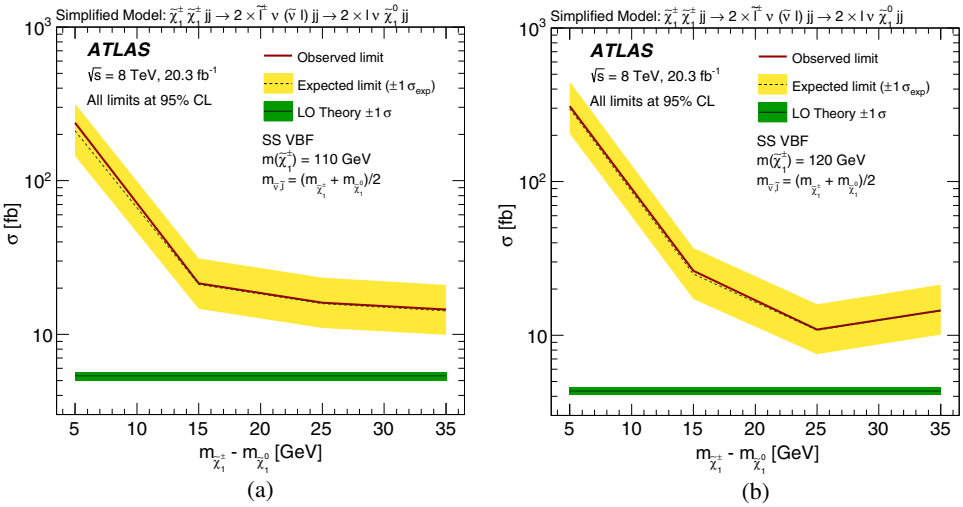

FIG. 14. The 95% CL upper limit on the signal cross section for VBF $\tilde{\chi}_1^\pm\tilde{\chi}_1^\pm$ production for (a) $m(\tilde{\chi}_1^\pm) = 110$ GeV and (b) $m(\tilde{\chi}_1^\pm) = 120$ GeV. The limits are set with respect to the mass difference between the $\tilde{\chi}_1^\pm$ and $\tilde{\chi}_1^0$, and use the results from the same-sign, two-lepton VBF analysis.

signal point, the signal region with the best expected limit is used. The upper limits on the cross section for direct stau production are shown in Fig. 12 for combined $\tilde{\tau}_L\tilde{\tau}_L$ and $\tilde{\tau}_R\tilde{\tau}_R$ production, where the observed limit is nearly always above the theoretical prediction. One scenario of combined $\tilde{\tau}_L\tilde{\tau}_L$ and $\tilde{\tau}_R\tilde{\tau}_R$ production is excluded, where the $\tilde{\tau}_R$ mass is 109 GeV and the $\tilde{\chi}_1^0$ is massless. For this scenario, cross sections above 0.115 pb are excluded, where the theoretical cross section at NLO is 0.128 pb. No scenarios can be excluded where only $\tilde{\tau}_R\tilde{\tau}_R$ production or $\tilde{\tau}_L\tilde{\tau}_L$ production is considered. Cross sections above 0.06 (0.21) pb are excluded for $\tilde{\tau}_R\tilde{\tau}_R$ ($\tilde{\tau}_L\tilde{\tau}_L$) production with a $\tilde{\tau}_R$ ($\tilde{\tau}_L$) mass of 109 GeV and a massless $\tilde{\chi}_1^0$, where the theoretical cross section at NLO is 0.04 (0.09) pb. For this scenario [$m(\tilde{\tau}_R) = 109$ GeV, $m(\tilde{\chi}_1^0) = 0$ GeV], the expected yields from $\tilde{\tau}_R\tilde{\tau}_R$ production are larger than from $\tilde{\tau}_L\tilde{\tau}_L$ in the signal region, making the experimental limits stronger for $\tilde{\tau}_R\tilde{\tau}_R$ production. However, for other mass points the experimental limit is generally weaker for $\tilde{\tau}_R\tilde{\tau}_R$ production due to

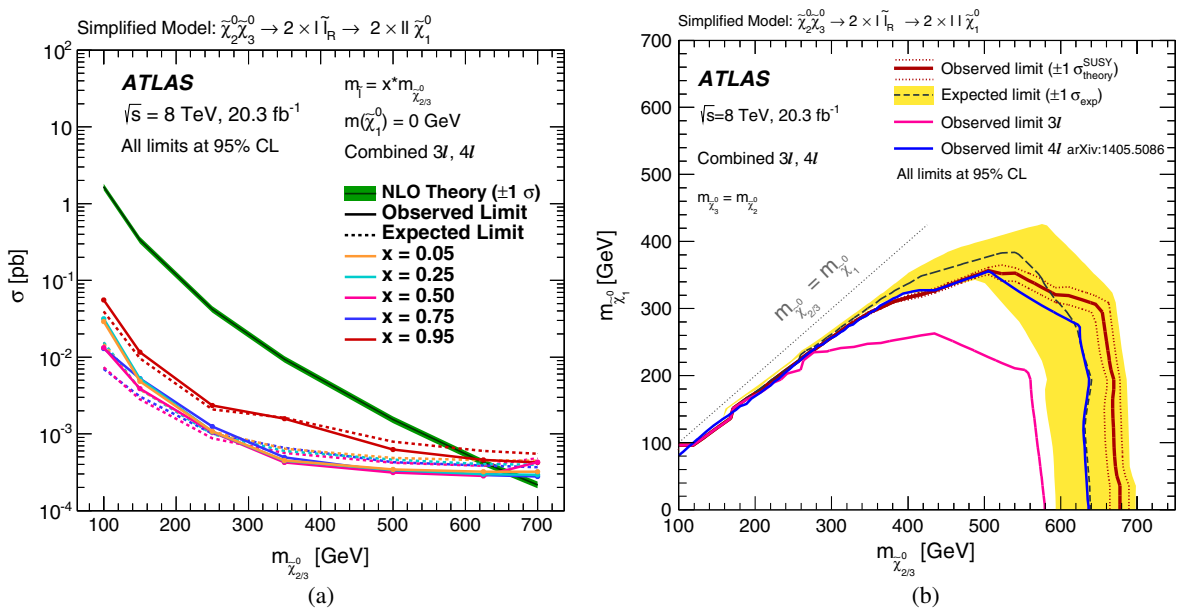

FIG. 15. The 95% CL exclusion limits on $\tilde{\chi}_2^0\tilde{\chi}_3^0$ production with $\tilde{\ell}_R$-mediated decays, (a) where the $\tilde{\chi}_1^0$ is massless and the intermediate slepton mass is set to 5%, 25%, 50%, 75%, and 95% of the $\tilde{\chi}_2^0$ mass, and (b) as a function of the $\tilde{\chi}_2^0$ and $\tilde{\chi}_1^0$ masses, where the slepton mass is halfway between the $\tilde{\chi}_2^0$ and $\tilde{\chi}_1^0$ masses. The limits in (a) and (b) are set using a combination of the 3ℓ analysis from Ref. [20] and the 4ℓ analysis from Ref. [21].

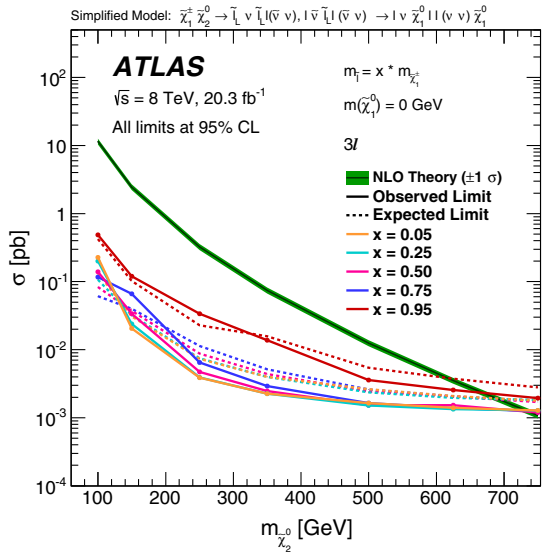

FIG. 16. The 95% CL upper cross-section limits on $\tilde{\chi}_1^\pm \tilde{\chi}_2^0$ production with $\tilde{\ell}_L$-mediated decays, where the $\tilde{\chi}_1^0$ is massless and the intermediate slepton mass is set to 5%, 25%, 50%, 75%, and 95% of the $\tilde{\chi}_1^\pm$ mass. The limits are set using the 3ℓ analysis from Ref. [20].

the lower production cross section. These limits on direct production of stau pairs improve upon the previous limits in Ref. [22], particularly for stau masses below ~150 GeV.

B. Direct chargino production

The opposite-sign, two-lepton analysis in Ref. [19] is used to reinterpret the limits on $\tilde{\chi}_1^+$ production decaying through sleptons, where the slepton mass is varied between the $\tilde{\chi}_1^\pm$ and $\tilde{\chi}_1^0$ masses. Scenarios where the slepton mass is 5%, 25%, 50%, 75%, and 95% of the $\tilde{\chi}_1^\pm$ mass are studied for a massless $\tilde{\chi}_1^0$, and the limits are shown in Fig. 13(a). For the majority of the $\tilde{\chi}_1^\pm$ masses considered, the slepton mass does not have a significant effect on the sensitivity, and $\tilde{\chi}_1^\pm$ masses are excluded up to ~500 GeV. The sensitivity is reduced for a very small mass splitting between the chargino and the slepton ($x = 0.95$), as in this case leptons from the $\tilde{\chi}_1^\pm \to \tilde{\nu}\ell$ decays have low momentum, making these events difficult to reconstruct in the two lepton final state.

Limits are also set in the $\tilde{\chi}_1^+ \tilde{\chi}_1^-$ scenario with $\tilde{\ell}_L$-mediated decays, with slepton masses set halfway between the $\tilde{\chi}_1^\pm$ and the $\tilde{\chi}_1^0$ masses, where both the $\tilde{\chi}_1^\pm$ and the $\tilde{\chi}_1^0$ masses are varied. Figure 13(b) shows the opposite-sign, two-lepton analysis presented in Sec. VIII A, which provides new sensitivity to compressed scenarios for $\tilde{\chi}_1^\pm$ masses below ~220 GeV. The 2ℓ analysis in Ref. [19] continues to dominate the sensitivity to scenarios with large mass splittings, excluding $\tilde{\chi}_1^\pm$ masses up to ~465 GeV.

The same-sign, two-lepton VBF analysis described in Sec. IX is used to set limits on VBF $\tilde{\chi}_1^\pm \tilde{\chi}_1^\pm$ production, where the $\tilde{\chi}_1^\pm$ decays through sleptons. Figures 14(a) and 14(b) show the 95% CL upper limits on the cross section for $m(\tilde{\chi}_1^\pm) = 110$ GeV and $m(\tilde{\chi}_1^\pm) = 120$ GeV, as a function of the mass splitting between the chargino and the neutralino. The best observed upper limit on the VBF $\tilde{\chi}_1^\pm \tilde{\chi}_1^\pm$ production cross section is found for a $\tilde{\chi}_1^\pm$ mass of 120 GeV and $m(\tilde{\chi}_1^\pm) - m(\tilde{\chi}_1^0) = 25$ GeV, where the theoretical cross section at LO is 4.33 fb and the excluded cross section is 10.9 fb. The sensitivity is slightly stronger for higher $\tilde{\chi}_1^\pm$ masses, since these scenarios were used for optimizing the signal selection.

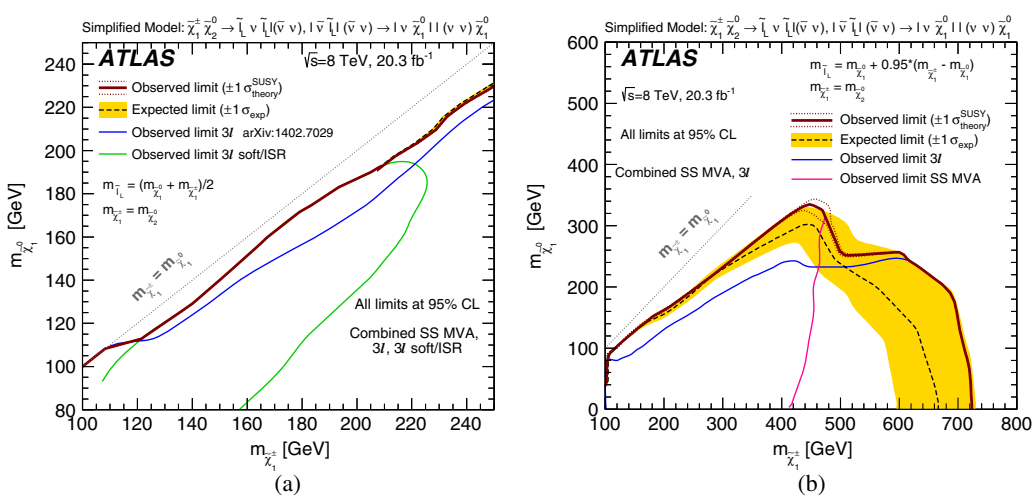

FIG. 17. The 95% CL exclusion limits on $\tilde{\chi}_1^\pm \tilde{\chi}_2^0$ production with $\tilde{\ell}_L$-mediated decays, as a function of the $\tilde{\chi}_1^\pm$ and $\tilde{\chi}_1^0$ masses, where the intermediate slepton mass is set to the $\tilde{\chi}_1^0$ mass plus (a) 50% or (b) 95% of the difference between the $\tilde{\chi}_1^\pm$ and the $\tilde{\chi}_1^0$ masses. The limits in (a) are set using a combination of the 3ℓ analysis from Ref. [20] and the same-sign, two-lepton analysis from this article, while the limits in (b) use the combination of the three-lepton and same-sign, two-lepton analyses from this article.

C. Direct neutralino production

The combination of the three-lepton analysis in Ref. [20] and four-lepton analysis in Ref. [21] is used to set limits on $\tilde{\chi}_2^0\tilde{\chi}_3^0$ production with $\tilde{\ell}_R$-mediated decays, where the slepton mass is varied between the $\tilde{\chi}_2^0$ and $\tilde{\chi}_1^0$ masses. Scenarios where the slepton mass is 5%, 25%, 50%, 75%, and 95% of the $\tilde{\chi}_2^0$ mass are studied for a massless $\tilde{\chi}_1^0$, and the limits are shown in Fig. 15(a). For the majority of $\tilde{\chi}_2^0$ masses considered, the slepton mass does not have a significant effect on the sensitivity, and $\tilde{\chi}_2^0$ masses are excluded up to ~600 GeV. The sensitivity is reduced for a very small mass splitting between the $\tilde{\chi}_2^0$ and slepton ($x = 0.95$) as the lepton produced in the $\tilde{\chi}_2^0 \to \ell\tilde{\ell}_R$ decay has low momentum. The reduced sensitivity is not seen for a very small mass splitting between the slepton and the LSP ($x = 0.05$) as the lepton produced in the $\tilde{\ell}_R \to \ell\tilde{\chi}_1^0$ decay can carry some of the momentum of the slepton.

Limits are also set in the $\tilde{\chi}_2^0\tilde{\chi}_3^0$ scenario with $\tilde{\ell}_R$-mediated decays, with slepton masses set halfway between the $\tilde{\chi}_2^0$ and the $\tilde{\chi}_1^0$ masses, where both the $\tilde{\chi}_2^0$ and the $\tilde{\chi}_1^0$ masses are varied. The combination of the three- and four-lepton analysis is again used here and limits are shown in Fig. 15(b), where $\tilde{\chi}_2^0$, $\tilde{\chi}_3^0$ masses up to 670 GeV are excluded, improving the previous limits by 30 GeV for $\tilde{\chi}_1^0$ masses below 200 GeV.

D. Direct neutralino-chargino production

The three-lepton analysis in Ref. [20] is used to reinterpret the limits on $\tilde{\chi}_1^\pm\tilde{\chi}_2^0$ production decaying through sleptons. Scenarios where the slepton mass is 5%, 25%, 50%, 75%, and 95% of the $\tilde{\chi}_1^\pm$ mass are studied for a massless $\tilde{\chi}_1^0$. The limits on these variable slepton mass scenarios are shown in Fig. 16. For the majority of $\tilde{\chi}_1^\pm$ masses considered, the slepton mass does not have a significant effect on the sensitivity, and $\tilde{\chi}_1^\pm$ masses are excluded up to ~700 GeV. The same reduction in sensitivity is seen for a small mass splitting between the $\tilde{\chi}_2^0$ and slepton ($x = 0.95$) as in the $\tilde{\chi}_2^0\tilde{\chi}_3^0$ interpretation in Sec. X C. For $\tilde{\chi}_1^\pm\tilde{\chi}_2^0$ production scenarios decaying through SM W, Z, or Higgs bosons [20], the results in Fig. 16 would be degraded due to lower branching fractions into leptonic final states. The pMSSM scenario in Sec. X F shows the sensitivity to SUSY scenarios without sleptons in the $\tilde{\chi}_1^\pm\tilde{\chi}_2^0$ decay chain.

Limits are also set in the $\tilde{\chi}_1^\pm\tilde{\chi}_2^0$ scenarios with $\tilde{\ell}_L$-mediated decays, with slepton masses set halfway and at 95% between the $\tilde{\chi}_1^\pm$ and the $\tilde{\chi}_1^0$ masses, where both the $\tilde{\chi}_1^\pm$ and the $\tilde{\chi}_1^0$ masses are varied. Figures 17(a) and 17(b) show that the combination of the published and new analyses gives an improved sensitivity to compressed scenarios up to $\tilde{\chi}_1^\pm$ masses of ~250 GeV. In scenarios with large mass splittings, $\tilde{\chi}_1^\pm$ masses are excluded up to ~700 GeV for slepton masses set to the $\tilde{\chi}_1^0$ mass plus 50% or 95% of the difference between the $\tilde{\chi}_1^\pm$ and the $\tilde{\chi}_1^0$ masses. In the compressed areas of the $\tilde{\chi}_1^\pm\tilde{\chi}_2^0$ scenario with $\tilde{\ell}_L$-mediated decays, and slepton masses set halfway (95%) between the $\tilde{\chi}_1^\pm$ and the $\tilde{\chi}_1^0$ masses, the three-lepton (same-sign, two-lepton) analysis has the strongest sensitivity.

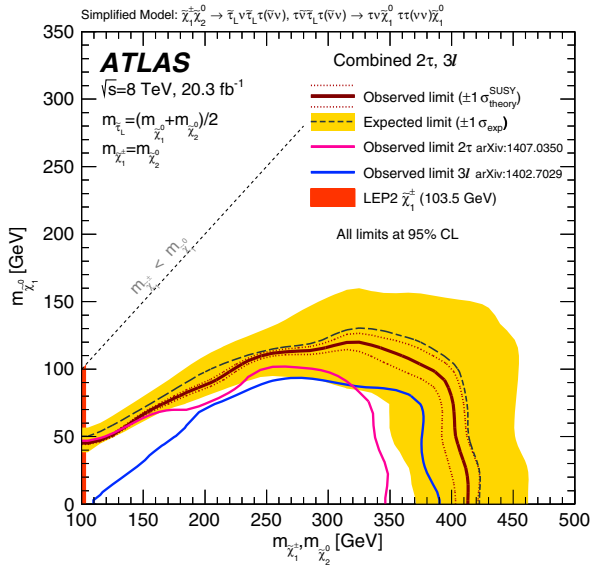

FIG. 18. The 95% CL exclusion limits on $\tilde{\chi}_1^\pm\tilde{\chi}_2^0$ production with $\tilde{\tau}$-mediated decays, as a function of the $\tilde{\chi}_1^\pm$ and $\tilde{\chi}_1^0$ masses. The limits are set using a combination of the 3ℓ analysis from Ref. [20] and the 2τ analysis from Ref. [22].

Finally, limits are set in the $\tilde{\chi}_1^\pm\tilde{\chi}_2^0$ scenario with $\tilde{\tau}$-mediated decays, using combined results from the two-tau analysis in Ref. [22] and the three-lepton analysis in Ref. [20]. Figure 18 shows that the sensitivity to large $\tilde{\chi}_1^\pm$ masses is improved by 20 GeV with the new combination, where $\tilde{\chi}_1^\pm$ masses are excluded up to ~400 GeV for massless $\tilde{\chi}_1^0$.

E. Summary of simplified electroweakino production

The ATLAS results for electroweakino searches at 8 TeV in the framework of simplified models are summarized in Figs. 19(a) and 19(b) in the $m(\tilde{\chi}_1^\pm,\tilde{\chi}_2^0)$-$m(\tilde{\chi}_1^0)$ plane. As explained in Sec. II, each of the $\tilde{\chi}_1^\pm/\tilde{\chi}_2^0/\tilde{\chi}_3^0$ decays considered in the plot is assumed to have a 100% branching fraction, and the production cross section is for pure wino $\tilde{\chi}_1^+\tilde{\chi}_1^-$ and $\tilde{\chi}_1^\pm\tilde{\chi}_2^0$, and pure higgsino $\tilde{\chi}_2^0\tilde{\chi}_3^0$. The limits for $\tilde{\chi}_1^+\tilde{\chi}_1^-$ and $\tilde{\chi}_1^\pm\tilde{\chi}_2^0$ production with decays mediated by SM bosons are summarized in Fig. 19(a). All of the limits are from the two-lepton, three-lepton, and Wh analyses from Refs. [19,20,23]. The new analyses targeting compressed spectra presented in this article have only a small sensitivity to these scenarios and did not significantly improve upon published limits. The limits for $\tilde{\chi}_1^+\tilde{\chi}_1^-$, $\tilde{\chi}_1^\pm\tilde{\chi}_2^0$, and $\tilde{\chi}_2^0\tilde{\chi}_3^0$ production with $\tilde{\ell}$-mediated decays are

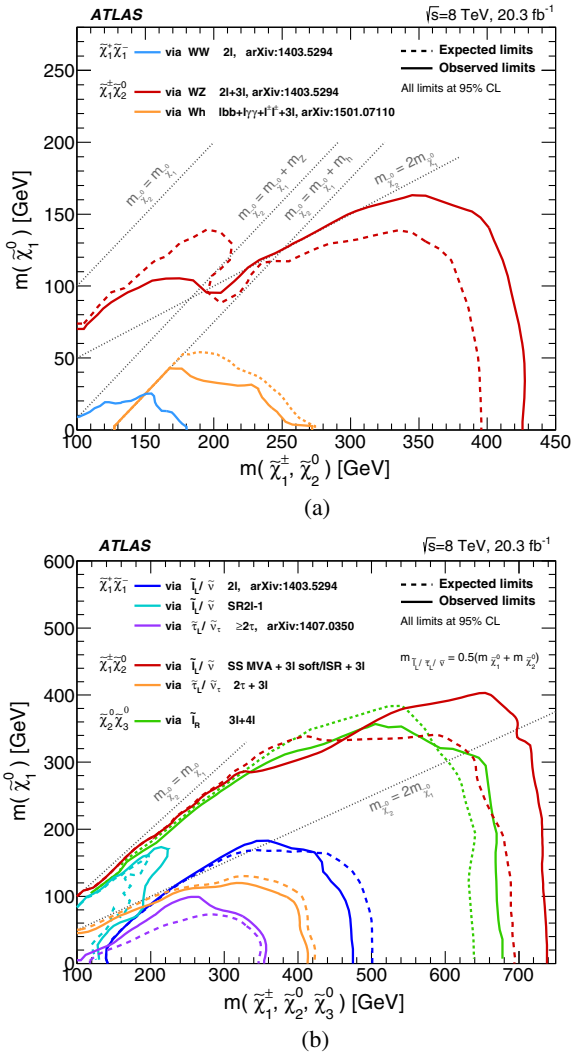

FIG. 19. The 95% CL exclusion limits on $\tilde{\chi}_1^+\tilde{\chi}_1^-$, $\tilde{\chi}_1^\pm\tilde{\chi}_2^0$, and $\tilde{\chi}_2^0\tilde{\chi}_3^0$ production with (a) SM-boson-mediated decays and (b) $\tilde{\ell}$-mediated decays, as a function of the $\tilde{\chi}_1^\pm$, $\tilde{\chi}_2^0$, and $\tilde{\chi}_1^0$ masses. The production cross section is for pure wino $\tilde{\chi}_1^+\tilde{\chi}_1^-$ and $\tilde{\chi}_1^\pm\tilde{\chi}_2^0$, and pure higgsino $\tilde{\chi}_2^0\tilde{\chi}_3^0$.

summarized in Fig. 19(b). The limits are from the new analyses in Secs. X B–X D and the previously published analyses.

F. pMSSM

The two-lepton, three-lepton, and Wh analyses from Refs. [19,20,23] are combined to improve the sensitivity in the considered pMSSM scenario where the EW SUSY production and the decays through W, Z, or h bosons are dominant. The 95% CL exclusion in the pMSSM $\mu - M_2$ plane for the scenario of heavy sleptons, $\tan\beta = 10$, and $M_1 = 50$ GeV is shown in Fig. 20. Including the Wh analysis in the new combination results in a stronger limit at high values of M_2, in particular in the intermediate μ region.

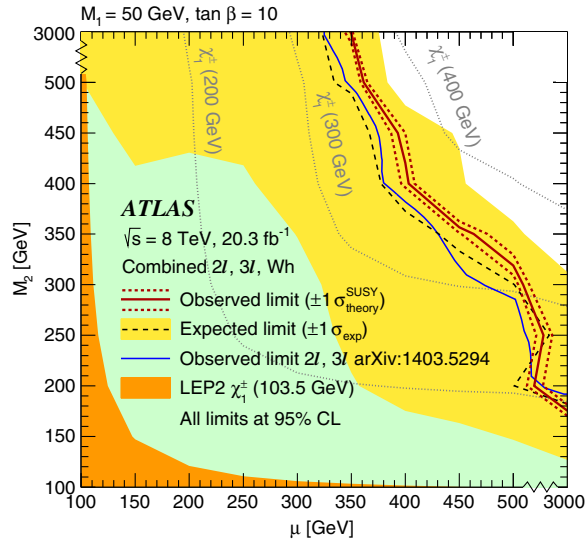

FIG. 20. The 95% CL exclusion limit in the pMSSM scenario, using a combination of the 2ℓ and 3ℓ analyses from Ref. [19] and the Wh analysis from Ref. [23]. The areas excluded by the -1σ expected limit are shown in green. The blue contour corresponds to the limits from the combination of the 2ℓ and 3ℓ analyses from Ref. [19]. The grey dotted contours show the chargino mass isolines.

G. NUHM2

The two-, three-, and four-lepton analyses from Refs. [19–21] are combined to set limits in a new interpretation for the NUHM2 model. The 95% CL exclusion in the NUHM2 $m_{1/2} - \mu$ plane is shown in Fig. 21, where the three-lepton analysis offers the best sensitivity

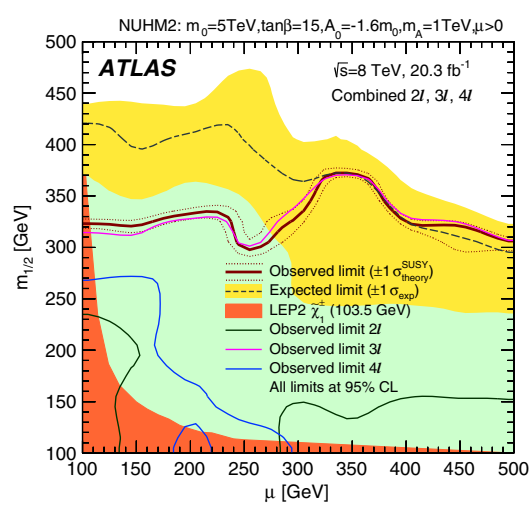

FIG. 21. The 95% CL exclusion limit in the NUHM2 scenario, using a combination of the 2ℓ, 3ℓ, and 4ℓ analyses from Refs. [19–21]. The areas excluded by the -1σ expected limit are shown in green. The black, pink, and blue contours correspond to the limits from the 2ℓ, 3ℓ, and 4ℓ analyses, respectively.

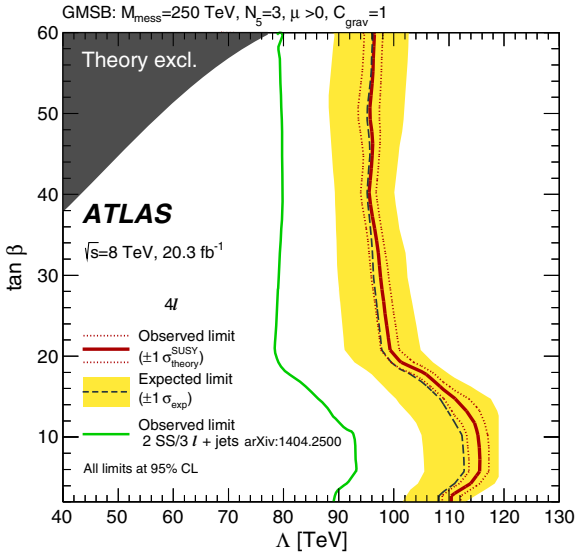

FIG. 22. The 95% CL exclusion limit in the GMSB scenario, using the 4ℓ analysis from Ref. [21]. The green contour corresponds to the limit from the $2SS/3\ell + \text{jets}$ analysis from Ref. [119].

and drives the combined limit. The results in the three-lepton signal regions lead to a weaker observed exclusion than expected for the compressed scenarios in the high-$m_{1/2}$, low-μ region. In general, $m_{1/2}$ values up to 300 GeV are excluded in the NUHM2 model.

H. GMSB

The four-lepton analysis from Ref. [21] is reinterpreted in the GMSB model described in Sec. II. The 95% CL exclusion in the GMSB Λ-$\tan\beta$ plane is shown in Fig. 22, where Λ values up to 94 TeV are excluded for all values of $\tan\beta$. For $\tan\beta = 10$, Λ values below 113 TeV are excluded. These results improve upon the previous limit in Ref. [119] by 20 TeV (15 TeV) in the low (high) $\tan\beta$ region.

XI. CONCLUSION

This article summarizes and extends the search for the production of electroweak SUSY particles using 20 fb^{-1} of $\sqrt{s} = 8$ TeV pp collision data collected with the ATLAS detector at the LHC. New analyses targeting scenarios with compressed mass spectra, VBF production of charginos and neutralinos, and the direct production of stau pairs provide sensitivity to EW SUSY scenarios not optimally covered in previous publications. The new and previous results are combined to set exclusion limits in a wide range of simplified and phenomenological SUSY models. For $\tilde{\chi}_1^+\tilde{\chi}_1^-$ production with $\tilde{\ell}_L$-mediated decays, $\tilde{\chi}_1^\pm$ with masses up to ~500 GeV are excluded. In the $\tilde{\chi}_1^\pm\tilde{\chi}_2^0$ and $\tilde{\chi}_2^0\tilde{\chi}_3^0$ scenarios with $\tilde{\ell}_L$-mediated decays, $\tilde{\chi}_1^\pm$ and $\tilde{\chi}_2^0$ masses are excluded up to 700 GeV and 670 GeV, respectively. For all three $\tilde{\ell}_L$-mediated decay scenarios, the value of the slepton mass is not seen to have a significant effect on the sensitivity. Exclusions are also set in pMSSM, NUHM2, and GMSB models, improving upon previous limits.

ACKNOWLEDGMENTS

We thank CERN for the very successful operation of the LHC, as well as the support staff from our institutions without whom ATLAS could not be operated efficiently. We thank Sabine Kraml for her advice while preparing the model files of the NUHM2 grid. We acknowledge the support of ANPCyT, Argentina; YerPhI, Armenia; ARC, Australia; BMWFW and FWF, Austria; ANAS, Azerbaijan; SSTC, Belarus; CNPq and FAPESP, Brazil; NSERC, NRC, and CFI, Canada; CERN; CONICYT, Chile; CAS, MOST, and NSFC, China; COLCIENCIAS, Colombia; MSMT CR, MPO CR, and VSC CR, Czech Republic; DNRF, DNSRC, and Lundbeck Foundation, Denmark; EPLANET, ERC, and NSRF, European Union; IN2P3-CNRS, CEA-DSM/IRFU, France; GNSF, Georgia; BMBF, DFG, HGF, MPG, and AvH Foundation, Germany; GSRT and NSRF, Greece; RGC, Hong Kong SAR, China; ISF, MINERVA, GIF, I-CORE, and Benoziyo Center, Israel; INFN, Italy; MEXT and JSPS, Japan; CNRST, Morocco; FOM and NWO, Netherlands; BRF and RCN, Norway; MNiSW and NCN, Poland; GRICES and FCT, Portugal; MNE/IFA, Romania; MES of Russia and NRC KI, Russian Federation; JINR; MSTD, Serbia; MSSR, Slovakia; ARRS and MIZŠ, Slovenia; DST/NRF, South Africa; MINECO, Spain; SRC and Wallenberg Foundation, Sweden; SER, SNSF, and Cantons of Bern and Geneva, Switzerland; NSC, Taiwan; TAEK, Turkey; STFC, the Royal Society and Leverhulme Trust, United Kingdom; DOE and NSF, United States of America. The crucial computing support from all WLCG partners is acknowledged gratefully, in particular from CERN and the ATLAS Tier-1 facilities at TRIUMF (Canada), NDGF (Denmark, Norway, Sweden), CC-IN2P3 (France), KIT/GridKA (Germany), INFN-CNAF (Italy), NL-T1 (Netherlands), PIC (Spain), ASGC (Taiwan), RAL (UK), and BNL (USA) and in the Tier-2 facilities worldwide.

APPENDIX: CROSS-SECTION CALCULATION FOR THE SAME-SIGN CHARGINO-PAIR PRODUCTION VIA VECTOR-BOSON FUSION

The cross sections for same-sign chargino-pair production via vector-boson fusion (including radiative processes) are calculated to LO in the strong coupling constant using MadGraph 5-1.3.33 [57]. The default

value of 99 is used for the maximum number of QCD and QED couplings. Same-sign chargino pairs are generated in association with two additional partons with $|\eta| < 5$ and no p_T requirement. No jet-parton matching is performed. All SUSY particles, except for the $\tilde{\chi}_1^{\pm}$, $\tilde{\chi}_1^0$, $\tilde{\chi}_2^0$, $\tilde{\ell}$, and $\tilde{\nu}$, are decoupled by setting their physical masses to ~100 TeV. The $\tilde{\chi}_1^{\pm}$ and $\tilde{\chi}_2^0$ are assumed to be mass degenerate. The sleptons are assumed to be mass degenerate with sneutrinos and have masses set halfway between $\tilde{\chi}_1^{\pm}$ and $\tilde{\chi}_1^0$ masses. Cross sections are also calculated using MadGraph 5-2.2.3 and are in agreement with those calculated using MadGraph 5-1.3.33. Details from the "`proc_card.dat`" are provided below.

```
import model mssm
define p=g u c d s u~ c~ d~ s~
define j=g u c d s u~ c~ d~ s~
define l+=e+ mu+
define l-=e- mu-
define vl=ve vm vt
define vl~ = ve~ vm~ vt~
generate   pp>x1+x1+jj@1
addprocess pp>x1-x1-jj@2
output -f
```


[1] H. Miyazawa, Prog. Theor. Phys. **36**, 1266 (1966).
[2] P. Ramond, Phys. Rev. D **3**, 2415 (1971).
[3] Y. A. Gol'fand and E. P. Likhtman, JETP Lett. **13**, 323 (1971).
[4] A. Neveu and J. H. Schwarz, Nucl. Phys. **B31**, 86 (1971).
[5] A. Neveu and J. H. Schwarz, Phys. Rev. D **4**, 1109 (1971).
[6] J. Gervais and B. Sakita, Nucl. Phys. **B34**, 632 (1971).
[7] D. V. Volkov and V. P. Akulov, Phys. Lett. **46B**, 109 (1973).
[8] J. Wess and B. Zumino, Phys. Lett. **49B**, 52 (1974).
[9] J. Wess and B. Zumino, Nucl. Phys. **B70**, 39 (1974).
[10] S. Weinberg, Phys. Rev. D **13**, 974 (1976).
[11] E. Gildener, Phys. Rev. D **14**, 1667 (1976).
[12] S. Weinberg, Phys. Rev. D **19**, 1277 (1979).
[13] L. Susskind, Phys. Rev. D **20**, 2619 (1979).
[14] P. Fayet, Phys. Lett. **64B**, 159 (1976).
[15] P. Fayet, Phys. Lett. **69B**, (1977) 489.
[16] G. R. Farrar and P. Fayet, Phys. Lett. **76B**, 575 (1978).
[17] P. Fayet, Phys. Lett. **84B**, 416 (1979).
[18] S. Dimopoulos and H. Georgi, Nucl. Phys. **B193**, 150 (1981).
[19] ATLAS Collaboration, J. High Energy Phys. 05 (2014) 071.
[20] ATLAS Collaboration, J. High Energy Phys. 04 (2014) 169.
[21] ATLAS Collaboration, Phys. Rev. D **90**, 052001 (2014).
[22] ATLAS Collaboration, J. High Energy Phys. 10 (2014) 96.
[23] ATLAS Collaboration, Eur. Phys. J. C **75**, 208 (2015).
[24] Z. Han, G. D. Kribs, A. Martin, and A. Menon, Phys. Rev. D **89**, 075007 (2014).
[25] R. Barbieri and G. Giudice, Nucl. Phys. **B306**, 63 (1988).
[26] B. de Carlos and J. A. Casas, Phys. Lett. B **309**, 320 (1993).
[27] A. G. Delannoy *et al.*, arXiv:1308.0355.
[28] K. Griest and D. Seckel, Phys. Rev. D **43**, 3191 (1991).
[29] G. Hinshaw *et al.*, Astrophys. J. Suppl. Ser. **208**, 19 (2013).
[30] V. Abazov *et al.* (D0 Collaboration), Phys. Lett. B **680**, 34 (2009).
[31] T. Aaltonen *et al.* (CDF Collaboration), Phys. Rev. Lett. **101**, 251801 (2008).
[32] CMS Collaboration, Phys. Rev. D **90**, 092007 (2014).
[33] CMS Collaboration, Eur. Phys. J. C **74**, 3036 (2014).
[34] CMS Collaboration, J. High Energy Phys. 11 (2015) 189.
[35] The LEP SUSY Working Group and the ALEPH, DELPHI, L3 and OPAL experiments, notes LEPSUSYWG/01-03.1, 04-01.1, http://lepsusy.web.cern.ch/lepsusy/Welcome.html.
[36] S. Schael *et al.* (ALEPH Collaboration), Phys. Lett. B **583**, 247 (2004).
[37] J. Abdallah *et al.* (DELPHI Collaboration), Eur. Phys. J. C **31**, 421 (2003).
[38] M. Acciarri *et al.* (L3 Collaboration), Phys. Lett. B **472**, 420 (2000).
[39] G. Abbiendi *et al.* (OPAL Collaboration), Eur. Phys. J. C **35**, 1 (2004).
[40] J. Alwall, P. C. Schuster, and N. Toro, Phys. Rev. D **79**, 075020 (2009).
[41] A. Djouadi *et al.*, arXiv:hep-ph/9901246.
[42] J. R. Ellis, T. Falk, K. A. Olive, and Y. Santoso, Nucl. Phys. **B652**, 259 (2003).
[43] J. R. Ellis, K. A. Olive, and Y. Santoso, Phys. Lett. B **539**, 107 (2002).
[44] M. Dine and W. Fischler, Phys. Lett. **110B**, 227 (1982).
[45] L. Alvarez-Gaume, M. Claudson, and M. B. Wise, Nucl. Phys. **B207**, 96 (1982).
[46] C. R. Nappi and B. A. Ovrut, Phys. Lett. **113B**, 175 (1982).
[47] M. Dine and A. E. Nelson, Phys. Rev. D **48**, 1277 (1993).
[48] M. Dine, A. E. Nelson, and Y. Shirman, Phys. Rev. D **51**, 1362 (1995).
[49] M. Dine, A. E. Nelson, Y. Nir, and Y. Shirman, Phys. Rev. D **53**, 2658 (1996).
[50] W. Beenakker, R. Höpker, M. Spira, and P. M. Zerwas, Nucl. Phys. **B492**, 51 (1997).
[51] B. Fuks, M. Klasen, D. R. Lamprea, and M. Rothering, J. High Energy Phys. 10 (2012) 081.
[52] B. Fuks, M. Klasen, D. R. Lamprea, and M. Rothering, Eur. Phys. J. C **73**, 2480 (2013).
[53] B. Fuks, M. Klasen, D. R. Lamprea, and M. Rothering, J. High Energy Phys. 01 (2014) 168.

[54] M. Krämer *et al.*, arXiv:1206.2892.
[55] G.-C. Cho, K. Hagiwara, J. Kanzaki, T. Plehn, D. Rainwater, and T. Stelzer, Phys. Rev. D **73**, 054002 (2006).
[56] B. Dutta, A. Gurrola, W. Johns, T. Kamon, P. Sheldon, and K. Sinha, Phys. Rev. D **87**, 035029 (2013).
[57] J. Alwall, P. Demin, S. de Visscher, R. Frederix, M. Herquet, F. Maltoni, T. Plehn, D. L. Rainwater, and T. Stelzer, J. High Energy Phys. 09 (2007) 028.
[58] J. Alwall, R. Frederix, S. Frixione, V. Hirschi, F. Maltoni, O. Mattelaer, H.-S. Shao, T. Stelzer, P. Torrielli, and M. Zaro, J. High Energy Phys. 07 (2014) 079.
[59] H. Baer, V. Barger, P. Huang, D. Mickelson, A. Mustafayev, W. Sreethawong, and X. Tata, J. High Energy Phys. 12 (2013) 013.
[60] ATLAS Collaboration, JINST **3**, S08003 (2008).
[61] ATLAS Collaboration, Eur. Phys. J. C **72**, 1849 (2012).
[62] P. Nason, J. High Energy Phys. 11 (2004) 040.
[63] S. Frixione, P. Nason, and C. Oleari, J. High Energy Phys. 11 (2007) 070.
[64] T. Sjöstrand, S. Mrenna, and P. Z. Skands, J. High Energy Phys. 05 (2006) 026.
[65] J. M. Campbell and R. K. Ellis, Phys. Rev. D **60**, 113006 (1999).
[66] J. M. Campbell, R. K. Ellis, and C. Williams, J. High Energy Phys. 07 (2011) 018.
[67] ATLAS Collaboration, Report No. ATL-PHYS-PUB-2012-003 (2012), http://cdsweb.cern.ch/record/1474107.
[68] H.-L. Lai, M. Guzzi, J. Huston, Z. Li, P. M. Nadolsky, J. Pumplin, and C.-P. Yuan, Phys. Rev. D **82**, 074024 (2010).
[69] T. Gleisberg, S. Höche, F. Krauss, M. Schönherr, S. Schumann, F. Siegert, and J. Winter, J. High Energy Phys. 02 (2009) 007.
[70] N. Kauer and G. Passarino, J. High Energy Phys. 08 (2012) 116.
[71] ATLAS Collaboration, Report No. ATL-PHYS-PUB-2011-009 (2011), http://cdsweb.cern.ch/record/1363300.
[72] F. Campanario, V. Hankele, C. Oleari, S. Prestel, and D. Zeppenfeld, Phys. Rev. D **78**, 094012 (2008).
[73] J. Pumplin, D. R. Stump, J. Huston, H.-L. Lai, P. Nadolsky, and W.-K. Tung, J. High Energy Phys. 07 (2002) 012.
[74] S. Dittmaier *et al.*, arXiv:1201.3084.
[75] M. L. Mangano, F. Piccinini, A. D. Polosa, M. Moretti, and R. Pittau, J. High Energy Phys. 07 (2003) 001.
[76] A. Kardos, Z. Trócsányi, and C. G. Papadopoulos, Phys. Rev. D **85**, 054015 (2012).
[77] J. M. Campbell and R. K. Ellis, J. High Energy Phys. 07 (2012) 052.
[78] M. Cacciari, M. Czakon, M. Mangano, A. Mitov, and P. Nason, Phys. Lett. B **710**, 612 (2012).
[79] P. Bärnreuther, M. Czakon, and A. Mitov, Phys. Rev. Lett. **109**, 132001 (2012).
[80] M. Czakon and A. Mitov, J. High Energy Phys. 12 (2012) 054.
[81] M. Czakon and A. Mitov, J. High Energy Phys. 01 (2013) 080.
[82] M. Czakon, P. Fiedler, and A. Mitov, Phys. Rev. Lett. **110**, 252004 (2013).
[83] M. Czakon and A. Mitov, Comput. Phys. Commun. **185**, 2930 (2014).
[84] P. Z. Skands, Phys. Rev. D **82**, 074018 (2010).
[85] B. P. Kersevan and E. Richter-Was, Comput. Phys. Commun. **184**, 919 (2013).
[86] N. Kidonakis, Phys. Rev. D **83**, 091503 (2011).
[87] S. Frixione, E. Laenen, P. Motylinski, and B. R. Webber, J. High Energy Phys. 03 (2006) 092.
[88] S. Frixione, E. Laenen, P. Motylinski, C. White, and B. R. Webber, J. High Energy Phys. 07 (2008) 029.
[89] N. Kidonakis, Phys. Rev. D **81**, 054028 (2010).
[90] N. Kidonakis, Phys. Rev. D **82**, 054018 (2010).
[91] J. Campbell, R. K. Ellis, and R. Rontsch, Phys. Rev. D **87**, 114006 (2013).
[92] S. Catani, L. Cieri, G. Ferrera, D. de Florian, and M. Grazzini, Phys. Rev. Lett. **103**, 082001 (2009).
[93] A. D. Martin, W. J. Stirling, R. S. Thorne, and G. Watt, Eur. Phys. J. C **63**, 189 (2009).
[94] M. Bähr *et al.*, Eur. Phys. J. C **58**, 639 (2008).
[95] S. Gieseke and A. Rohr, Eur. Phys. J. C **72**, 2225 (2012).
[96] S. Agostinelli *et al.*, Nucl. Instrum. Methods Phys. Res., Sect. A **506**, 250 (2003).
[97] ATLAS Collaboration, Eur. Phys. J. C **70**, 823 (2010).
[98] ATLAS Collaboration, Report No. ATL-PHYS-PUB-2010-013 (2010), http://cdsweb.cern.ch/record/1300517.
[99] ATLAS Collaboration, Eur. Phys. J. C **74**, 3071 (2014).
[100] ATLAS Collaboration, Eur. Phys. J. C **74**, 3130 (2014).
[101] M. Cacciari, G. P. Salam, and G. Soyez, J. High Energy Phys. 04 (2008) 063.
[102] ATLAS Collaboration, Eur. Phys. J. C **75**, 17 (2015).
[103] ATLAS Collaboration, Eur. Phys. J. C **73**, 2305 (2013).
[104] ATLAS Collaboration, Report No. ATLAS-CONF-2014-004 (2014), http://cdsweb.cern.ch/record/1664335.
[105] ATLAS Collaboration, Eur. Phys. J. C **75**, 303 (2015).
[106] ATLAS Collaboration, Eur. Phys. J. C **72**, 1844 (2012).
[107] M. Baak, G. J. Besjes, D. Côté, A. Koutsman, J. Lorenz, and D. Short, Eur. Phys. J. C **75**, 153 (2015).
[108] A. L. Read, J. Phys. G **28**, 2693 (2002).
[109] C. Lester and D. Summers, Phys. Lett. B **463**, 99 (1999).
[110] A. Barr, C. Lester, and P. Stephens, J. Phys. G **29**, 2343 (2003).
[111] M. R. Buckley, J. D. Lykken, C. Rogan, and M. Spiropulu, Phys. Rev. D **89**, 055020 (2014).
[112] ATLAS Collaboration, Eur. Phys. J. C **71**, 1577 (2011).
[113] ATLAS Collaboration, Eur. Phys. J. C **73**, 2518 (2013).
[114] J. Alwall *et al.*, Eur. Phys. J. C **53**, 473 (2008).
[115] ATLAS Collaboration, Eur. Phys. J. C **72**, 2043 (2012).
[116] ATLAS Collaboration, Phys. Rev. D **92**, 012006 (2015).
[117] S. Alioli, P. Nason, C. Oleari, and E. Re, J. High Energy Phys. 06 (2010) 043.
[118] K. Arnold *et al.*, arXiv:1107.4038.
[119] ATLAS Collaboration, J. High Energy Phys. 06 (2014) 035.

G. Aad,[85] B. Abbott,[113] J. Abdallah,[151] O. Abdinov,[11] R. Aben,[107] M. Abolins,[90] O. S. AbouZeid,[158] H. Abramowicz,[153] H. Abreu,[152] R. Abreu,[116] Y. Abulaiti,[146a,146b] B. S. Acharya,[164a,164b,a] L. Adamczyk,[38a] D. L. Adams,[25] J. Adelman,[108] S. Adomeit,[100] T. Adye,[131] A. A. Affolder,[74] T. Agatonovic-Jovin,[13] J. Agricola,[54] J. A. Aguilar-Saavedra,[126a,126f] S. P. Ahlen,[22] F. Ahmadov,[65,b] G. Aielli,[133a,133b] H. Akerstedt,[146a,146b] T. P. A. Åkesson,[81] A. V. Akimov,[96] G. L. Alberghi,[20a,20b] J. Albert,[169] S. Albrand,[55] M. J. Alconada Verzini,[71] M. Aleksa,[30] I. N. Aleksandrov,[65] C. Alexa,[26b] G. Alexander,[153] T. Alexopoulos,[10] M. Alhroob,[113] G. Alimonti,[91a] L. Alio,[85] J. Alison,[31] S. P. Alkire,[35] B. M. M. Allbrooke,[149] P. P. Allport,[18] A. Aloisio,[104a,104b] A. Alonso,[36] F. Alonso,[71] C. Alpigiani,[138] A. Altheimer,[35] B. Alvarez Gonzalez,[30] D. Álvarez Piqueras,[167] M. G. Alviggi,[104a,104b] B. T. Amadio,[15] K. Amako,[66] Y. Amaral Coutinho,[24a] C. Amelung,[23] D. Amidei,[89] S. P. Amor Dos Santos,[126a,126c] A. Amorim,[126a,126b] S. Amoroso,[48] N. Amram,[153] G. Amundsen,[23] C. Anastopoulos,[139] L. S. Ancu,[49] N. Andari,[108] T. Andeen,[35] C. F. Anders,[58b] G. Anders,[30] J. K. Anders,[74] K. J. Anderson,[31] A. Andreazza,[91a,91b] V. Andrei,[58a] S. Angelidakis,[9] I. Angelozzi,[107] P. Anger,[44] A. Angerami,[35] F. Anghinolfi,[30] A. V. Anisenkov,[109,c] N. Anjos,[12] A. Annovi,[124a,124b] M. Antonelli,[47] A. Antonov,[98] J. Antos,[144b] D. J. Antrim,[163] F. Anulli,[132a] M. Aoki,[66] L. Aperio Bella,[18] G. Arabidze,[90] Y. Arai,[66] J. P. Araque,[126a] A. T. H. Arce,[45] F. A. Arduh,[71] J-F. Arguin,[95] S. Argyropoulos,[63] M. Arik,[19a] A. J. Armbruster,[30] O. Arnaez,[30] H. Arnold,[48] M. Arratia,[28] O. Arslan,[21] A. Artamonov,[97] G. Artoni,[23] S. Asai,[155] N. Asbah,[42] A. Ashkenazi,[153] B. Åsman,[146a,146b] L. Asquith,[149] K. Assamagan,[25] R. Astalos,[144a] M. Atkinson,[165] N. B. Atlay,[141] K. Augsten,[128] M. Aurousseau,[145b] G. Avolio,[30] B. Axen,[15] M. K. Ayoub,[117] G. Azuelos,[95,d] M. A. Baak,[30] A. E. Baas,[58a] M. J. Baca,[18] C. Bacci,[134a,134b] H. Bachacou,[136] K. Bachas,[154] M. Backes,[30] M. Backhaus,[30] P. Bagiacchi,[132a,132b] P. Bagnaia,[132a,132b] Y. Bai,[33a] T. Bain,[35] J. T. Baines,[131] O. K. Baker,[176] E. M. Baldin,[109,c] P. Balek,[129] T. Balestri,[148] F. Balli,[84] W. K. Balunas,[122] E. Banas,[39] Sw. Banerjee,[173] A. A. E. Bannoura,[175] L. Barak,[30] E. L. Barberio,[88] D. Barberis,[50a,50b] M. Barbero,[85] T. Barillari,[101] M. Barisonzi,[164a,164b] T. Barklow,[143] N. Barlow,[28] S. L. Barnes,[84] B. M. Barnett,[131] R. M. Barnett,[15] Z. Barnovska,[5] A. Baroncelli,[134a] G. Barone,[23] A. J. Barr,[120] F. Barreiro,[82] J. Barreiro Guimarães da Costa,[57] R. Bartoldus,[143] A. E. Barton,[72] P. Bartos,[144a] A. Basalaev,[123] A. Bassalat,[117] A. Basye,[165] R. L. Bates,[53] S. J. Batista,[158] J. R. Batley,[28] M. Battaglia,[137] M. Bauce,[132a,132b] F. Bauer,[136] H. S. Bawa,[143,e] J. B. Beacham,[111] M. D. Beattie,[72] T. Beau,[80] P. H. Beauchemin,[161] R. Beccherle,[124a,124b] P. Bechtle,[21] H. P. Beck,[17,f] K. Becker,[120] M. Becker,[83] M. Beckingham,[170] C. Becot,[117] A. J. Beddall,[19b] A. Beddall,[19b] V. A. Bednyakov,[65] C. P. Bee,[148] L. J. Beemster,[107] T. A. Beermann,[30] M. Begel,[25] J. K. Behr,[120] C. Belanger-Champagne,[87] W. H. Bell,[49] G. Bella,[153] L. Bellagamba,[20a] A. Bellerive,[29] M. Bellomo,[86] K. Belotskiy,[98] O. Beltramello,[30] O. Benary,[153] D. Benchekroun,[135a] M. Bender,[100] K. Bendtz,[146a,146b] N. Benekos,[10] Y. Benhammou,[153] E. Benhar Noccioli,[49] J. A. Benitez Garcia,[159b] D. P. Benjamin,[45] J. R. Bensinger,[23] S. Bentvelsen,[107] L. Beresford,[120] M. Beretta,[47] D. Berge,[107] E. Bergeaas Kuutmann,[166] N. Berger,[5] F. Berghaus,[169] J. Beringer,[15] C. Bernard,[22] N. R. Bernard,[86] C. Bernius,[110] F. U. Bernlochner,[21] T. Berry,[77] P. Berta,[129] C. Bertella,[83] G. Bertoli,[146a,146b] F. Bertolucci,[124a,124b] C. Bertsche,[113] D. Bertsche,[113] M. I. Besana,[91a] G. J. Besjes,[36] O. Bessidskaia Bylund,[146a,146b] M. Bessner,[42] N. Besson,[136] C. Betancourt,[48] S. Bethke,[101] A. J. Bevan,[76] W. Bhimji,[15] R. M. Bianchi,[125] L. Bianchini,[23] M. Bianco,[30] O. Biebel,[100] D. Biedermann,[16] S. P. Bieniek,[78] N. V. Biesuz,[124a,124b] M. Biglietti,[134a] J. Bilbao De Mendizabal,[49] H. Bilokon,[47] M. Bindi,[54] S. Binet,[117] A. Bingul,[19b] C. Bini,[132a,132b] S. Biondi,[20a,20b] D. M. Bjergaard,[45] C. W. Black,[150] J. E. Black,[143] K. M. Black,[22] D. Blackburn,[138] R. E. Blair,[6] J.-B. Blanchard,[136] J. E. Blanco,[77] T. Blazek,[144a] I. Bloch,[42] C. Blocker,[23] W. Blum,[83,†] U. Blumenschein,[54] S. Blunier,[32a] G. J. Bobbink,[107] V. S. Bobrovnikov,[109,c] S. S. Bocchetta,[81] A. Bocci,[45] C. Bock,[100] M. Boehler,[48] J. A. Bogaerts,[30] D. Bogavac,[13] A. G. Bogdanchikov,[109] C. Bohm,[146a] V. Boisvert,[77] T. Bold,[38a] V. Boldea,[26b] A. S. Boldyrev,[99] M. Bomben,[80] M. Bona,[76] M. Boonekamp,[136] A. Borisov,[130] G. Borissov,[72] S. Borroni,[42] J. Bortfeldt,[100] V. Bortolotto,[60a,60b,60c] K. Bos,[107] D. Boscherini,[20a] M. Bosman,[12] J. Boudreau,[125] J. Bouffard,[2] E. V. Bouhova-Thacker,[72] D. Boumediene,[34] C. Bourdarios,[117] N. Bousson,[114] S. K. Boutle,[53] A. Boveia,[30] J. Boyd,[30] I. R. Boyko,[65] I. Bozic,[13] J. Bracinik,[18] A. Brandt,[8] G. Brandt,[54] O. Brandt,[58a] U. Bratzler,[156] B. Brau,[86] J. E. Brau,[116] H. M. Braun,[175,†] W. D. Breaden Madden,[53] K. Brendlinger,[122] A. J. Brennan,[88] L. Brenner,[107] R. Brenner,[166] S. Bressler,[172] T. M. Bristow,[46] D. Britton,[53] D. Britzger,[42] F. M. Brochu,[28] I. Brock,[21] R. Brock,[90] J. Bronner,[101] G. Brooijmans,[35] T. Brooks,[77] W. K. Brooks,[32b] J. Brosamer,[15] E. Brost,[116] P. A. Bruckman de Renstrom,[39] D. Bruncko,[144b] R. Bruneliere,[48] A. Bruni,[20a] G. Bruni,[20a] M. Bruschi,[20a] N. Bruscino,[21] L. Bryngemark,[81] T. Buanes,[14] Q. Buat,[142] P. Buchholz,[141] A. G. Buckley,[53] S. I. Buda,[26b] I. A. Budagov,[65] F. Buehrer,[48] L. Bugge,[119] M. K. Bugge,[119] O. Bulekov,[98] D. Bullock,[8] H. Burckhart,[30] S. Burdin,[74] C. D. Burgard,[48] B. Burghgrave,[108] S. Burke,[131] I. Burmeister,[43] E. Busato,[34] D. Büscher,[48] V. Büscher,[83] P. Bussey,[53] J. M. Butler,[22] A. I. Butt,[3] C. M. Buttar,[53] J. M. Butterworth,[78] P. Butti,[107] W. Buttinger,[25] A. Buzatu,[53]

A. R. Buzykaev,[109,c] S. Cabrera Urbán,[167] D. Caforio,[128] V. M. Cairo,[37a,37b] O. Cakir,[4a] N. Calace,[49] P. Calafiura,[15] A. Calandri,[136] G. Calderini,[80] P. Calfayan,[100] L. P. Caloba,[24a] D. Calvet,[34] S. Calvet,[34] R. Camacho Toro,[31] S. Camarda,[42] P. Camarri,[133a,133b] D. Cameron,[119] R. Caminal Armadans,[165] S. Campana,[30] M. Campanelli,[78] A. Campoverde,[148] V. Canale,[104a,104b] A. Canepa,[159a] M. Cano Bret,[33e] J. Cantero,[82] R. Cantrill,[126a] T. Cao,[40] M. D. M. Capeans Garrido,[30] I. Caprini,[26b] M. Caprini,[26b] M. Capua,[37a,37b] R. Caputo,[83] R. M. Carbone,[35] R. Cardarelli,[133a] F. Cardillo,[48] T. Carli,[30] G. Carlino,[104a] L. Carminati,[91a,91b] S. Caron,[106] E. Carquin,[32a] G. D. Carrillo-Montoya,[30] J. R. Carter,[28] J. Carvalho,[126a,126c] D. Casadei,[78] M. P. Casado,[12] M. Casolino,[12] E. Castaneda-Miranda,[145a] A. Castelli,[107] V. Castillo Gimenez,[167] N. F. Castro,[126a,g] P. Catastini,[57] A. Catinaccio,[30] J. R. Catmore,[119] A. Cattai,[30] J. Caudron,[83] V. Cavaliere,[165] D. Cavalli,[91a] M. Cavalli-Sforza,[12] V. Cavasinni,[124a,124b] F. Ceradini,[134a,134b] B. C. Cerio,[45] K. Cerny,[129] A. S. Cerqueira,[24b] A. Cerri,[149] L. Cerrito,[76] F. Cerutti,[15] M. Cerv,[30] A. Cervelli,[17] S. A. Cetin,[19c] A. Chafaq,[135a] D. Chakraborty,[108] I. Chalupkova,[129] Y. L. Chan,[60a] P. Chang,[165] J. D. Chapman,[28] D. G. Charlton,[18] C. C. Chau,[158] C. A. Chavez Barajas,[149] S. Cheatham,[152] A. Chegwidden,[90] S. Chekanov,[6] S. V. Chekulaev,[159a] G. A. Chelkov,[65,h] M. A. Chelstowska,[89] C. Chen,[64] H. Chen,[25] K. Chen,[148] L. Chen,[33d,i] S. Chen,[33c] S. Chen,[155] X. Chen,[33f] Y. Chen,[67] H. C. Cheng,[89] Y. Cheng,[31] A. Cheplakov,[65] E. Cheremushkina,[130] R. Cherkaoui El Moursli,[135e] V. Chernyatin,[25,†] E. Cheu,[7] L. Chevalier,[136] V. Chiarella,[47] G. Chiarelli,[124a,124b] G. Chiodini,[73a] A. S. Chisholm,[18] R. T. Chislett,[78] A. Chitan,[26b] M. V. Chizhov,[65] K. Choi,[61] S. Chouridou,[9] B. K. B. Chow,[100] V. Christodoulou,[78] D. Chromek-Burckhart,[30] J. Chudoba,[127] A. J. Chuinard,[87] J. J. Chwastowski,[39] L. Chytka,[115] G. Ciapetti,[132a,132b] A. K. Ciftci,[4a] D. Cinca,[53] V. Cindro,[75] I. A. Cioara,[21] A. Ciocio,[15] F. Cirotto,[104a,104b] Z. H. Citron,[172] M. Ciubancan,[26b] A. Clark,[49] B. L. Clark,[57] P. J. Clark,[46] R. N. Clarke,[15] C. Clement,[146a,146b] Y. Coadou,[85] M. Cobal,[164a,164c] A. Coccaro,[49] J. Cochran,[64] L. Coffey,[23] J. G. Cogan,[143] L. Colasurdo,[106] B. Cole,[35] S. Cole,[108] A. P. Colijn,[107] J. Collot,[55] T. Colombo,[58c] G. Compostella,[101] P. Conde Muiño,[126a,126b] E. Coniavitis,[48] S. H. Connell,[145b] I. A. Connelly,[77] V. Consorti,[48] S. Constantinescu,[26b] C. Conta,[121a,121b] G. Conti,[30] F. Conventi,[104a,j] M. Cooke,[15] B. D. Cooper,[78] A. M. Cooper-Sarkar,[120] T. Cornelissen,[175] M. Corradi,[20a] F. Corriveau,[87,k] A. Corso-Radu,[163] A. Cortes-Gonzalez,[12] G. Cortiana,[101] G. Costa,[91a] M. J. Costa,[167] D. Costanzo,[139] D. Côté,[8] G. Cottin,[28] G. Cowan,[77] B. E. Cox,[84] K. Cranmer,[110] G. Cree,[29] S. Crépé-Renaudin,[55] F. Crescioli,[80] W. A. Cribbs,[146a,146b] M. Crispin Ortuzar,[120] M. Cristinziani,[21] V. Croft,[106] G. Crosetti,[37a,37b] T. Cuhadar Donszelmann,[139] J. Cummings,[176] M. Curatolo,[47] J. Cúth,[83] C. Cuthbert,[150] H. Czirr,[141] P. Czodrowski,[3] S. D'Auria,[53] M. D'Onofrio,[74] M. J. Da Cunha Sargedas De Sousa,[126a,126b] C. Da Via,[84] W. Dabrowski,[38a] A. Dafinca,[120] T. Dai,[89] O. Dale,[14] F. Dallaire,[95] C. Dallapiccola,[86] M. Dam,[36] J. R. Dandoy,[31] N. P. Dang,[48] A. C. Daniells,[18] M. Danninger,[168] M. Dano Hoffmann,[136] V. Dao,[48] G. Darbo,[50a] S. Darmora,[8] J. Dassoulas,[3] A. Dattagupta,[61] W. Davey,[21] C. David,[169] T. Davidek,[129] E. Davies,[120,l] M. Davies,[153] P. Davison,[78] Y. Davygora,[58a] E. Dawe,[88] I. Dawson,[139] R. K. Daya-Ishmukhametova,[86] K. De,[8] R. de Asmundis,[104a] A. De Benedetti,[113] S. De Castro,[20a,20b] S. De Cecco,[80] N. De Groot,[106] P. de Jong,[107] H. De la Torre,[82] F. De Lorenzi,[64] D. De Pedis,[132a] A. De Salvo,[132a] U. De Sanctis,[149] A. De Santo,[149] J. B. De Vivie De Regie,[117] W. J. Dearnaley,[72] R. Debbe,[25] C. Debenedetti,[137] D. V. Dedovich,[65] I. Deigaard,[107] J. Del Peso,[82] T. Del Prete,[124a,124b] D. Delgove,[117] F. Deliot,[136] C. M. Delitzsch,[49] M. Deliyergiyev,[75] A. Dell'Acqua,[30] L. Dell'Asta,[22] M. Dell'Orso,[124a,124b] M. Della Pietra,[104a,j] D. della Volpe,[49] M. Delmastro,[5] P. A. Delsart,[55] C. Deluca,[107] D. A. DeMarco,[158] S. Demers,[176] M. Demichev,[65] A. Demilly,[80] S. P. Denisov,[130] D. Derendarz,[39] J. E. Derkaoui,[135d] F. Derue,[80] P. Dervan,[74] K. Desch,[21] C. Deterre,[42] K. Dette,[43] P. O. Deviveiros,[30] A. Dewhurst,[131] S. Dhaliwal,[23] A. Di Ciaccio,[133a,133b] L. Di Ciaccio,[5] A. Di Domenico,[132a,132b] C. Di Donato,[104a,104b] A. Di Girolamo,[30] B. Di Girolamo,[30] A. Di Mattia,[152] B. Di Micco,[134a,134b] R. Di Nardo,[47] A. Di Simone,[48] R. Di Sipio,[158] D. Di Valentino,[29] C. Diaconu,[85] M. Diamond,[158] F. A. Dias,[46] M. A. Diaz,[32a] E. B. Diehl,[89] J. Dietrich,[16] S. Diglio,[85] A. Dimitrievska,[13] J. Dingfelder,[21] P. Dita,[26b] S. Dita,[26b] F. Dittus,[30] F. Djama,[85] T. Djobava,[51b] J. I. Djuvsland,[58a] M. A. B. do Vale,[24c] D. Dobos,[30] M. Dobre,[26b] C. Doglioni,[81] T. Dohmae,[155] J. Dolejsi,[129] Z. Dolezal,[129] B. A. Dolgoshein,[98,†] M. Donadelli,[24d] S. Donati,[124a,124b] P. Dondero,[121a,121b] J. Donini,[34] J. Dopke,[131] A. Doria,[104a] M. T. Dova,[71] A. T. Doyle,[53] E. Drechsler,[54] M. Dris,[10] E. Dubreuil,[34] E. Duchovni,[172] G. Duckeck,[100] O. A. Ducu,[26b,85] D. Duda,[107] A. Dudarev,[30] L. Duflot,[117] L. Duguid,[77] M. Dührssen,[30] M. Dunford,[58a] H. Duran Yildiz,[4a] M. Düren,[52] A. Durglishvili,[51b] D. Duschinger,[44] B. Dutta,[42] M. Dyndal,[38a] C. Eckardt,[42] K. M. Ecker,[101] R. C. Edgar,[89] W. Edson,[2] N. C. Edwards,[46] W. Ehrenfeld,[21] T. Eifert,[30] G. Eigen,[14] K. Einsweiler,[15] T. Ekelof,[166] M. El Kacimi,[135c] M. Ellert,[166] S. Elles,[5] F. Ellinghaus,[175] A. A. Elliot,[169] N. Ellis,[30] J. Elmsheuser,[100] M. Elsing,[30] D. Emeliyanov,[131] Y. Enari,[155] O. C. Endner,[83] M. Endo,[118] J. Erdmann,[43] A. Ereditato,[17] G. Ernis,[175] J. Ernst,[2] M. Ernst,[25] S. Errede,[165] E. Ertel,[83] M. Escalier,[117] H. Esch,[43] C. Escobar,[125] B. Esposito,[47] A. I. Etienvre,[136] E. Etzion,[153] H. Evans,[61] A. Ezhilov,[123]

L. Fabbri,[20a,20b] G. Facini,[31] R. M. Fakhrutdinov,[130] S. Falciano,[132a] R. J. Falla,[78] J. Faltova,[129] Y. Fang,[33a] M. Fanti,[91a,91b] A. Farbin,[8] A. Farilla,[134a] T. Farooque,[12] S. Farrell,[15] S. M. Farrington,[170] P. Farthouat,[30] F. Fassi,[135e] P. Fassnacht,[30] D. Fassouliotis,[9] M. Faucci Giannelli,[77] A. Favareto,[50a,50b] L. Fayard,[117] O. L. Fedin,[123,m] W. Fedorko,[168] S. Feigl,[30] L. Feligioni,[85] C. Feng,[33d] E. J. Feng,[30] H. Feng,[89] A. B. Fenyuk,[130] L. Feremenga,[8] P. Fernandez Martinez,[167] S. Fernandez Perez,[30] J. Ferrando,[53] A. Ferrari,[166] P. Ferrari,[107] R. Ferrari,[121a] D. E. Ferreira de Lima,[53] A. Ferrer,[167] D. Ferrere,[49] C. Ferretti,[89] A. Ferretto Parodi,[50a,50b] M. Fiascaris,[31] F. Fiedler,[83] A. Filipčič,[75] M. Filipuzzi,[42] F. Filthaut,[106] M. Fincke-Keeler,[169] K. D. Finelli,[150] M. C. N. Fiolhais,[126a,126c] L. Fiorini,[167] A. Firan,[40] A. Fischer,[2] C. Fischer,[12] J. Fischer,[175] W. C. Fisher,[90] N. Flaschel,[42] I. Fleck,[141] P. Fleischmann,[89] G. T. Fletcher,[139] G. Fletcher,[76] R. R. M. Fletcher,[122] T. Flick,[175] A. Floderus,[81] L. R. Flores Castillo,[60a] M. J. Flowerdew,[101] A. Formica,[136] A. Forti,[84] D. Fournier,[117] H. Fox,[72] S. Fracchia,[12] P. Francavilla,[80] M. Franchini,[20a,20b] D. Francis,[30] L. Franconi,[119] M. Franklin,[57] M. Frate,[163] M. Fraternali,[121a,121b] D. Freeborn,[78] S. T. French,[28] F. Friedrich,[44] D. Froidevaux,[30] J. A. Frost,[120] C. Fukunaga,[156] E. Fullana Torregrosa,[83] B. G. Fulsom,[143] T. Fusayasu,[102] J. Fuster,[167] C. Gabaldon,[55] O. Gabizon,[175] A. Gabrielli,[20a,20b] A. Gabrielli,[15] G. P. Gach,[18] S. Gadatsch,[30] S. Gadomski,[49] G. Gagliardi,[50a,50b] P. Gagnon,[61] C. Galea,[106] B. Galhardo,[126a,126c] E. J. Gallas,[120] B. J. Gallop,[131] P. Gallus,[128] G. Galster,[36] K. K. Gan,[111] J. Gao,[33b,85] Y. Gao,[46] Y. S. Gao,[143,e] F. M. Garay Walls,[46] F. Garberson,[176] C. García,[167] J. E. García Navarro,[167] M. Garcia-Sciveres,[15] R. W. Gardner,[31] N. Garelli,[143] V. Garonne,[119] C. Gatti,[47] A. Gaudiello,[50a,50b] G. Gaudio,[121a] B. Gaur,[141] L. Gauthier,[95] P. Gauzzi,[132a,132b] I. L. Gavrilenko,[96] C. Gay,[168] G. Gaycken,[21] E. N. Gazis,[10] P. Ge,[33d] Z. Gecse,[168] C. N. P. Gee,[131] Ch. Geich-Gimbel,[21] M. P. Geisler,[58a] C. Gemme,[50a] M. H. Genest,[55] S. Gentile,[132a,132b] M. George,[54] S. George,[77] D. Gerbaudo,[163] A. Gershon,[153] S. Ghasemi,[141] H. Ghazlane,[135b] B. Giacobbe,[20a] S. Giagu,[132a,132b] V. Giangiobbe,[12] P. Giannetti,[124a,124b] B. Gibbard,[25] S. M. Gibson,[77] M. Gignac,[168] M. Gilchriese,[15] T. P. S. Gillam,[28] D. Gillberg,[30] G. Gilles,[34] D. M. Gingrich,[3,d] N. Giokaris,[9] M. P. Giordani,[164a,164c] F. M. Giorgi,[20a] F. M. Giorgi,[16] P. F. Giraud,[136] P. Giromini,[47] D. Giugni,[91a] C. Giuliani,[101] M. Giulini,[58b] B. K. Gjelsten,[119] S. Gkaitatzis,[154] I. Gkialas,[154] E. L. Gkougkousis,[117] L. K. Gladilin,[99] C. Glasman,[82] J. Glatzer,[30] P. C. F. Glaysher,[46] A. Glazov,[42] M. Goblirsch-Kolb,[101] J. R. Goddard,[76] J. Godlewski,[39] S. Goldfarb,[89] T. Golling,[49] D. Golubkov,[130] A. Gomes,[126a,126b,126d] R. Gonçalo,[126a] J. Goncalves Pinto Firmino Da Costa,[136] L. Gonella,[21] S. González de la Hoz,[167] G. Gonzalez Parra,[12] S. Gonzalez-Sevilla,[49] L. Goossens,[30] P. A. Gorbounov,[97] H. A. Gordon,[25] I. Gorelov,[105] B. Gorini,[30] E. Gorini,[73a,73b] A. Gorišek,[75] E. Gornicki,[39] A. T. Goshaw,[45] C. Gössling,[43] M. I. Gostkin,[65] D. Goujdami,[135c] A. G. Goussiou,[138] N. Govender,[145b] E. Gozani,[152] H. M. X. Grabas,[137] L. Graber,[54] I. Grabowska-Bold,[38a] P. O. J. Gradin,[166] P. Grafström,[20a,20b] J. Gramling,[49] E. Gramstad,[119] S. Grancagnolo,[16] V. Gratchev,[123] H. M. Gray,[30] E. Graziani,[134a] Z. D. Greenwood,[79,n] C. Grefe,[21] K. Gregersen,[78] I. M. Gregor,[42] P. Grenier,[143] J. Griffiths,[8] A. A. Grillo,[137] K. Grimm,[72] S. Grinstein,[12,o] Ph. Gris,[34] J.-F. Grivaz,[117] J. P. Grohs,[44] A. Grohsjean,[42] E. Gross,[172] J. Grosse-Knetter,[54] G. C. Grossi,[79] Z. J. Grout,[149] L. Guan,[89] J. Guenther,[128] F. Guescini,[49] D. Guest,[163] O. Gueta,[153] E. Guido,[50a,50b] T. Guillemin,[117] S. Guindon,[2] U. Gul,[53] C. Gumpert,[44] J. Guo,[33e] Y. Guo,[33b,p] S. Gupta,[120] G. Gustavino,[132a,132b] P. Gutierrez,[113] N. G. Gutierrez Ortiz,[78] C. Gutschow,[44] C. Guyot,[136] C. Gwenlan,[120] C. B. Gwilliam,[74] A. Haas,[110] C. Haber,[15] H. K. Hadavand,[8] N. Haddad,[135e] P. Haefner,[21] S. Hageböck,[21] Z. Hajduk,[39] H. Hakobyan,[177] M. Haleem,[42] J. Haley,[114] D. Hall,[120] G. Halladjian,[90] G. D. Hallewell,[85] K. Hamacher,[175] P. Hamal,[115] K. Hamano,[169] A. Hamilton,[145a] G. N. Hamity,[139] P. G. Hamnett,[42] L. Han,[33b] K. Hanagaki,[66,q] K. Hanawa,[155] M. Hance,[137] B. Haney,[122] P. Hanke,[58a] R. Hanna,[136] J. B. Hansen,[36] J. D. Hansen,[36] M. C. Hansen,[21] P. H. Hansen,[36] K. Hara,[160] A. S. Hard,[173] T. Harenberg,[175] F. Hariri,[117] S. Harkusha,[92] R. D. Harrington,[46] P. F. Harrison,[170] F. Hartjes,[107] M. Hasegawa,[67] Y. Hasegawa,[140] A. Hasib,[113] S. Hassani,[136] S. Haug,[17] R. Hauser,[90] L. Hauswald,[44] M. Havranek,[127] C. M. Hawkes,[18] R. J. Hawkings,[30] A. D. Hawkins,[81] T. Hayashi,[160] D. Hayden,[90] C. P. Hays,[120] J. M. Hays,[76] H. S. Hayward,[74] S. J. Haywood,[131] S. J. Head,[18] T. Heck,[83] V. Hedberg,[81] L. Heelan,[8] S. Heim,[122] T. Heim,[175] B. Heinemann,[15] L. Heinrich,[110] J. Hejbal,[127] L. Helary,[22] S. Hellman,[146a,146b] D. Hellmich,[21] C. Helsens,[12] J. Henderson,[120] R. C. W. Henderson,[72] Y. Heng,[173] C. Hengler,[42] S. Henkelmann,[168] A. Henrichs,[176] A. M. Henriques Correia,[30] S. Henrot-Versille,[117] G. H. Herbert,[16] Y. Hernández Jiménez,[167] G. Herten,[48] R. Hertenberger,[100] L. Hervas,[30] G. G. Hesketh,[78] N. P. Hessey,[107] J. W. Hetherly,[40] R. Hickling,[76] E. Higón-Rodriguez,[167] E. Hill,[169] J. C. Hill,[28] K. H. Hiller,[42] S. J. Hillier,[18] I. Hinchliffe,[15] E. Hines,[122] R. R. Hinman,[15] M. Hirose,[157] D. Hirschbuehl,[175] J. Hobbs,[148] N. Hod,[107] M. C. Hodgkinson,[139] P. Hodgson,[139] A. Hoecker,[30] M. R. Hoeferkamp,[105] F. Hoenig,[100] M. Hohlfeld,[83] D. Hohn,[21] T. R. Holmes,[15] M. Homann,[43] T. M. Hong,[125] W. H. Hopkins,[116] Y. Horii,[103] A. J. Horton,[142] J-Y. Hostachy,[55] S. Hou,[151] A. Hoummada,[135a] J. Howard,[120] J. Howarth,[42] M. Hrabovsky,[115] I. Hristova,[16] J. Hrivnac,[117] T. Hryn'ova,[5]

A. Hrynevich,[93] C. Hsu,[145c] P. J. Hsu,[151,r] S.-C. Hsu,[138] D. Hu,[35] Q. Hu,[33b] X. Hu,[89] Y. Huang,[42] Z. Hubacek,[128] F. Hubaut,[85] F. Huegging,[21] T. B. Huffman,[120] E. W. Hughes,[35] G. Hughes,[72] M. Huhtinen,[30] T. A. Hülsing,[83] N. Huseynov,[65,b] J. Huston,[90] J. Huth,[57] G. Iacobucci,[49] G. Iakovidis,[25] I. Ibragimov,[141] L. Iconomidou-Fayard,[117] E. Ideal,[176] Z. Idrissi,[135e] P. Iengo,[30] O. Igonkina,[107] T. Iizawa,[171] Y. Ikegami,[66] K. Ikematsu,[141] M. Ikeno,[66] Y. Ilchenko,[31,s] D. Iliadis,[154] N. Ilic,[143] T. Ince,[101] G. Introzzi,[121a,121b] P. Ioannou,[9] M. Iodice,[134a] K. Iordanidou,[35] V. Ippolito,[57] A. Irles Quiles,[167] C. Isaksson,[166] M. Ishino,[68] M. Ishitsuka,[157] R. Ishmukhametov,[111] C. Issever,[120] S. Istin,[19a] J. M. Iturbe Ponce,[84] R. Iuppa,[133a,133b] J. Ivarsson,[81] W. Iwanski,[39] H. Iwasaki,[66] J. M. Izen,[41] V. Izzo,[104a] S. Jabbar,[3] B. Jackson,[122] M. Jackson,[74] P. Jackson,[1] M. R. Jaekel,[30] V. Jain,[2] K. Jakobs,[48] S. Jakobsen,[30] T. Jakoubek,[127] J. Jakubek,[128] D. O. Jamin,[114] D. K. Jana,[79] E. Jansen,[78] R. Jansky,[62] J. Janssen,[21] M. Janus,[54] G. Jarlskog,[81] N. Javadov,[65,b] T. Javůrek,[48] L. Jeanty,[15] J. Jejelava,[51a,t] G.-Y. Jeng,[150] D. Jennens,[88] P. Jenni,[48,u] J. Jentzsch,[43] C. Jeske,[170] S. Jézéquel,[5] H. Ji,[173] J. Jia,[148] Y. Jiang,[33b] S. Jiggins,[78] J. Jimenez Pena,[167] S. Jin,[33a] A. Jinaru,[26b] O. Jinnouchi,[157] M. D. Joergensen,[36] P. Johansson,[139] K. A. Johns,[7] W. J. Johnson,[138] K. Jon-And,[146a,146b] G. Jones,[170] R. W. L. Jones,[72] T. J. Jones,[74] J. Jongmanns,[58a] P. M. Jorge,[126a,126b] K. D. Joshi,[84] J. Jovicevic,[159a] X. Ju,[173] P. Jussel,[62] A. Juste Rozas,[12,o] M. Kaci,[167] A. Kaczmarska,[39] M. Kado,[117] H. Kagan,[111] M. Kagan,[143] S. J. Kahn,[85] E. Kajomovitz,[45] C. W. Kalderon,[120] S. Kama,[40] A. Kamenshchikov,[130] N. Kanaya,[155] S. Kaneti,[28] V. A. Kantserov,[98] J. Kanzaki,[66] B. Kaplan,[110] L. S. Kaplan,[173] A. Kapliy,[31] D. Kar,[145c] K. Karakostas,[10] A. Karamaoun,[3] N. Karastathis,[10,107] M. J. Kareem,[54] E. Karentzos,[10] M. Karnevskiy,[83] S. N. Karpov,[65] Z. M. Karpova,[65] K. Karthik,[110] V. Kartvelishvili,[72] A. N. Karyukhin,[130] K. Kasahara,[160] L. Kashif,[173] R. D. Kass,[111] A. Kastanas,[14] Y. Kataoka,[155] C. Kato,[155] A. Katre,[49] J. Katzy,[42] K. Kawade,[103] K. Kawagoe,[70] T. Kawamoto,[155] G. Kawamura,[54] S. Kazama,[155] V. F. Kazanin,[109,c] R. Keeler,[169] R. Kehoe,[40] J. S. Keller,[42] J. J. Kempster,[77] H. Keoshkerian,[84] O. Kepka,[127] B. P. Kerševan,[75] S. Kersten,[175] R. A. Keyes,[87] F. Khalil-zada,[11] H. Khandanyan,[146a,146b] A. Khanov,[114] A. G. Kharlamov,[109,c] T. J. Khoo,[28] V. Khovanskiy,[97] E. Khramov,[65] J. Khubua,[51b,v] S. Kido,[67] H. Y. Kim,[8] S. H. Kim,[160] Y. K. Kim,[31] N. Kimura,[154] O. M. Kind,[16] B. T. King,[74] M. King,[167] S. B. King,[168] J. Kirk,[131] A. E. Kiryunin,[101] T. Kishimoto,[67] D. Kisielewska,[38a] F. Kiss,[48] K. Kiuchi,[160] O. Kivernyk,[136] E. Kladiva,[144b] M. H. Klein,[35] M. Klein,[74] U. Klein,[74] K. Kleinknecht,[83] P. Klimek,[146a,146b] A. Klimentov,[25] R. Klingenberg,[43] J. A. Klinger,[139] T. Klioutchnikova,[30] E.-E. Kluge,[58a] P. Kluit,[107] S. Kluth,[101] J. Knapik,[39] E. Kneringer,[62] E. B. F. G. Knoops,[85] A. Knue,[53] A. Kobayashi,[155] D. Kobayashi,[157] T. Kobayashi,[155] M. Kobel,[44] M. Kocian,[143] P. Kodys,[129] T. Koffas,[29] E. Koffeman,[107] L. A. Kogan,[120] S. Kohlmann,[175] Z. Kohout,[128] T. Kohriki,[66] T. Koi,[143] H. Kolanoski,[16] M. Kolb,[58b] I. Koletsou,[5] A. A. Komar,[96,†] Y. Komori,[155] T. Kondo,[66] N. Kondrashova,[42] K. Köneke,[48] A. C. König,[106] T. Kono,[66] R. Konoplich,[110,w] N. Konstantinidis,[78] R. Kopeliansky,[152] S. Koperny,[38a] L. Köpke,[83] A. K. Kopp,[48] K. Korcyl,[39] K. Kordas,[154] A. Korn,[78] A. A. Korol,[109,c] I. Korolkov,[12] E. V. Korolkova,[139] O. Kortner,[101] S. Kortner,[101] T. Kosek,[129] V. V. Kostyukhin,[21] V. M. Kotov,[65] A. Kotwal,[45] A. Kourkoumeli-Charalampidi,[154] C. Kourkoumelis,[9] V. Kouskoura,[25] A. Koutsman,[159a] R. Kowalewski,[169] T. Z. Kowalski,[38a] W. Kozanecki,[136] A. S. Kozhin,[130] V. A. Kramarenko,[99] G. Kramberger,[75] D. Krasnopevtsev,[98] M. W. Krasny,[80] A. Krasznahorkay,[30] J. K. Kraus,[21] A. Kravchenko,[25] S. Kreiss,[110] M. Kretz,[58c] J. Kretzschmar,[74] K. Kreutzfeldt,[52] P. Krieger,[158] K. Krizka,[31] K. Kroeninger,[43] H. Kroha,[101] J. Kroll,[122] J. Kroseberg,[21] J. Krstic,[13] U. Kruchonak,[65] H. Krüger,[21] N. Krumnack,[64] A. Kruse,[173] M. C. Kruse,[45] M. Kruskal,[22] T. Kubota,[88] H. Kucuk,[78] S. Kuday,[4b] S. Kuehn,[48] A. Kugel,[58c] F. Kuger,[174] A. Kuhl,[137] T. Kuhl,[42] V. Kukhtin,[65] R. Kukla,[136] Y. Kulchitsky,[92] S. Kuleshov,[32b] M. Kuna,[132a,132b] T. Kunigo,[68] A. Kupco,[127] H. Kurashige,[67] Y. A. Kurochkin,[92] V. Kus,[127] E. S. Kuwertz,[169] M. Kuze,[157] J. Kvita,[115] T. Kwan,[169] D. Kyriazopoulos,[139] A. La Rosa,[137] J. L. La Rosa Navarro,[24d] L. La Rotonda,[37a,37b] C. Lacasta,[167] F. Lacava,[132a,132b] J. Lacey,[29] H. Lacker,[16] D. Lacour,[80] V. R. Lacuesta,[167] E. Ladygin,[65] R. Lafaye,[5] B. Laforge,[80] T. Lagouri,[176] S. Lai,[54] L. Lambourne,[78] S. Lammers,[61] C. L. Lampen,[7] W. Lampl,[7] E. Lançon,[136] U. Landgraf,[48] M. P. J. Landon,[76] V. S. Lang,[58a] J. C. Lange,[12] A. J. Lankford,[163] F. Lanni,[25] K. Lantzsch,[21] A. Lanza,[121a] S. Laplace,[80] C. Lapoire,[30] J. F. Laporte,[136] T. Lari,[91a] F. Lasagni Manghi,[20a,20b] M. Lassnig,[30] P. Laurelli,[47] W. Lavrijsen,[15] A. T. Law,[137] P. Laycock,[74] T. Lazovich,[57] O. Le Dortz,[80] E. Le Guirriec,[85] E. Le Menedeu,[12] M. LeBlanc,[169] T. LeCompte,[6] F. Ledroit-Guillon,[55] C. A. Lee,[145a] S. C. Lee,[151] L. Lee,[1] G. Lefebvre,[80] M. Lefebvre,[169] F. Legger,[100] C. Leggett,[15] A. Lehan,[74] G. Lehmann Miotto,[30] X. Lei,[7] W. A. Leight,[29] A. Leisos,[154,x] A. G. Leister,[176] M. A. L. Leite,[24d] R. Leitner,[129] D. Lellouch,[172] B. Lemmer,[54] K. J. C. Leney,[78] T. Lenz,[21] B. Lenzi,[30] R. Leone,[7] S. Leone,[124a,124b] C. Leonidopoulos,[46] S. Leontsinis,[10] C. Leroy,[95] C. G. Lester,[28] M. Levchenko,[123] J. Levêque,[5] D. Levin,[89] L. J. Levinson,[172] M. Levy,[18] A. Lewis,[120] A. M. Leyko,[21] M. Leyton,[41] B. Li,[33b,y] H. Li,[148] H. L. Li,[31] L. Li,[45] L. Li,[33e] S. Li,[45] X. Li,[84] Y. Li,[33c,z] Z. Liang,[137] H. Liao,[34] B. Liberti,[133a] A. Liblong,[158] P. Lichard,[30] K. Lie,[165] J. Liebal,[21] W. Liebig,[14] C. Limbach,[21]

A. Limosani,[150] S. C. Lin,[151,aa] T. H. Lin,[83] F. Linde,[107] B. E. Lindquist,[148] J. T. Linnemann,[90] E. Lipeles,[122] A. Lipniacka,[14] M. Lisovyi,[58b] T. M. Liss,[165] D. Lissauer,[25] A. Lister,[168] A. M. Litke,[137] B. Liu,[151,bb] D. Liu,[151] H. Liu,[89] J. Liu,[85] J. B. Liu,[33b] K. Liu,[85] L. Liu,[165] M. Liu,[45] M. Liu,[33b] Y. Liu,[33b] M. Livan,[121a,121b] A. Lleres,[55] J. Llorente Merino,[82] S. L. Lloyd,[76] F. Lo Sterzo,[151] E. Lobodzinska,[42] P. Loch,[7] W. S. Lockman,[137] F. K. Loebinger,[84] A. E. Loevschall-Jensen,[36] K. M. Loew,[23] A. Loginov,[176] T. Lohse,[16] K. Lohwasser,[42] M. Lokajicek,[127] B. A. Long,[22] J. D. Long,[165] R. E. Long,[72] K. A. Looper,[111] L. Lopes,[126a] D. Lopez Mateos,[57] B. Lopez Paredes,[139] I. Lopez Paz,[12] J. Lorenz,[100] N. Lorenzo Martinez,[61] M. Losada,[162] P. J. Lösel,[100] X. Lou,[33a] A. Lounis,[117] J. Love,[6] P. A. Love,[72] H. Lu,[60a] N. Lu,[89] H. J. Lubatti,[138] C. Luci,[132a,132b] A. Lucotte,[55] C. Luedtke,[48] F. Luehring,[61] W. Lukas,[62] L. Luminari,[132a] O. Lundberg,[146a,146b] B. Lund-Jensen,[147] D. Lynn,[25] R. Lysak,[127] E. Lytken,[81] H. Ma,[25] L. L. Ma,[33d] G. Maccarrone,[47] A. Macchiolo,[101] C. M. Macdonald,[139] B. Maček,[75] J. Machado Miguens,[122,126b] D. Macina,[30] D. Madaffari,[85] R. Madar,[34] H. J. Maddocks,[72] W. F. Mader,[44] A. Madsen,[166] J. Maeda,[67] S. Maeland,[14] T. Maeno,[25] A. Maevskiy,[99] E. Magradze,[54] K. Mahboubi,[48] J. Mahlstedt,[107] C. Maiani,[136] C. Maidantchik,[24a] A. A. Maier,[101] T. Maier,[100] A. Maio,[126a,126b,126d] S. Majewski,[116] Y. Makida,[66] N. Makovec,[117] B. Malaescu,[80] Pa. Malecki,[39] V. P. Maleev,[123] F. Malek,[55] U. Mallik,[63] D. Malon,[6] C. Malone,[143] S. Maltezos,[10] V. M. Malyshev,[109] S. Malyukov,[30] J. Mamuzic,[42] G. Mancini,[47] B. Mandelli,[30] L. Mandelli,[91a] I. Mandić,[75] R. Mandrysch,[63] J. Maneira,[126a,126b] A. Manfredini,[101] L. Manhaes de Andrade Filho,[24b] J. Manjarres Ramos,[159b] A. Mann,[100] A. Manousakis-Katsikakis,[9] B. Mansoulie,[136] R. Mantifel,[87] M. Mantoani,[54] L. Mapelli,[30] L. March,[145c] G. Marchiori,[80] M. Marcisovsky,[127] C. P. Marino,[169] M. Marjanovic,[13] D. E. Marley,[89] F. Marroquim,[24a] S. P. Marsden,[84] Z. Marshall,[15] L. F. Marti,[17] S. Marti-Garcia,[167] B. Martin,[90] T. A. Martin,[170] V. J. Martin,[46] B. Martin dit Latour,[14] M. Martinez,[12,o] S. Martin-Haugh,[131] V. S. Martoiu,[26b] A. C. Martyniuk,[78] M. Marx,[138] F. Marzano,[132a] A. Marzin,[30] L. Masetti,[83] T. Mashimo,[155] R. Mashinistov,[96] J. Masik,[84] A. L. Maslennikov,[109,c] I. Massa,[20a,20b] L. Massa,[20a,20b] P. Mastrandrea,[5] A. Mastroberardino,[37a,37b] T. Masubuchi,[155] P. Mättig,[175] J. Mattmann,[83] J. Maurer,[26b] S. J. Maxfield,[74] D. A. Maximov,[109,c] R. Mazini,[151] S. M. Mazza,[91a,91b] G. Mc Goldrick,[158] S. P. Mc Kee,[89] A. McCarn,[89] R. L. McCarthy,[148] T. G. McCarthy,[29] N. A. McCubbin,[131] K. W. McFarlane,[56,†] J. A. Mcfayden,[78] G. Mchedlidze,[54] S. J. McMahon,[131] R. A. McPherson,[169,k] M. Medinnis,[42] S. Meehan,[145a] S. Mehlhase,[100] A. Mehta,[74] K. Meier,[58a] C. Meineck,[100] B. Meirose,[41] B. R. Mellado Garcia,[145c] F. Meloni,[17] A. Mengarelli,[20a,20b] S. Menke,[101] E. Meoni,[161] K. M. Mercurio,[57] S. Mergelmeyer,[21] P. Mermod,[49] L. Merola,[104a,104b] C. Meroni,[91a] F. S. Merritt,[31] A. Messina,[132a,132b] J. Metcalfe,[25] A. S. Mete,[163] C. Meyer,[83] C. Meyer,[122] J-P. Meyer,[136] J. Meyer,[107] H. Meyer Zu Theenhausen,[58a] R. P. Middleton,[131] S. Miglioranzi,[164a,164c] L. Mijović,[21] G. Mikenberg,[172] M. Mikestikova,[127] M. Mikuž,[75] M. Milesi,[88] A. Milic,[30] D. W. Miller,[31] C. Mills,[46] A. Milov,[172] D. A. Milstead,[146a,146b] A. A. Minaenko,[130] Y. Minami,[155] I. A. Minashvili,[65] A. I. Mincer,[110] B. Mindur,[38a] M. Mineev,[65] Y. Ming,[173] L. M. Mir,[12] K. P. Mistry,[122] T. Mitani,[171] J. Mitrevski,[100] V. A. Mitsou,[167] A. Miucci,[49] P. S. Miyagawa,[139] J. U. Mjörnmark,[81] T. Moa,[146a,146b] K. Mochizuki,[85] S. Mohapatra,[35] W. Mohr,[48] S. Molander,[146a,146b] R. Moles-Valls,[21] R. Monden,[68] K. Mönig,[42] C. Monini,[55] J. Monk,[36] E. Monnier,[85] A. Montalbano,[148] J. Montejo Berlingen,[12] F. Monticelli,[71] S. Monzani,[132a,132b] R. W. Moore,[3] N. Morange,[117] D. Moreno,[162] M. Moreno Llácer,[54] P. Morettini,[50a] D. Mori,[142] T. Mori,[155] M. Morii,[57] M. Morinaga,[155] V. Morisbak,[119] S. Moritz,[83] A. K. Morley,[150] G. Mornacchi,[30] J. D. Morris,[76] S. S. Mortensen,[36] A. Morton,[53] L. Morvaj,[103] M. Mosidze,[51b] J. Moss,[143] K. Motohashi,[157] R. Mount,[143] E. Mountricha,[25] S. V. Mouraviev,[96,†] E. J. W. Moyse,[86] S. Muanza,[85] R. D. Mudd,[18] F. Mueller,[101] J. Mueller,[125] R. S. P. Mueller,[100] T. Mueller,[28] D. Muenstermann,[49] P. Mullen,[53] G. A. Mullier,[17] J. A. Murillo Quijada,[18] W. J. Murray,[170,131] H. Musheghyan,[54] E. Musto,[152] A. G. Myagkov,[130,cc] M. Myska,[128] B. P. Nachman,[143] O. Nackenhorst,[54] J. Nadal,[54] K. Nagai,[120] R. Nagai,[157] Y. Nagai,[85] K. Nagano,[66] A. Nagarkar,[111] Y. Nagasaka,[59] K. Nagata,[160] M. Nagel,[101] E. Nagy,[85] A. M. Nairz,[30] Y. Nakahama,[30] K. Nakamura,[66] T. Nakamura,[155] I. Nakano,[112] H. Namasivayam,[41] R. F. Naranjo Garcia,[42] R. Narayan,[31] D. I. Narrias Villar,[58a] T. Naumann,[42] G. Navarro,[162] R. Nayyar,[7] H. A. Neal,[89] P. Yu. Nechaeva,[96] T. J. Neep,[84] P. D. Nef,[143] A. Negri,[121a,121b] M. Negrini,[20a] S. Nektarijevic,[106] C. Nellist,[117] A. Nelson,[163] S. Nemecek,[127] P. Nemethy,[110] A. A. Nepomuceno,[24a] M. Nessi,[30,dd] M. S. Neubauer,[165] M. Neumann,[175] R. M. Neves,[110] P. Nevski,[25] P. R. Newman,[18] D. H. Nguyen,[6] R. B. Nickerson,[120] R. Nicolaidou,[136] B. Nicquevert,[30] J. Nielsen,[137] N. Nikiforou,[35] A. Nikiforov,[16] V. Nikolaenko,[130,cc] I. Nikolic-Audit,[80] K. Nikolopoulos,[18] J. K. Nilsen,[119] P. Nilsson,[25] Y. Ninomiya,[155] A. Nisati,[132a] R. Nisius,[101] T. Nobe,[155] M. Nomachi,[118] I. Nomidis,[29] T. Nooney,[76] S. Norberg,[113] M. Nordberg,[30] O. Novgorodova,[44] S. Nowak,[101] M. Nozaki,[66] L. Nozka,[115] K. Ntekas,[10] G. Nunes Hanninger,[88] T. Nunnemann,[100] E. Nurse,[78] F. Nuti,[88] B. J. O'Brien,[46] F. O'grady,[7] D. C. O'Neil,[142] V. O'Shea,[53] F. G. Oakham,[29,d] H. Oberlack,[101] T. Obermann,[21] J. Ocariz,[80] A. Ochi,[67] I. Ochoa,[35] J. P. Ochoa-Ricoux,[32a] S. Oda,[70]

S. Odaka,[66] H. Ogren,[61] A. Oh,[84] S. H. Oh,[45] C. C. Ohm,[15] H. Ohman,[166] H. Oide,[30] W. Okamura,[118] H. Okawa,[160] Y. Okumura,[31] T. Okuyama,[66] A. Olariu,[26b] S. A. Olivares Pino,[46] D. Oliveira Damazio,[25] A. Olszewski,[39] J. Olszowska,[39] A. Onofre,[126a,126e] K. Onogi,[103] P. U. E. Onyisi,[31,s] C. J. Oram,[159a] M. J. Oreglia,[31] Y. Oren,[153] D. Orestano,[134a,134b] N. Orlando,[154] C. Oropeza Barrera,[53] R. S. Orr,[158] B. Osculati,[50a,50b] R. Ospanov,[84] G. Otero y Garzon,[27] H. Otono,[70] M. Ouchrif,[135d] F. Ould-Saada,[119] A. Ouraou,[136] K. P. Oussoren,[107] Q. Ouyang,[33a] A. Ovcharova,[15] M. Owen,[53] R. E. Owen,[18] V. E. Ozcan,[19a] N. Ozturk,[8] K. Pachal,[142] A. Pacheco Pages,[12] C. Padilla Aranda,[12] M. Pagáčová,[48] S. Pagan Griso,[15] E. Paganis,[139] F. Paige,[25] P. Pais,[86] K. Pajchel,[119] G. Palacino,[159b] S. Palestini,[30] M. Palka,[38b] D. Pallin,[34] A. Palma,[126a,126b] Y. B. Pan,[173] E. St. Panagiotopoulou,[10] C. E. Pandini,[80] J. G. Panduro Vazquez,[77] P. Pani,[146a,146b] S. Panitkin,[25] D. Pantea,[26b] L. Paolozzi,[49] Th. D. Papadopoulou,[10] K. Papageorgiou,[154] A. Paramonov,[6] D. Paredes Hernandez,[154] M. A. Parker,[28] K. A. Parker,[139] F. Parodi,[50a,50b] J. A. Parsons,[35] U. Parzefall,[48] E. Pasqualucci,[132a] S. Passaggio,[50a] F. Pastore,[134a,134b,†] Fr. Pastore,[77] G. Pásztor,[29] S. Pataraia,[175] N. D. Patel,[150] J. R. Pater,[84] T. Pauly,[30] J. Pearce,[169] B. Pearson,[113] L. E. Pedersen,[36] M. Pedersen,[119] S. Pedraza Lopez,[167] R. Pedro,[126a,126b] S. V. Peleganchuk,[109,c] D. Pelikan,[166] O. Penc,[127] C. Peng,[33a] H. Peng,[33b] B. Penning,[31] J. Penwell,[61] D. V. Perepelitsa,[25] E. Perez Codina,[159a] M. T. Pérez García-Estañ,[167] L. Perini,[91a,91b] H. Pernegger,[30] S. Perrella,[104a,104b] R. Peschke,[42] V. D. Peshekhonov,[65] K. Peters,[30] R. F. Y. Peters,[84] B. A. Petersen,[30] T. C. Petersen,[36] E. Petit,[42] A. Petridis,[1] C. Petridou,[154] P. Petroff,[117] E. Petrolo,[132a] F. Petrucci,[134a,134b] N. E. Pettersson,[157] R. Pezoa,[32b] P. W. Phillips,[131] G. Piacquadio,[143] E. Pianori,[170] A. Picazio,[49] E. Piccaro,[76] M. Piccinini,[20a,20b] M. A. Pickering,[120] R. Piegaia,[27] D. T. Pignotti,[111] J. E. Pilcher,[31] A. D. Pilkington,[84] A. W. J. Pin,[84] J. Pina,[126a,126b,126d] M. Pinamonti,[164a,164c,ee] J. L. Pinfold,[3] A. Pingel,[36] S. Pires,[80] H. Pirumov,[42] M. Pitt,[172] C. Pizio,[91a,91b] L. Plazak,[144a] M.-A. Pleier,[25] V. Pleskot,[129] E. Plotnikova,[65] P. Plucinski,[146a,146b] D. Pluth,[64] R. Poettgen,[146a,146b] L. Poggioli,[117] D. Pohl,[21] G. Polesello,[121a] A. Poley,[42] A. Policicchio,[37a,37b] R. Polifka,[158] A. Polini,[20a] C. S. Pollard,[53] V. Polychronakos,[25] K. Pommès,[30] L. Pontecorvo,[132a] B. G. Pope,[90] G. A. Popeneciu,[26c] D. S. Popovic,[13] A. Poppleton,[30] S. Pospisil,[128] K. Potamianos,[15] I. N. Potrap,[65] C. J. Potter,[149] C. T. Potter,[116] G. Poulard,[30] J. Poveda,[30] V. Pozdnyakov,[65] P. Pralavorio,[85] A. Pranko,[15] S. Prasad,[30] S. Prell,[64] D. Price,[84] L. E. Price,[6] M. Primavera,[73a] S. Prince,[87] M. Proissl,[46] K. Prokofiev,[60c] F. Prokoshin,[32b] E. Protopapadaki,[136] S. Protopopescu,[25] J. Proudfoot,[6] M. Przybycien,[38a] E. Ptacek,[116] D. Puddu,[134a,134b] E. Pueschel,[86] D. Puldon,[148] M. Purohit,[25,ff] P. Puzo,[117] J. Qian,[89] G. Qin,[53] Y. Qin,[84] A. Quadt,[54] D. R. Quarrie,[15] W. B. Quayle,[164a,164b] M. Queitsch-Maitland,[84] D. Quilty,[53] S. Raddum,[119] V. Radeka,[25] V. Radescu,[42] S. K. Radhakrishnan,[148] P. Radloff,[116] P. Rados,[88] F. Ragusa,[91a,91b] G. Rahal,[178] S. Rajagopalan,[25] M. Rammensee,[30] C. Rangel-Smith,[166] F. Rauscher,[100] S. Rave,[83] T. Ravenscroft,[53] M. Raymond,[30] A. L. Read,[119] N. P. Readioff,[74] D. M. Rebuzzi,[121a,121b] A. Redelbach,[174] G. Redlinger,[25] R. Reece,[137] K. Reeves,[41] L. Rehnisch,[16] J. Reichert,[122] H. Reisin,[27] C. Rembser,[30] H. Ren,[33a] A. Renaud,[117] M. Rescigno,[132a] S. Resconi,[91a] O. L. Rezanova,[109,c] P. Reznicek,[129] R. Rezvani,[95] R. Richter,[101] S. Richter,[78] E. Richter-Was,[38b] O. Ricken,[21] M. Ridel,[80] P. Rieck,[16] C. J. Riegel,[175] J. Rieger,[54] O. Rifki,[113] M. Rijssenbeek,[148] A. Rimoldi,[121a,121b] L. Rinaldi,[20a] B. Ristić,[49] E. Ritsch,[30] I. Riu,[12] F. Rizatdinova,[114] E. Rizvi,[76] S. H. Robertson,[87,k] A. Robichaud-Veronneau,[87] D. Robinson,[28] J. E. M. Robinson,[42] A. Robson,[53] C. Roda,[124a,124b] S. Roe,[30] O. Røhne,[119] A. Romaniouk,[98] M. Romano,[20a,20b] S. M. Romano Saez,[34] E. Romero Adam,[167] N. Rompotis,[138] M. Ronzani,[48] L. Roos,[80] E. Ros,[167] S. Rosati,[132a] K. Rosbach,[48] P. Rose,[137] P. L. Rosendahl,[14] O. Rosenthal,[141] V. Rossetti,[146a,146b] E. Rossi,[104a,104b] L. P. Rossi,[50a] J. H. N. Rosten,[28] R. Rosten,[138] M. Rotaru,[26b] I. Roth,[172] J. Rothberg,[138] D. Rousseau,[117] C. R. Royon,[136] A. Rozanov,[85] Y. Rozen,[152] X. Ruan,[145c] F. Rubbo,[143] I. Rubinskiy,[42] V. I. Rud,[99] C. Rudolph,[44] M. S. Rudolph,[158] F. Rühr,[48] A. Ruiz-Martinez,[30] Z. Rurikova,[48] N. A. Rusakovich,[65] A. Ruschke,[100] H. L. Russell,[138] J. P. Rutherfoord,[7] N. Ruthmann,[30] Y. F. Ryabov,[123] M. Rybar,[165] G. Rybkin,[117] N. C. Ryder,[120] A. F. Saavedra,[150] G. Sabato,[107] S. Sacerdoti,[27] A. Saddique,[3] H. F-W. Sadrozinski,[137] R. Sadykov,[65] F. Safai Tehrani,[132a] P. Saha,[108] M. Sahinsoy,[58a] M. Saimpert,[136] T. Saito,[155] H. Sakamoto,[155] Y. Sakurai,[171] G. Salamanna,[134a,134b] A. Salamon,[133a] J. E. Salazar Loyola,[32b] M. Saleem,[113] D. Salek,[107] P. H. Sales De Bruin,[138] D. Salihagic,[101] A. Salnikov,[143] J. Salt,[167] D. Salvatore,[37a,37b] F. Salvatore,[149] A. Salvucci,[60a] A. Salzburger,[30] D. Sammel,[48] D. Sampsonidis,[154] A. Sanchez,[104a,104b] J. Sánchez,[167] V. Sanchez Martinez,[167] H. Sandaker,[119] R. L. Sandbach,[76] H. G. Sander,[83] M. P. Sanders,[100] M. Sandhoff,[175] C. Sandoval,[162] R. Sandstroem,[101] D. P. C. Sankey,[131] M. Sannino,[50a,50b] A. Sansoni,[47] C. Santoni,[34] R. Santonico,[133a,133b] H. Santos,[126a] I. Santoyo Castillo,[149] K. Sapp,[125] A. Sapronov,[65] J. G. Saraiva,[126a,126d] B. Sarrazin,[21] O. Sasaki,[66] Y. Sasaki,[155] K. Sato,[160] G. Sauvage,[5,†] E. Sauvan,[5] G. Savage,[77] P. Savard,[158,d] C. Sawyer,[131] L. Sawyer,[79,n] J. Saxon,[31] C. Sbarra,[20a] A. Sbrizzi,[20a,20b] T. Scanlon,[78] D. A. Scannicchio,[163] M. Scarcella,[150] V. Scarfone,[37a,37b] J. Schaarschmidt,[172] P. Schacht,[101] D. Schaefer,[30] R. Schaefer,[42] J. Schaeffer,[83]

S. Schaepe,[21] S. Schaetzel,[58b] U. Schäfer,[83] A. C. Schaffer,[117] D. Schaile,[100] R. D. Schamberger,[148] V. Scharf,[58a] V. A. Schegelsky,[123] D. Scheirich,[129] M. Schernau,[163] C. Schiavi,[50a,50b] C. Schillo,[48] M. Schioppa,[37a,37b] S. Schlenker,[30] K. Schmieden,[30] C. Schmitt,[83] S. Schmitt,[58b] S. Schmitt,[42] B. Schneider,[159a] Y. J. Schnellbach,[74] U. Schnoor,[44] L. Schoeffel,[136] A. Schoening,[58b] B. D. Schoenrock,[90] E. Schopf,[21] A. L. S. Schorlemmer,[54] M. Schott,[83] D. Schouten,[159a] J. Schovancova,[8] S. Schramm,[49] M. Schreyer,[174] N. Schuh,[83] M. J. Schultens,[21] H.-C. Schultz-Coulon,[58a] H. Schulz,[16] M. Schumacher,[48] B. A. Schumm,[137] Ph. Schune,[136] C. Schwanenberger,[84] A. Schwartzman,[143] T. A. Schwarz,[89] Ph. Schwegler,[101] H. Schweiger,[84] Ph. Schwemling,[136] R. Schwienhorst,[90] J. Schwindling,[136] T. Schwindt,[21] F. G. Sciacca,[17] E. Scifo,[117] G. Sciolla,[23] F. Scuri,[124a,124b] F. Scutti,[21] J. Searcy,[89] G. Sedov,[42] E. Sedykh,[123] P. Seema,[21] S. C. Seidel,[105] A. Seiden,[137] F. Seifert,[128] J. M. Seixas,[24a] G. Sekhniaidze,[104a] K. Sekhon,[89] S. J. Sekula,[40] D. M. Seliverstov,[123,†] N. Semprini-Cesari,[20a,20b] C. Serfon,[30] L. Serin,[117] L. Serkin,[164a,164b] T. Serre,[85] M. Sessa,[134a,134b] R. Seuster,[159a] H. Severini,[113] T. Sfiligoj,[75] F. Sforza,[30] A. Sfyrla,[30] E. Shabalina,[54] M. Shamim,[116] L. Y. Shan,[33a] R. Shang,[165] J. T. Shank,[22] M. Shapiro,[15] P. B. Shatalov,[97] K. Shaw,[164a,164b] S. M. Shaw,[84] A. Shcherbakova,[146a,146b] C. Y. Shehu,[149] P. Sherwood,[78] L. Shi,[151,gg] S. Shimizu,[67] C. O. Shimmin,[163] M. Shimojima,[102] M. Shiyakova,[65] A. Shmeleva,[96] D. Shoaleh Saadi,[95] M. J. Shochet,[31] S. Shojaii,[91a,91b] S. Shrestha,[111] E. Shulga,[98] M. A. Shupe,[7] S. Shushkevich,[42] P. Sicho,[127] P. E. Sidebo,[147] O. Sidiropoulou,[174] D. Sidorov,[114] A. Sidoti,[20a,20b] F. Siegert,[44] Dj. Sijacki,[13] J. Silva,[126a,126d] Y. Silver,[153] S. B. Silverstein,[146a] V. Simak,[128] O. Simard,[5] Lj. Simic,[13] S. Simion,[117] E. Simioni,[83] B. Simmons,[78] D. Simon,[34] P. Sinervo,[158] N. B. Sinev,[116] M. Sioli,[20a,20b] G. Siragusa,[174] A. N. Sisakyan,[65,†] S. Yu. Sivoklokov,[99] J. Sjölin,[146a,146b] T. B. Sjursen,[14] M. B. Skinner,[72] H. P. Skottowe,[57] P. Skubic,[113] M. Slater,[18] T. Slavicek,[128] M. Slawinska,[107] K. Sliwa,[161] V. Smakhtin,[172] B. H. Smart,[46] L. Smestad,[14] S. Yu. Smirnov,[98] Y. Smirnov,[98] L. N. Smirnova,[99,hh] O. Smirnova,[81] M. N. K. Smith,[35] R. W. Smith,[35] M. Smizanska,[72] K. Smolek,[128] A. A. Snesarev,[96] G. Snidero,[76] S. Snyder,[25] R. Sobie,[169,k] F. Socher,[44] A. Soffer,[153] D. A. Soh,[151,gg] G. Sokhrannyi,[75] C. A. Solans,[30] M. Solar,[128] J. Solc,[128] E. Yu. Soldatov,[98] U. Soldevila,[167] A. A. Solodkov,[130] A. Soloshenko,[65] O. V. Solovyanov,[130] V. Solovyev,[123] P. Sommer,[48] H. Y. Song,[33b,y] N. Soni,[1] A. Sood,[15] A. Sopczak,[128] B. Sopko,[128] V. Sopko,[128] V. Sorin,[12] D. Sosa,[58b] M. Sosebee,[8] C. L. Sotiropoulou,[124a,124b] R. Soualah,[164a,164c] A. M. Soukharev,[109,c] D. South,[42] B. C. Sowden,[77] S. Spagnolo,[73a,73b] M. Spalla,[124a,124b] M. Spangenberg,[170] F. Spanò,[77] W. R. Spearman,[57] D. Sperlich,[16] F. Spettel,[101] R. Spighi,[20a] G. Spigo,[30] L. A. Spiller,[88] M. Spousta,[129] R. D. St. Denis,[53,†] A. Stabile,[91a] S. Staerz,[44] J. Stahlman,[122] R. Stamen,[58a] S. Stamm,[16] E. Stanecka,[39] C. Stanescu,[134a] M. Stanescu-Bellu,[42] M. M. Stanitzki,[42] S. Stapnes,[119] E. A. Starchenko,[130] J. Stark,[55] P. Staroba,[127] P. Starovoitov,[58a] R. Staszewski,[39] P. Steinberg,[25] B. Stelzer,[142] H. J. Stelzer,[30] O. Stelzer-Chilton,[159a] H. Stenzel,[52] G. A. Stewart,[53] J. A. Stillings,[21] M. C. Stockton,[87] M. Stoebe,[87] G. Stoicea,[26b] P. Stolte,[54] S. Stonjek,[101] A. R. Stradling,[8] A. Straessner,[44] M. E. Stramaglia,[17] J. Strandberg,[147] S. Strandberg,[146a,146b] A. Strandlie,[119] E. Strauss,[143] M. Strauss,[113] P. Strizenec,[144b] R. Ströhmer,[174] D. M. Strom,[116] R. Stroynowski,[40] A. Strubig,[106] S. A. Stucci,[17] B. Stugu,[14] N. A. Styles,[42] D. Su,[143] J. Su,[125] R. Subramaniam,[79] A. Succurro,[12] S. Suchek,[58a] Y. Sugaya,[118] M. Suk,[128] V. V. Sulin,[96] S. Sultansoy,[4c] T. Sumida,[68] S. Sun,[57] X. Sun,[33a] J. E. Sundermann,[48] K. Suruliz,[149] G. Susinno,[37a,37b] M. R. Sutton,[149] S. Suzuki,[66] M. Svatos,[127] M. Swiatlowski,[143] I. Sykora,[144a] T. Sykora,[129] D. Ta,[48] C. Taccini,[134a,134b] K. Tackmann,[42] J. Taenzer,[158] A. Taffard,[163] R. Tafirout,[159a] N. Taiblum,[153] H. Takai,[25] R. Takashima,[69] H. Takeda,[67] T. Takeshita,[140] Y. Takubo,[66] M. Talby,[85] A. A. Talyshev,[109,c] J. Y. C. Tam,[174] K. G. Tan,[88] J. Tanaka,[155] R. Tanaka,[117] S. Tanaka,[66] B. B. Tannenwald,[111] N. Tannoury,[21] S. Tapia Araya,[32b] S. Tapprogge,[83] S. Tarem,[152] F. Tarrade,[29] G. F. Tartarelli,[91a] P. Tas,[129] M. Tasevsky,[127] T. Tashiro,[68] E. Tassi,[37a,37b] A. Tavares Delgado,[126a,126b] Y. Tayalati,[135d] F. E. Taylor,[94] G. N. Taylor,[88] P. T. E. Taylor,[88] W. Taylor,[159b] F. A. Teischinger,[30] M. Teixeira Dias Castanheira,[76] P. Teixeira-Dias,[77] K. K. Temming,[48] D. Temple,[142] H. Ten Kate,[30] P. K. Teng,[151] J. J. Teoh,[118] F. Tepel,[175] S. Terada,[66] K. Terashi,[155] J. Terron,[82] S. Terzo,[101] M. Testa,[47] R. J. Teuscher,[158,k] T. Theveneaux-Pelzer,[34] J. P. Thomas,[18] J. Thomas-Wilsker,[77] E. N. Thompson,[35] P. D. Thompson,[18] R. J. Thompson,[84] A. S. Thompson,[53] L. A. Thomsen,[176] E. Thomson,[122] M. Thomson,[28] R. P. Thun,[89,†] M. J. Tibbetts,[15] R. E. Ticse Torres,[85] V. O. Tikhomirov,[96,ii] Yu. A. Tikhonov,[109,c] S. Timoshenko,[98] E. Tiouchichine,[85] P. Tipton,[176] S. Tisserant,[85] K. Todome,[157] T. Todorov,[5,†] S. Todorova-Nova,[129] J. Tojo,[70] S. Tokár,[144a] K. Tokushuku,[66] K. Tollefson,[90] E. Tolley,[57] L. Tomlinson,[84] M. Tomoto,[103] L. Tompkins,[143,jj] K. Toms,[105] E. Torrence,[116] H. Torres,[142] E. Torró Pastor,[138] J. Toth,[85,kk] F. Touchard,[85] D. R. Tovey,[139] T. Trefzger,[174] L. Tremblet,[30] A. Tricoli,[30] I. M. Trigger,[159a] S. Trincaz-Duvoid,[80] M. F. Tripiana,[12] W. Trischuk,[158] B. Trocmé,[55] C. Troncon,[91a] M. Trottier-McDonald,[15] M. Trovatelli,[169] L. Truong,[164a,164c] M. Trzebinski,[39] A. Trzupek,[39] C. Tsarouchas,[30] J. C-L. Tseng,[120] P. V. Tsiareshka,[92] D. Tsionou,[154] G. Tsipolitis,[10] N. Tsirintanis,[9] S. Tsiskaridze,[12] V. Tsiskaridze,[48]

E. G. Tskhadadze,[51a] K. M. Tsui,[60a] I. I. Tsukerman,[97] V. Tsulaia,[15] S. Tsuno,[66] D. Tsybychev,[148] A. Tudorache,[26b] V. Tudorache,[26b] A. N. Tuna,[57] S. A. Tupputi,[20a,20b] S. Turchikhin,[99,hh] D. Turecek,[128] R. Turra,[91a,91b] A. J. Turvey,[40] P. M. Tuts,[35] A. Tykhonov,[49] M. Tylmad,[146a,146b] M. Tyndel,[131] I. Ueda,[155] R. Ueno,[29] M. Ughetto,[146a,146b] M. Ugland,[14] F. Ukegawa,[160] G. Unal,[30] A. Undrus,[25] G. Unel,[163] F. C. Ungaro,[48] Y. Unno,[66] C. Unverdorben,[100] J. Urban,[144b] P. Urquijo,[88] P. Urrejola,[83] G. Usai,[8] A. Usanova,[62] L. Vacavant,[85] V. Vacek,[128] B. Vachon,[87] C. Valderanis,[83] N. Valencic,[107] S. Valentinetti,[20a,20b] A. Valero,[167] L. Valery,[12] S. Valkar,[129] S. Vallecorsa,[49] J. A. Valls Ferrer,[167] W. Van Den Wollenberg,[107] P. C. Van Der Deijl,[107] R. van der Geer,[107] H. van der Graaf,[107] N. van Eldik,[152] P. van Gemmeren,[6] J. Van Nieuwkoop,[142] I. van Vulpen,[107] M. C. van Woerden,[30] M. Vanadia,[132a,132b] W. Vandelli,[30] R. Vanguri,[122] A. Vaniachine,[6] F. Vannucci,[80] G. Vardanyan,[177] R. Vari,[132a] E. W. Varnes,[7] T. Varol,[40] D. Varouchas,[80] A. Vartapetian,[8] K. E. Varvell,[150] F. Vazeille,[34] T. Vazquez Schroeder,[87] J. Veatch,[7] L. M. Veloce,[158] F. Veloso,[126a,126c] T. Velz,[21] S. Veneziano,[132a] A. Ventura,[73a,73b] D. Ventura,[86] M. Venturi,[169] N. Venturi,[158] A. Venturini,[23] V. Vercesi,[121a] M. Verducci,[132a,132b] W. Verkerke,[107] J. C. Vermeulen,[107] A. Vest,[44] M. C. Vetterli,[142,d] O. Viazlo,[81] I. Vichou,[165] T. Vickey,[139] O. E. Vickey Boeriu,[139] G. H. A. Viehhauser,[120] S. Viel,[15] R. Vigne,[62] M. Villa,[20a,20b] M. Villaplana Perez,[91a,91b] E. Vilucchi,[47] M. G. Vincter,[29] V. B. Vinogradov,[65] I. Vivarelli,[149] F. Vives Vaque,[3] S. Vlachos,[10] D. Vladoiu,[100] M. Vlasak,[128] M. Vogel,[32a] P. Vokac,[128] G. Volpi,[124a,124b] M. Volpi,[88] H. von der Schmitt,[101] H. von Radziewski,[48] E. von Toerne,[21] V. Vorobel,[129] K. Vorobev,[98] M. Vos,[167] R. Voss,[30] J. H. Vossebeld,[74] N. Vranjes,[13] M. Vranjes Milosavljevic,[13] V. Vrba,[127] M. Vreeswijk,[107] R. Vuillermet,[30] I. Vukotic,[31] Z. Vykydal,[128] P. Wagner,[21] W. Wagner,[175] H. Wahlberg,[71] S. Wahrmund,[44] J. Wakabayashi,[103] J. Walder,[72] R. Walker,[100] W. Walkowiak,[141] C. Wang,[151] F. Wang,[173] H. Wang,[15] H. Wang,[40] J. Wang,[42] J. Wang,[150] K. Wang,[87] R. Wang,[6] S. M. Wang,[151] T. Wang,[21] T. Wang,[35] X. Wang,[176] C. Wanotayaroj,[116] A. Warburton,[87] C. P. Ward,[28] D. R. Wardrope,[78] A. Washbrook,[46] C. Wasicki,[42] P. M. Watkins,[18] A. T. Watson,[18] I. J. Watson,[150] M. F. Watson,[18] G. Watts,[138] S. Watts,[84] B. M. Waugh,[78] S. Webb,[84] M. S. Weber,[17] S. W. Weber,[174] J. S. Webster,[31] A. R. Weidberg,[120] B. Weinert,[61] J. Weingarten,[54] C. Weiser,[48] H. Weits,[107] P. S. Wells,[30] T. Wenaus,[25] T. Wengler,[30] S. Wenig,[30] N. Wermes,[21] M. Werner,[48] P. Werner,[30] M. Wessels,[58a] J. Wetter,[161] K. Whalen,[116] A. M. Wharton,[72] A. White,[8] M. J. White,[1] R. White,[32b] S. White,[124a,124b] D. Whiteson,[163] F. J. Wickens,[131] W. Wiedenmann,[173] M. Wielers,[131] P. Wienemann,[21] C. Wiglesworth,[36] L. A. M. Wiik-Fuchs,[21] A. Wildauer,[101] H. G. Wilkens,[30] H. H. Williams,[122] S. Williams,[107] C. Willis,[90] S. Willocq,[86] A. Wilson,[89] J. A. Wilson,[18] I. Wingerter-Seez,[5] F. Winklmeier,[116] B. T. Winter,[21] M. Wittgen,[143] J. Wittkowski,[100] S. J. Wollstadt,[83] M. W. Wolter,[39] H. Wolters,[126a,126c] B. K. Wosiek,[39] J. Wotschack,[30] M. J. Woudstra,[84] K. W. Wozniak,[39] M. Wu,[55] M. Wu,[31] S. L. Wu,[173] X. Wu,[49] Y. Wu,[89] T. R. Wyatt,[84] B. M. Wynne,[46] S. Xella,[36] D. Xu,[33a] L. Xu,[25] B. Yabsley,[150] S. Yacoob,[145a] R. Yakabe,[67] M. Yamada,[66] D. Yamaguchi,[157] Y. Yamaguchi,[118] A. Yamamoto,[66] S. Yamamoto,[155] T. Yamanaka,[155] K. Yamauchi,[103] Y. Yamazaki,[67] Z. Yan,[22] H. Yang,[33e] H. Yang,[173] Y. Yang,[151] W-M. Yao,[15] Y. C. Yap,[80] Y. Yasu,[66] E. Yatsenko,[5] K. H. Yau Wong,[21] J. Ye,[40] S. Ye,[25] I. Yeletskikh,[65] A. L. Yen,[57] E. Yildirim,[42] K. Yorita,[171] R. Yoshida,[6] K. Yoshihara,[122] C. Young,[143] C. J. S. Young,[30] S. Youssef,[22] D. R. Yu,[15] J. Yu,[8] J. M. Yu,[89] J. Yu,[114] L. Yuan,[67] S. P. Y. Yuen,[21] A. Yurkewicz,[108] I. Yusuff,[28,ll] B. Zabinski,[39] R. Zaidan,[63] A. M. Zaitsev,[130,cc] J. Zalieckas,[14] A. Zaman,[148] S. Zambito,[57] L. Zanello,[132a,132b] D. Zanzi,[88] C. Zeitnitz,[175] M. Zeman,[128] A. Zemla,[38a] Q. Zeng,[143] K. Zengel,[23] O. Zenin,[130] T. Ženiš,[144a] D. Zerwas,[117] D. Zhang,[89] F. Zhang,[173] G. Zhang,[33b] H. Zhang,[33c] J. Zhang,[6] L. Zhang,[48] R. Zhang,[33b,i] X. Zhang,[33d] Z. Zhang,[117] X. Zhao,[40] Y. Zhao,[33d,117] Z. Zhao,[33b] A. Zhemchugov,[65] J. Zhong,[120] B. Zhou,[89] C. Zhou,[45] L. Zhou,[35] L. Zhou,[40] M. Zhou,[148] N. Zhou,[33f] C. G. Zhu,[33d] H. Zhu,[33a] J. Zhu,[89] Y. Zhu,[33b] X. Zhuang,[33a] K. Zhukov,[96] A. Zibell,[174] D. Zieminska,[61] N. I. Zimine,[65] C. Zimmermann,[83] S. Zimmermann,[48] Z. Zinonos,[54] M. Zinser,[83] M. Ziolkowski,[141] L. Živković,[13] G. Zobernig,[173] A. Zoccoli,[20a,20b] M. zur Nedden,[16] G. Zurzolo,[104a,104b] and L. Zwalinski[30]

(ATLAS Collaboration)

[1]*Department of Physics, University of Adelaide, Adelaide, Australia*
[2]*Physics Department, SUNY Albany, Albany, New York, USA*
[3]*Department of Physics, University of Alberta, Edmonton, Alberta, Canada*
[4a]*Department of Physics, Ankara University, Ankara, Turkey*
[4b]*Istanbul Aydin University, Istanbul, Turkey*
[4c]*Division of Physics, TOBB University of Economics and Technology, Ankara, Turkey*
[5]*LAPP, CNRS/IN2P3 and Université Savoie Mont Blanc, Annecy-le-Vieux, France*
[6]*High Energy Physics Division, Argonne National Laboratory, Argonne, Illinois, USA*

[7]Department of Physics, University of Arizona, Tucson, Arizona, USA
[8]Department of Physics, The University of Texas at Arlington, Arlington, Texas, USA
[9]Physics Department, University of Athens, Athens, Greece
[10]Physics Department, National Technical University of Athens, Zografou, Greece
[11]Institute of Physics, Azerbaijan Academy of Sciences, Baku, Azerbaijan
[12]Institut de Física d'Altes Energies and Departament de Física de la Universitat Autònoma de Barcelona, Barcelona, Spain
[13]Institute of Physics, University of Belgrade, Belgrade, Serbia
[14]Department for Physics and Technology, University of Bergen, Bergen, Norway
[15]Physics Division, Lawrence Berkeley National Laboratory and University of California, Berkeley, California, USA
[16]Department of Physics, Humboldt University, Berlin, Germany
[17]Albert Einstein Center for Fundamental Physics and Laboratory for High Energy Physics, University of Bern, Bern, Switzerland
[18]School of Physics and Astronomy, University of Birmingham, Birmingham, United Kingdom
[19a]Department of Physics, Bogazici University, Istanbul, Turkey
[19b]Department of Physics Engineering, Gaziantep University, Gaziantep, Turkey
[19c]Department of Physics, Dogus University, Istanbul, Turkey
[20a]INFN Sezione di Bologna, Italy
[20b]Dipartimento di Fisica e Astronomia, Università di Bologna, Bologna, Italy
[21]Physikalisches Institut, University of Bonn, Bonn, Germany
[22]Department of Physics, Boston University, Boston, Massachusetts, USA
[23]Department of Physics, Brandeis University, Waltham, Massachusetts, USA
[24a]Universidade Federal do Rio De Janeiro COPPE/EE/IF, Rio de Janeiro, Brazil
[24b]Electrical Circuits Department, Federal University of Juiz de Fora (UFJF), Juiz de Fora, Brazil
[24c]Federal University of Sao Joao del Rei (UFSJ), Sao Joao del Rei, Brazil
[24d]Instituto de Fisica, Universidade de Sao Paulo, Sao Paulo, Brazil
[25]Physics Department, Brookhaven National Laboratory, Upton, New York, USA
[26a]Transilvania University of Brasov, Brasov, Romania
[26b]National Institute of Physics and Nuclear Engineering, Bucharest, Romania
[26c]National Institute for Research and Development of Isotopic and Molecular Technologies, Physics Department, Cluj Napoca, Romania
[26d]University Politehnica Bucharest, Bucharest, Romania
[26e]West University in Timisoara, Timisoara, Romania
[27]Departamento de Física, Universidad de Buenos Aires, Buenos Aires, Argentina
[28]Cavendish Laboratory, University of Cambridge, Cambridge, United Kingdom
[29]Department of Physics, Carleton University, Ottawa, Ontario, Canada
[30]CERN, Geneva, Switzerland
[31]Enrico Fermi Institute, University of Chicago, Chicago, Illinois, USA
[32a]Departamento de Física, Pontificia Universidad Católica de Chile, Santiago, Chile
[32b]Departamento de Física, Universidad Técnica Federico Santa María, Valparaíso, Chile
[33a]Institute of High Energy Physics, Chinese Academy of Sciences, Beijing, China
[33b]Department of Modern Physics, University of Science and Technology of China, Anhui, China
[33c]Department of Physics, Nanjing University, Jiangsu, China
[33d]School of Physics, Shandong University, Shandong, China
[33e]Department of Physics and Astronomy, Shanghai Key Laboratory for Particle Physics and Cosmology, Shanghai Jiao Tong University, Shanghai, China
[33f]Physics Department, Tsinghua University, Beijing 100084, China
[34]Laboratoire de Physique Corpusculaire, Clermont Université and Université Blaise Pascal and CNRS/IN2P3, Clermont-Ferrand, France
[35]Nevis Laboratory, Columbia University, Irvington, New York, USA
[36]Niels Bohr Institute, University of Copenhagen, Kobenhavn, Denmark
[37a]INFN Gruppo Collegato di Cosenza, Laboratori Nazionali di Frascati, Italy
[37b]Dipartimento di Fisica, Università della Calabria, Rende, Italy
[38a]AGH University of Science and Technology, Faculty of Physics and Applied Computer Science, Krakow, Poland
[38b]Marian Smoluchowski Institute of Physics, Jagiellonian University, Krakow, Poland
[39]Institute of Nuclear Physics Polish Academy of Sciences, Krakow, Poland
[40]Physics Department, Southern Methodist University, Dallas, Texas, USA
[41]Physics Department, University of Texas at Dallas, Richardson, Texas, USA

[42]DESY, Hamburg and Zeuthen, Germany
[43]Institut für Experimentelle Physik IV, Technische Universität Dortmund, Dortmund, Germany
[44]Institut für Kern- und Teilchenphysik, Technische Universität Dresden, Dresden, Germany
[45]Department of Physics, Duke University, Durham, North Carolina, USA
[46]SUPA—School of Physics and Astronomy, University of Edinburgh, Edinburgh, United Kingdom
[47]INFN Laboratori Nazionali di Frascati, Frascati, Italy
[48]Fakultät für Mathematik und Physik, Albert-Ludwigs-Universität, Freiburg, Germany
[49]Section de Physique, Université de Genève, Geneva, Switzerland
[50a]INFN Sezione di Genova, Italy
[50b]Dipartimento di Fisica, Università di Genova, Genova, Italy
[51a]E. Andronikashvili Institute of Physics, Iv. Javakhishvili Tbilisi State University, Tbilisi, Georgia
[51b]High Energy Physics Institute, Tbilisi State University, Tbilisi, Georgia
[52]II Physikalisches Institut, Justus-Liebig-Universität Giessen, Giessen, Germany
[53]SUPA—School of Physics and Astronomy, University of Glasgow, Glasgow, United Kingdom
[54]II Physikalisches Institut, Georg-August-Universität, Göttingen, Germany
[55]Laboratoire de Physique Subatomique et de Cosmologie, Université Grenoble-Alpes, CNRS/IN2P3, Grenoble, France
[56]Department of Physics, Hampton University, Hampton, Virginia, USA
[57]Laboratory for Particle Physics and Cosmology, Harvard University, Cambridge, Massachusetts, USA
[58a]Kirchhoff-Institut für Physik, Ruprecht-Karls-Universität Heidelberg, Heidelberg, Germany
[58b]Physikalisches Institut, Ruprecht-Karls-Universität Heidelberg, Heidelberg, Germany
[58c]ZITI Institut für technische Informatik, Ruprecht-Karls-Universität Heidelberg, Mannheim, Germany
[59]Faculty of Applied Information Science, Hiroshima Institute of Technology, Hiroshima, Japan
[60a]Department of Physics, The Chinese University of Hong Kong, Shatin, N.T., Hong Kong, China
[60b]Department of Physics, The University of Hong Kong, Hong Kong, China
[60c]Department of Physics, The Hong Kong University of Science and Technology, Clear Water Bay, Kowloon, Hong Kong, China
[61]Department of Physics, Indiana University, Bloomington, Indiana, USA
[62]Institut für Astro- und Teilchenphysik, Leopold-Franzens-Universität, Innsbruck, Austria
[63]University of Iowa, Iowa City, Iowa, USA
[64]Department of Physics and Astronomy, Iowa State University, Ames, Iowa, USA
[65]Joint Institute for Nuclear Research, JINR Dubna, Dubna, Russia
[66]KEK, High Energy Accelerator Research Organization, Tsukuba, Japan
[67]Graduate School of Science, Kobe University, Kobe, Japan
[68]Faculty of Science, Kyoto University, Kyoto, Japan
[69]Kyoto University of Education, Kyoto, Japan
[70]Department of Physics, Kyushu University, Fukuoka, Japan
[71]Instituto de Física La Plata, Universidad Nacional de La Plata and CONICET, La Plata, Argentina
[72]Physics Department, Lancaster University, Lancaster, United Kingdom
[73a]INFN Sezione di Lecce, Italy
[73b]Dipartimento di Matematica e Fisica, Università del Salento, Lecce, Italy
[74]Oliver Lodge Laboratory, University of Liverpool, Liverpool, United Kingdom
[75]Department of Physics, Jožef Stefan Institute and University of Ljubljana, Ljubljana, Slovenia
[76]School of Physics and Astronomy, Queen Mary University of London, London, United Kingdom
[77]Department of Physics, Royal Holloway University of London, Surrey, United Kingdom
[78]Department of Physics and Astronomy, University College London, London, United Kingdom
[79]Louisiana Tech University, Ruston, Louisiana, USA
[80]Laboratoire de Physique Nucléaire et de Hautes Energies, UPMC and Université Paris-Diderot and CNRS/IN2P3, Paris, France
[81]Fysiska Institutionen, Lunds Universitet, Lund, Sweden
[82]Departamento de Física Teorica C-15, Universidad Autonoma de Madrid, Madrid, Spain
[83]Institut für Physik, Universität Mainz, Mainz, Germany
[84]School of Physics and Astronomy, University of Manchester, Manchester, United Kingdom
[85]CPPM, Aix-Marseille Université and CNRS/IN2P3, Marseille, France
[86]Department of Physics, University of Massachusetts, Amherst, Massachusetts, USA
[87]Department of Physics, McGill University, Montreal, Quebec, Canada
[88]School of Physics, University of Melbourne, Victoria, Australia
[89]Department of Physics, The University of Michigan, Ann Arbor, Michigan, USA
[90]Department of Physics and Astronomy, Michigan State University, East Lansing, Michigan, USA
[91a]INFN Sezione di Milano, Italy

[91b]Dipartimento di Fisica, Università di Milano, Milano, Italy
[92]B.I. Stepanov Institute of Physics, National Academy of Sciences of Belarus, Minsk, Republic of Belarus
[93]National Scientific and Educational Centre for Particle and High Energy Physics, Minsk, Republic of Belarus
[94]Department of Physics, Massachusetts Institute of Technology, Cambridge, Massachusetts, USA
[95]Group of Particle Physics, University of Montreal, Montreal, Quebec, Canada
[96]P.N. Lebedev Institute of Physics, Academy of Sciences, Moscow, Russia
[97]Institute for Theoretical and Experimental Physics (ITEP), Moscow, Russia
[98]National Research Nuclear University MEPhI, Moscow, Russia
[99]D.V. Skobeltsyn Institute of Nuclear Physics, M.V. Lomonosov Moscow State University, Moscow, Russia
[100]Fakultät für Physik, Ludwig-Maximilians-Universität München, München, Germany
[101]Max-Planck-Institut für Physik (Werner-Heisenberg-Institut), München, Germany
[102]Nagasaki Institute of Applied Science, Nagasaki, Japan
[103]Graduate School of Science and Kobayashi-Maskawa Institute, Nagoya University, Nagoya, Japan
[104a]INFN Sezione di Napoli, Italy
[104b]Dipartimento di Fisica, Università di Napoli, Napoli, Italy
[105]Department of Physics and Astronomy, University of New Mexico, Albuquerque, New Mexico, USA
[106]Institute for Mathematics, Astrophysics and Particle Physics, Radboud University Nijmegen/Nikhef, Nijmegen, Netherlands
[107]Nikhef National Institute for Subatomic Physics and University of Amsterdam, Amsterdam, Netherlands
[108]Department of Physics, Northern Illinois University, DeKalb, Illinois, USA
[109]Budker Institute of Nuclear Physics, SB RAS, Novosibirsk, Russia
[110]Department of Physics, New York University, New York, New York, USA
[111]Ohio State University, Columbus, Ohio, USA
[112]Faculty of Science, Okayama University, Okayama, Japan
[113]Homer L. Dodge Department of Physics and Astronomy, University of Oklahoma, Norman, Oklahoma, USA
[114]Department of Physics, Oklahoma State University, Stillwater, Oklahoma, USA
[115]Palacký University, RCPTM, Olomouc, Czech Republic
[116]Center for High Energy Physics, University of Oregon, Eugene, Oregon, USA
[117]LAL, Université Paris-Sud and CNRS/IN2P3, Orsay, France
[118]Graduate School of Science, Osaka University, Osaka, Japan
[119]Department of Physics, University of Oslo, Oslo, Norway
[120]Department of Physics, Oxford University, Oxford, United Kingdom
[121a]INFN Sezione di Pavia, Italy
[121b]Dipartimento di Fisica, Università di Pavia, Pavia, Italy
[122]Department of Physics, University of Pennsylvania, Philadelphia, Pennsylvania, USA
[123]National Research Centre "Kurchatov Institute" B.P.Konstantinov Petersburg Nuclear Physics Institute, St. Petersburg, Russia
[124a]INFN Sezione di Pisa, Italy
[124b]Dipartimento di Fisica E. Fermi, Università di Pisa, Pisa, Italy
[125]Department of Physics and Astronomy, University of Pittsburgh, Pittsburgh, Pennsylvania, USA
[126a]Laboratório de Instrumentação e Física Experimental de Partículas—LIP, Lisboa, Portugal
[126b]Faculdade de Ciências, Universidade de Lisboa, Lisboa, Portugal
[126c]Department of Physics, University of Coimbra, Coimbra, Portugal
[126d]Centro de Física Nuclear da Universidade de Lisboa, Lisboa, Portugal
[126e]Departamento de Física, Universidade do Minho, Braga, Portugal
[126f]Departamento de Física Teorica y del Cosmos and CAFPE, Universidad de Granada, Granada, Spain
[126g]Departamento de Física and CEFITEC of Faculdade de Ciencias e Tecnologia, Universidade Nova de Lisboa, Caparica, Portugal
[127]Institute of Physics, Academy of Sciences of the Czech Republic, Praha, Czech Republic
[128]Czech Technical University in Prague, Praha, Czech Republic
[129]Faculty of Mathematics and Physics, Charles University in Prague, Praha, Czech Republic
[130]State Research Center Institute for High Energy Physics (Protvino), NRC KI, Russia
[131]Particle Physics Department, Rutherford Appleton Laboratory, Didcot, United Kingdom
[132a]INFN Sezione di Roma, Italy
[132b]Dipartimento di Fisica, Sapienza Università di Roma, Roma, Italy
[133a]INFN Sezione di Roma Tor Vergata, Italy
[133b]Dipartimento di Fisica, Università di Roma Tor Vergata, Roma, Italy
[134a]INFN Sezione di Roma Tre, Italy

[134b]*Dipartimento di Matematica e Fisica, Università Roma Tre, Roma, Italy*
[135a]*Faculté des Sciences Ain Chock, Réseau Universitaire de Physique des Hautes Energies—Université Hassan II, Casablanca, Morocco*
[135b]*Centre National de l'Energie des Sciences Techniques Nucleaires, Rabat, Morocco*
[135c]*Faculté des Sciences Semlalia, Université Cadi Ayyad, LPHEA-Marrakech, Morocco*
[135d]*Faculté des Sciences, Université Mohamed Premier and LPTPM, Oujda, Morocco*
[135e]*Faculté des sciences, Université Mohammed V, Rabat, Morocco*
[136]*DSM/IRFU (Institut de Recherches sur les Lois Fondamentales de l'Univers), CEA Saclay (Commissariat à l'Energie Atomique et aux Energies Alternatives), Gif-sur-Yvette, France*
[137]*Santa Cruz Institute for Particle Physics, University of California Santa Cruz, Santa Cruz, California, USA*
[138]*Department of Physics, University of Washington, Seattle, Washington, USA*
[139]*Department of Physics and Astronomy, University of Sheffield, Sheffield, United Kingdom*
[140]*Department of Physics, Shinshu University, Nagano, Japan*
[141]*Fachbereich Physik, Universität Siegen, Siegen, Germany*
[142]*Department of Physics, Simon Fraser University, Burnaby, British Columbia, Canada*
[143]*SLAC National Accelerator Laboratory, Stanford, California, USA*
[144a]*Faculty of Mathematics, Physics & Informatics, Comenius University, Bratislava, Slovak Republic*
[144b]*Department of Subnuclear Physics, Institute of Experimental Physics of the Slovak Academy of Sciences, Kosice, Slovak Republic*
[145a]*Department of Physics, University of Cape Town, Cape Town, South Africa*
[145b]*Department of Physics, University of Johannesburg, Johannesburg, South Africa*
[145c]*School of Physics, University of the Witwatersrand, Johannesburg, South Africa*
[146a]*Department of Physics, Stockholm University, Sweden*
[146b]*The Oskar Klein Centre, Stockholm, Sweden*
[147]*Physics Department, Royal Institute of Technology, Stockholm, Sweden*
[148]*Departments of Physics & Astronomy and Chemistry, Stony Brook University, Stony Brook New York, USA*
[149]*Department of Physics and Astronomy, University of Sussex, Brighton, United Kingdom*
[150]*School of Physics, University of Sydney, Sydney, Australia*
[151]*Institute of Physics, Academia Sinica, Taipei, Taiwan*
[152]*Department of Physics, Technion: Israel Institute of Technology, Haifa, Israel*
[153]*Raymond and Beverly Sackler School of Physics and Astronomy, Tel Aviv University, Tel Aviv, Israel*
[154]*Department of Physics, Aristotle University of Thessaloniki, Thessaloniki, Greece*
[155]*International Center for Elementary Particle Physics and Department of Physics, The University of Tokyo, Tokyo, Japan*
[156]*Graduate School of Science and Technology, Tokyo Metropolitan University, Tokyo, Japan*
[157]*Department of Physics, Tokyo Institute of Technology, Tokyo, Japan*
[158]*Department of Physics, University of Toronto, Toronto, Ontario, Canada*
[159a]*TRIUMF, Vancouver, British Columbia, Canada*
[159b]*Department of Physics and Astronomy, York University, Toronto Ontario, Canada*
[160]*Faculty of Pure and Applied Sciences, and Center for Integrated Research in Fundamental Science and Engineering, University of Tsukuba, Tsukuba, Japan*
[161]*Department of Physics and Astronomy, Tufts University, Medford, Massachusetts, USA*
[162]*Centro de Investigaciones, Universidad Antonio Narino, Bogota, Colombia*
[163]*Department of Physics and Astronomy, University of California Irvine, Irvine, California, USA*
[164a]*INFN Gruppo Collegato di Udine, Sezione di Trieste, Udine, Italy*
[164b]*ICTP, Trieste, Italy*
[164c]*Dipartimento di Chimica, Fisica e Ambiente, Università di Udine, Udine, Italy*
[165]*Department of Physics, University of Illinois, Urbana, Illinois, USA*
[166]*Department of Physics and Astronomy, University of Uppsala, Uppsala, Sweden*
[167]*Instituto de Física Corpuscular (IFIC) and Departamento de Física Atómica, Molecular y Nuclear and Departamento de Ingeniería Electrónica and Instituto de Microelectrónica de Barcelona (IMB-CNM), University of Valencia and CSIC, Valencia, Spain*
[168]*Department of Physics, University of British Columbia, Vancouver, British Columbia, Canada*
[169]*Department of Physics and Astronomy, University of Victoria, Victoria, British Columbia, Canada*
[170]*Department of Physics, University of Warwick, Coventry, United Kingdom*
[171]*Waseda University, Tokyo, Japan*
[172]*Department of Particle Physics, The Weizmann Institute of Science, Rehovot, Israel*
[173]*Department of Physics, University of Wisconsin, Madison, Wisconsin, USA*

[174]Fakultät für Physik und Astronomie, Julius-Maximilians-Universität, Würzburg, Germany
[175]Fachbereich C Physik, Bergische Universität Wuppertal, Wuppertal, Germany
[176]Department of Physics, Yale University, New Haven, Connecticut, USA
[177]Yerevan Physics Institute, Yerevan, Armenia
[178]Centre de Calcul de l'Institut National de Physique Nucléaire et de Physique des Particules (IN2P3), Villeurbanne, France

[†]Deceased.
[a]Also at Department of Physics, King's College London, London, United Kingdom.
[b]Also at Institute of Physics, Azerbaijan Academy of Sciences, Baku, Azerbaijan.
[c]Also at Novosibirsk State University, Novosibirsk, Russia.
[d]Also at TRIUMF, Vancouver BC, Canada.
[e]Also at Department of Physics, California State University, Fresno, CA, USA.
[f]Also at Department of Physics, University of Fribourg, Fribourg, Switzerland.
[g]Also at Departamento de Física e Astronomia, Faculdade de Ciencias, Universidade do Porto, Portugal.
[h]Also at Tomsk State University, Tomsk, Russia.
[i]Also at CPPM, Aix-Marseille Université and CNRS/IN2P3, Marseille, France.
[j]Also at Universita di Napoli Parthenope, Napoli, Italy.
[k]Also at Institute of Particle Physics (IPP), Canada.
[l]Also at Particle Physics Department, Rutherford Appleton Laboratory, Didcot, United Kingdom.
[m]Also at Department of Physics, St. Petersburg State Polytechnical University, St. Petersburg, Russia.
[n]Also at Louisiana Tech University, Ruston, LA, USA.
[o]Also at Institucio Catalana de Recerca i Estudis Avancats, ICREA, Barcelona, Spain.
[p]Also at Department of Physics, The University of Michigan, Ann Arbor, MI, USA.
[q]Also at Graduate School of Science, Osaka University, Osaka, Japan.
[r]Also at Department of Physics, National Tsing Hua University, Taiwan.
[s]Also at Department of Physics, The University of Texas at Austin, Austin, TX, USA.
[t]Also at Institute of Theoretical Physics, Ilia State University, Tbilisi, Georgia.
[u]Also at CERN, Geneva, Switzerland.
[v]Also at Georgian Technical University (GTU),Tbilisi, Georgia.
[w]Also at Manhattan College, New York, NY, USA.
[x]Also at Hellenic Open University, Patras, Greece.
[y]Also at Institute of Physics, Academia Sinica, Taipei, Taiwan.
[z]Also at LAL, Université Paris-Sud and CNRS/IN2P3, Orsay, France.
[aa]Also at Academia Sinica Grid Computing, Institute of Physics, Academia Sinica, Taipei, Taiwan.
[bb]Also at School of Physics, Shandong University, Shandong, China.
[cc]Also at Moscow Institute of Physics and Technology State University, Dolgoprudny, Russia.
[dd]Also at Section de Physique, Université de Genève, Geneva, Switzerland.
[ee]Also at International School for Advanced Studies (SISSA), Trieste, Italy.
[ff]Also at Department of Physics and Astronomy, University of South Carolina, Columbia, SC, USA.
[gg]Also at School of Physics and Engineering, Sun Yat-sen University, Guangzhou, China.
[hh]Also at Faculty of Physics, M.V.Lomonosov Moscow State University, Moscow, Russia.
[ii]Also at National Research Nuclear University MEPhI, Moscow, Russia.
[jj]Also at Department of Physics, Stanford University, Stanford, CA, USA.
[kk]Also at Institute for Particle and Nuclear Physics, Wigner Research Centre for Physics, Budapest, Hungary.
[ll]Also at University of Malaya, Department of Physics, Kuala Lumpur, Malaysia.